

Copyright
by
Scott Davenport McVicar
2016

The Dissertation Committee for Scott Davenport McVicar Certifies that this is the approved version of the following dissertation:

PEGylated Tissue Repair Peptide TP508 Derivatives as Second Generation Drugs for Radiomitigation and Other Systemic Applications

Committee:

Darrell Carney, Ph.D., Supervisor

Jose Barral, M.D., Ph.D., Chair

Konrad Pazdrak, M.D., Ph.D.

Krishna Rajarathnam, Ph.D.

William Calhoun, M.D.

Gerald Fuller, Ph.D.

Dean, Graduate School

**PEGylated Tissue Repair Peptide TP508 Derivatives as Second
Generation Drugs for Radiomitigation and Other Systemic Applications**

by

Scott Davenport McVicar, B.Sc.

Dissertation

Presented to the Faculty of the Graduate School of

The University of Texas Medical Branch

in Partial Fulfillment

of the Requirements

for the Degree of

Doctor of Philosophy

The University of Texas Medical Branch

November, 2016

Dedication

To my beloved wife, Kristine.

Acknowledgements

All research is built on the hard work and insight of those who have come before. I would like to thank all of the members of the Carney Lab, past and present, for elucidating the therapeutic properties of TP508. I would also like to thank the staff of Chrysalis BioTherapeutics, particularly Dr. Laurie Sower and Dr. Kempaiah Rayavara, for their research support and scientific collaboration. Thanks to my dissertation committee for their time and feedback. Special thanks to my external committee member, Dr. Gerald Fuller, for making himself extraordinarily available to review and discuss my research, and for reviewing my journal article drafts prior to submission.

**PEGylated Tissue Repair Peptide TP508 Derivatives as Second
Generation Drugs for Radiomitigation and Other Systemic
Applications**

Publication No. _____

Scott Davenport McVicar

The University of Texas Medical Branch, 2016

Supervisor: Dr. Darrell Carney

TP508 is a therapeutic peptide that represents a specific receptor-binding domain of human thrombin with many potential clinical applications. However, it shares several weaknesses common to peptides when administered systemically, such as a short circulating half-life and rapid proteolytic degradation. One FDA-approved method for modifying therapeutic peptides and small proteins to improve these characteristics is through covalent attachment to polyethylene glycol moieties, a process known as PEGylation. Because TP508 is currently being evaluated as a nuclear countermeasure drug for radiomitigation, this project was initiated to evaluate several different PEGylated TP508 derivatives in an attempt to increase TP508 efficacy or decrease the therapeutic dose required for efficacy. We demonstrate that the circulating half-life of TP508 derivatives increase in a size-dependent manner with the length of polyethylene glycol attached to TP508. The PEGylated TP508 derivatives were evaluated for biological activity to determine if increased half-life correlated with increased activity using a combination of *in vitro* and *in vivo* methods. *In vitro* activity of TP508 derivatives was demonstrated in human dermal microvascular endothelial cells (HDMEC) where TP508 and its derivatives accelerated repair of radiation induced DNA double strand breaks. To test *in vivo* activity, murine models for mitigation of ionizing radiation using outbred male CD-1 mice were used. These studies demonstrated that injection of only two of the TP508 derivatives enhanced aortic explant angiogenesis when the explants were cultured on extracellular matrix *ex vivo*. Moreover, equimolar doses of TP508 and two of the TP508 derivatives injected intraperitoneally into male CD-1 mice 24h after receiving 8Gy ionizing radiation showed enhanced closure of full-thickness dorsal excisions, with the PEGylated TP508 derivatives restoring the wound healing rate to that of unirradiated mice. These results have identified two TP508 derivatives that may be promising second-generation drugs for radiomitigation and tissue repair applications where the peptide must be administered systemically.

TABLE OF CONTENTS

List of Tables	xii
List of Figures.....	xiii
List of Abbreviations	xviii
Section 1: Introduction.....	1
Chapter 1: TP508 as a therapeutic drug product	1
A. The origin of TP508.....	1
B. Physiological Tissue Repair Activities of TP508	4
C. Preclinical Studies Demonstrating TP508 Potential Efficacy.....	5
D. Cardiovascular Effects of TP508.....	8
E. Clinical Trials with TP508	12
F. Physico-Chemical Properties of TP508.....	15
Chapter 2: Modifying polypeptide drug products for improved efficacy through PEGylation	21
A. PEGylation as a Means to Increase Biological Half-Life	21
B. Polypeptide Modification with Polyethylene Glycol for Improved Therapeutic Efficacy	23

C. Hypothesis and Aims	28
Section 2: Results	29
Chapter 3: Characterization of PEGylated TP508 Derivatives	29
A. Identity And Purity of PEGylated TP508 Derivatives.....	29
B. Plasma Half-Life of TP508 and TP508 Derivatives	33
Chapter 4: Biological activity of TP508 Derivatives.....	40
A. Initial Work to Establish a Simple <i>In-Vitro</i> Assay for TP508 Activity Using WI-38 Fibroblasts.....	40
B. Use of a Mouse Aortic Ring Assay for Angiogenic Activity of TP508 Administered <i>In Vivo</i>	48
C. Bone Marrow Cell Proliferation in Response to TP508	57
D. Effect of TP508 and PEGylated TP508 Derivatives on Healing of Wounds in Irradiated Mice.....	61
E. Use of <i>In Vitro</i> Assays to Better Understand How Steric Hindrance of TP508 Derivatives May Effect Their Biological Activity or Lack Thereof....	69
Section 3: Discussion.....	104
Chapter 5: Discussion and conclusions	104
A. Goal of Project.....	104

B. Characterization of TP508 Derivatives	104
C. Biological Activity of the TP508 Derivatives <i>In Vivo</i>	106
D. Relative Specific Activity of the PEGylated TP508 Derivatives <i>In Vitro</i>	109
E. Future Directions	115
F. Conclusions	122
Section 4: Materials and Methods	124
A. TP508 derivative peptide synthesis	124
B. Plasma half-life	125
C. In-gel fluorescence assay	126
D. WI-38 cell culture	126
E. RNA isolation from WI-38 cells	127
F. MTT assay	127
G. Aortic ring assay using <i>in vivo</i> pretreatment	128
H. Immunofluorescent imaging of aortic rings	128
I. Femur section immunohistochemistry	129
J. Wound closure rate in a murine Radiation Combined with Injury (RCI) model	129
K. Aortic explants with <i>in vitro</i> TP508 treatment	130
L. Endothelial tube formation	130
M. γ H2AX assay	131

Appendix A - Original macro by RJ Blatt for automated analysis of endothelial sprouting in the in vitro mouse aortic ring assay using ImagePro 7.0	133
Appendix B - Optimized macro used for analysis of TP508 and TP508 derivative biological activity in ImagePro Plus 7.0.....	133
Bibliography	139
Vita	148

LIST OF TABLES

Table 1.1 – Color coding of TP508 residues and relative amino acid positions in human prothrombin and thrombin	18
Table 3.1 – Plasma half-life and attendant statistics for TP508 and PEGylated TP508 derivatives	36
Table 4.1 – Gene candidates for RT-qPCR method development for a quantitative dose dependent assay for TP508 biological activity	41

LIST OF FIGURES

Figure 1.1 - Two-receptor model of thrombin activity	3
Figure 1.2 - Animal models of surgically induced ischemia	7
Figure 1.3 – Physico-chemical summary of TP508 properties.....	15
Figure 1.4 – Conformation of TP508 within human prothrombin, and ensemble of predicted TP508 conformations in aqueous solution.....	17
Figure 2.1 – Chemical structure of polyethylene glycol.....	22
Figure 2.2 – Reaction scheme for covalent attachment of PEG-NHS to primary amine on protein	24
Figure 2.3 – Reaction scheme for covalent bond formation between PEG-maleimide and thiol sidechain of cysteine residue in protein.....	25
Figure 2.4 – Illustration of binding avidity of a multivalent PEGylated polypeptide	26
Figure 2.5 – Receptor occupancy of multivalent PEGylated polypeptides and free monomeric peptide at the same concentration.....	27
Figure 3.1 – SDS-PAGE of TP508 derivatives	31
Figure 3.2 – Western Blotting of TP508 derivatives using anti-TP508B Rb411 polyclonal antibody.....	32

Figure 3.3 – Decay curves for TAMRA fluorescently-labeled TP508 & TP508 derivatives	35
Figure 3.4 – In-gel fluorescence of TAMRA-TP508 biological half-life samples.	37
Figure 3.5 – Total TAMRA-TP508 concentration determined from the in-gel fluorescence assay as compared to the plate-based fluorescence assay	38
Figure 4.1 – PhosphoImager workflow for analysis of transcriptional response of WI-38 fibroblasts to TP508.....	39
Figure 4.2 – Comparison of WI-38 fibroblast transcriptional response for selected genes in response to TP508 stimulation by qPCR and PhosphoImager analysis.....	44
Figure 4.3 – MTT cell viability results for WI-38 cell proliferation after 24h treatment with TP508 and thrombin	45
Figure 4.4 – Fluorescent competition assay workflow	46
Figure 4.5 – Fluorescent competition assay of TAMRA-TP508.....	47
Figure 4.6 – Workflow for aortic ring assay with <i>in vivo</i> pre-treatment with TP508	51
Figure 4.7 – Phase contrast microscopy of aortic rings with <i>in vivo</i> pretreatment at Day 5.....	52
Figure 4.8 – Percentage of aortic rings displaying endothelial sprouting at Days 4-6 after <i>in vivo</i> pretreatment	53

Figure 4.9 – Number of endothelial sprouts at Days 4-6 after <i>in vivo</i> pretreatment..	55
Figure 4.10 – Phase contrast and immunofluorescent images of aortic rings with <i>in vivo</i> TP508 treatment	56
Figure 4.11 – H&E staining and PCNA immunofluorescent staining of longitudinal bone marrow sections from naïve CD-1 mice 24h after TP508 pretreatment	58
Figure 4.12 – Quantitation of PCNA+ cells in bone marrow sections from CD-1 mice 24h after TP508 pretreatment	59
Figure 4.13 – Workflow for assessing wound closure rates in murine RCI model	62
Figure 4.14 – WoundZoom images of from Day 0 – Day 15 in RCI model	64
Figure 4.15 – Mean wound areas in RCI model at various days post-wounding ...	65
Figure 4.16 – Mean rate of wound closure per day in RCI model.....	66
Figure 4.17 – Comparative aortic sprouting with <i>in vivo</i> and <i>in vitro</i> TP508 treatment	72
Figure 4.18 – WimSprout analysis of endothelial sprouting	74
Figure 4.19 – Endothelial sprouting analysis using angiogenesis macro in ImagePro Plus 7.0.....	76
Figure 4.20 – Effect of aortic ring position within thoracic aorta on endothelial sprouting.....	78
Figure 4.21 – Plating order effect on endothelial sprouting in the <i>in vitro</i> aortic ring assay	79

Figure 4.22 – Concentration dependent effect of TP508 dosage <i>in vitro</i> on endothelial sprouting in aortic ring assay	80
Figure 4.23 – Endothelial sprouting activity profile of TP508 and TP508 derivatives using <i>in vitro</i> dosing in the mouse aortic ring assay	84
Figure 4.24 – Endothelial tube formation in HDMEC alone.....	86
Figure 4.25 – Endothelial tube formation at 16h in HDMEC alone and in co-culture with pericytes at ratios of 1:100, 1:10 and 1:1 pericyte:HDMEC	88
Figure 4.26 – Quantitation of fold increase in total tube length in 1:100 pericyte:HDMEC co-culture	90
Figure 4.27 – TP508 treatment maintains the capacity of 1:100 pericyte:HDMEC co-cultures to form endothelial tube networks following 3 Gy ionizing radiation	92
Figure 4.28 – CellProfiler overlay of nuclear outlines (blue) on images of γ H2AX foci (green) in HDMEC after 3 Gy ionizing radiation.....	95
Figure 4.29 – Quantitation of γ H2AX foci per nucleus in HDMEC after 3 Gy ionizing radiation	96
Figure 4.30 – CellProfiler overlay of nuclear outlines (blue) on images of γ H2AX foci (green) in HDMEC after 6 Gy ionizing radiation.....	98
Figure 4.31 – Quantitation of γ H2AX foci per nucleus in HDMEC after 6 Gy ionizing radiation	100

Figure 4.32 – Quantitation of the number of γ H2AX foci per nucleus in HDMEC
pretreated with TP508 derivatives, at 5h post-6 Gy ionizing radiation 102

Figure 5.1 – The SELEX aptamer-generation approach..... 117

Figure 5.2 - TRICEPS™ reagent-based ligand-receptor capture 119

LIST OF ABBREVIATIONS

ACN	Acetonitrile
CI	Confidence interval
DMEM/F-12	Dulbecco's Modified Eagle Medium/Nutrient Mixture F-12
DPBS	Dulbecco's phosphate buffered saline
DSB	Double-strand breaks
DTNB	3,3'-dithiobis(6-nitro)-benzoic acid (Ellman's Reagent)
EBM	Endothelial basal medium
ECM	Extracellular matrix
EDTA	Ethylenediaminetetraacetic acid
EGM2-MV	Endothelial growth medium for microvascular cells
ELISA	Enzyme-linked immunosorbent assay
eNOS	Endothelial nitric oxide synthase
FBS	Fetal bovine serum
GRAS	Generally recognized as safe (FDA designation)
H-ARS	Hematopoietic-acute radiation syndrome
HDMEC	Primary adult human dermal microvascular endothelial cells
hPC-PL	Primary human pericytes derived from placenta
HPLC	High performance liquid chromatography
HUVEC	Human umbilical vein endothelial cells
i.m.	Intramuscular (injection route)
i.p.	Intraperitoneal (injection route)

ITT	Intent to treat population (in clinical studies)
i.v.	Intravenous (injection route)
kDa	kiloDaltons
MMP	Matrix metalloproteinase
MRN	(MRE11-RAD50-NBS1)
MTT	3-(4,5-Dimethylthiazol-2-yl)-2,5-diphenyltetrazolium bromide
NPAP	Non-proteolytically activated receptor
NHS	N hydroxysuccinimide
NZW	New Zealand White (rabbit strain)
p-ATM	Phosphorylated ataxia telangiectasia mutated
PBMC	Peripheral blood mononuclear cells
PEG	Polyethylene glycol
PLGA	Poly(lactic co-glycolic acid)
PP	Per protocol population (in clinical studies)
p-Rad50	Phosphorylated RAD50
pQCT	Peripheral quantitative computed tomography
RCI	Radiation combined with injury
s.c.	Subcutaneous (injection route)
SD	Standard deviation
SDS-PAGE	Sodium dodecyl sulfate - polyacrylamide gel electrophoresis
SEM	Standard error of the mean
TAMRA	Tetramethylrhodamine
TGF- β	Transforming growth factor beta

TGS	Tris-Glycine-Sodium dodecyl sulfate buffer
VEGF	Vascular endothelial growth factor

SECTION 1: INTRODUCTION

Chapter 1: TP508 as a therapeutic drug product

A. THE ORIGIN OF TP508

TP508 is a synthetic peptide with numerous potential clinical applications in the area of tissue repair. It is comprised of a 23 amino acid polypeptide sequence identical to a segment of prothrombin, synthesized with an –NH₂ endcap at the C-terminus (AGYKPDEGKRGDACEGSDGGPFV-NH₂). This sequence was originally discovered in the Carney laboratory (1) during a screening project to identify the receptor binding region of thrombin by synthesizing and determining which sequences specifically competed for high-affinity thrombin binding sites on fibroblasts (1). TP508 does not possess the serine protease activity of native thrombin, but has been found to stimulate a number of mid-stage wound healing events. Under normal physiological conditions, much of the TP508 sequence lies buried within the three-dimensional structures of thrombin and prothrombin. However, under high salt conditions, or when bound to a surface, thrombin undergoes a conformational change that exposes this region for binding to cell surface molecules (2).

Thrombin is most generally known for its role in blood coagulation. However, it also plays a necessary role in the inflammatory phase of wound healing (3-7). Thrombin's serine protease activity, in addition to cleavage of fibrinogen and platelet activation during hemostasis, has been demonstrated to initiate signaling in various cell types through cleavage of protease-activated receptors (PARs) (7, 8). However, earlier studies with

thrombin that was proteolytically inactivated by diisopropyl fluorophosphate (DIP-thrombin) demonstrated that both proteolytic activity and receptor binding are necessary for thrombin stimulation of cell proliferation (9). This determination came from the observation that DNA synthesis and cell proliferation initiated by α -thrombin required two activation signals, which could be mimicked using γ -thrombin to generate the enzymatic activity and diisopropyl fluorophosphate-inactivated α -thrombin (DIP-Thrombin) for binding (10). Because TP508 was shown to compete for high-affinity thrombin binding to fibroblasts, additional studies showed that TP508 stimulated non-proteolytic signals, similar to DIP-inactivated thrombin, but that stimulation of cell proliferation still required additional activation by proteolytically active α -thrombin.

Differential gene expression studies showed that the activity of TP508 generated non-proteolytic signals that were distinct from thrombin activation of the PAR1, 3 & 4 receptors and that TP508 induces transcription of annexin V while PAR1-activating peptide SFLLRNP does not (11). It has also been shown that while thrombin can upregulate the cytokine IL-1 β , peripheral blood mononuclear cells (PBMCs) with PAR1 knocked down also exhibit IL-1 β upregulation in the presence of TP508 while those stimulated with SFLLRNP do not, illustrating TP508 acts through an alternate receptor (12). Additional evidence for thrombin activity independent of its ability to cleave PAR receptors was illustrated using neutrophils, where inactivation of thrombin abolished chemotaxis, but not chemokinesis (13).

These studies helped to validate a two-receptor model of thrombin activation of cells (Figure 1.1, adapted from Olszewska et al. 2009) (14). In this model, in addition to

the proteolytic activity of α -thrombin through the PAR receptors, binding of α -thrombin, proteolytically inactive thrombin, or thrombin fragments containing the appropriate binding region (including TP508), bind to a second, non-proteolytically activated receptor (NPAR) to initiate the previously mentioned downstream effects (15). Since TP508 possesses an RGD integrin recognition motif within its primary sequence, it has been hypothesized that TP508 may act through integrin binding (16). There is some supporting primary evidence showing that TP508, when bound to a surface via thiol linkage to its Cys14 residue, binds to $\alpha_v\beta_3$ integrin (17). However, the activity of soluble TP508 *in vitro* and *in vivo*, its competition for high-affinity thrombin binding sites, and its activation of endothelial cell signaling are not consistent with a model involving integrin binding, crosslinking, or activation. It should be noted, however, that NPAR has yet to be isolated and fully characterized. Therefore, there remains a great deal of work to be done to fully understand the signals that are initiated in cells by TP508.

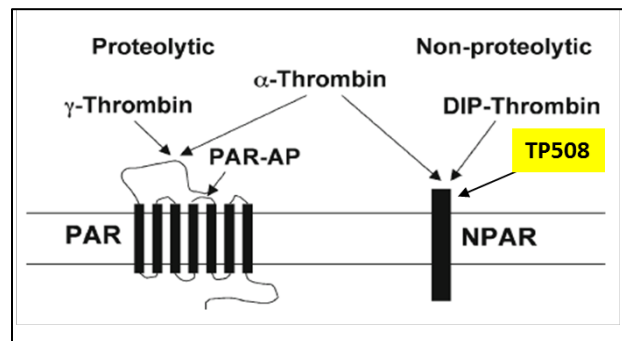


Figure 1.1 – Two-receptor model of thrombin activity. Proteolytic α -thrombin and γ -thrombin cleave the PAR receptors for activation of inflammatory effects. TP508, chemically inactivated thrombin (DIP-Thrombin) and α -thrombin also bind a non-proteolytically activated receptor to cause other downstream effects.

B. PHYSIOLOGICAL TISSUE REPAIR ACTIVITIES OF TP508

A number of studies have shown that TP508 stimulates wound healing effects including acceleration of angiogenesis (18, 19), enhancement of osteogenesis (20), induction of vascular endothelial nitric oxide signaling (21, 22), and enhanced proliferation of stem cells isolated from adipose tissue (23). Pre-clinical studies in various animal models demonstrate that TP508 accelerates closure of full-thickness dermal wounds (18, 24-26), accelerates bone fracture repair (27-30), restores normal wound healing rates in diabetic models of impaired wound healing (Burckart and Carney, unpublished), and attenuates damage from myocardial ischemic reperfusion injury and chronic ischemia (31-34).

It has been determined that the sequence of TP508 remains intact within an 11 kDa C-terminal major fragment of thrombin that is released when fibrin clots are broken down by neutrophil elastase (35). This suggests that TP508 represents the minimal peptide sequence necessary for mimicking a natural signaling molecule which enhances wound repair at the proliferation stage, by extending the duration of cell recruitment in large wounds via continuous stimulation as the clot breaks down, and stimulating angiogenesis in concert with well-studied growth factors (e.g. VEGF, TGF- β) (7). Furthermore, the timing of this signal is tightly regulated, only being released late in the inflammation phase when neutrophils have migrated into a fibrin clot and initiated degradation of the proteins trapped therein. This is consistent with the temporal regulation of other aspects of wound healing, such as the recruitment of inflammatory cells and subsequent resolution of inflammation at the early proliferation stage, or the tight control of matrix metalloproteinase activity during the remodeling stage of wound healing.

C. PRECLINICAL STUDIES DEMONSTRATING TP508 POTENTIAL EFFICACY

Due to its fundamental involvement in tissue regeneration, TP508 has the potential to be used for a wide variety of therapeutic indications. As a result, it has undergone a number of pre-clinical and clinical studies at the University of Texas Medical Branch (UTMB), at collaborator universities in the US and Europe, and through corporations who have licensed TP508 for therapeutic investigations including Orthologic Corporation, Capstone Technologies, and Chrysalis BioTherapeutics. Selected key studies from each therapeutic area are summarized herein. Particular focus has been given to studies that have not been reviewed elsewhere (27, 36-38).

Early preclinical studies established that TP508 accelerated healing when applied topically to full thickness excisional wounds in healthy male Sprague-Dawley rats (39). These rats received two dorsal full-thickness circular wounds 2 cm in diameter, with one wound receiving a single application of 0.1 µg TP508 administered topically in sterile saline, with the other wound receiving saline alone. A retrospective analysis of 18 separate experiments using this model was used to demonstrate consistent accelerated wound healing in response to TP508 (39). This analysis showed that by Day 7 post wounding, TP508 displayed an average of 59% closure, as compared to 42% closure in the saline control, a highly significant difference ($p < 0.001$). This is equivalent to a 40% increase in early rate of closure in response to TP508 as compared to saline control. By Day 10 post-wounding, TP508 treated wounds reached 86% closure, as compared to 77% closure with the saline control ($p < 0.001$). Thus, TP508 accelerates initiation of wound closure and also reduces the time to closure of these wounds. During this study, the most effective dosage of TP508 was established to occur in the range of 0.1 – 1.0 µg for the closure of full-

thickness dermal wounds of this size. At the higher concentration of 3.0 μg TP508/wound, the wound closure rate was not significantly different from that of the saline control, suggesting that 1.0 $\mu\text{g}/\text{mL}$ was the optimal effective dose of TP508.

Once it was established that TP508 accelerated wound healing in healthy animal models, preclinical studies focused on determining whether TP508 could accelerate or restore normal rates of healing in impaired wound healing models. These studies included animals with streptozotocin-induced diabetes representing Type 1 Diabetes, genetically obese *Lpr*^{-/-} mice as a standard Type 2 diabetic mouse model, and several models with induced dermal ischemia. In each of these model systems, TP508 showed significant acceleration of healing (Carney, unpublished). An example of the ischemic dermal studies is reviewed here.

Male Sprague-Dawley rats were examined for accelerated dermal wound healing in several models of ischemia (40). In the bipedicle flap model (Figure 1.2A), four dorsal 1.5 cm full thickness excisions (black circles) were rendered ischemic by creating a skin flap using 5 cm incisions (black lines) located to either side of the full thickness incisions, lifting the skin and dissecting any blood vessels connecting to the resulting flap. In this model, by Days 5 and 7 post-wounding, 0.1 μg TP508-treated wounds showed significant closure, while the saline-treated ischemic wounds had yet to begin closure. In the free graft model (Figure 1.2B), two 2 cm full thickness dorsal excisions were created, followed by complete removal of a rectangular section of skin 5 cm long x 6 cm wide, which was then reattached by interrupted sutures (black crosses along perimeter of rectangle). In this model, which represents the most severe form of ischemia tested, the excisional wounds

treated with 0.1 μg TP508 showed significantly more closure from Day 10 through Day 21 post-wounding. By Day 21, mean wound closure for the TP508-treated wounds was over 50%, as compared to $\sim 30\%$ for the saline control. In the cranial flap model (Figure 1.2C), wounding was performed in a similar manner to the free graft model, but no incision was performed at the cranial side of the wound. In this model, healing in the TP508-treated wounds was restored to non-ischemic levels, with mean wound sizes 63% of that of the saline control at Day 7, and 43% of the saline control at Day 10. A major finding of this study is that TP508 reduces the pathological conditions induced by ischemia, restoring the tissue to near normal healing rates. Tissue histology taken from the margins of the ischemic tissue suggest that TP508 does this through several mechanisms, including enhancing the early inflammation response with greater neutrophil recruitment at Day 1 post-wounding, accelerating early revascularization, and reducing chronic inflammation present in ischemic wounds at Day 14 post-wounding.

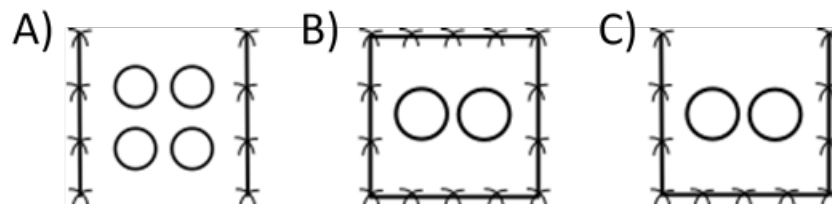


Figure 1.2 – Animal models of surgically induced ischemia. A) Bipedicle flap model; B) Free graft model; C) Cranial flap model.

TP508 has more recently been evaluated in acceleration of bone repair in a distraction osteogenesis model. In this model, male New Zealand white (NZW) rabbits receive a surgically induced tibial fracture, followed by external fixation and then gradual

traction to lengthen the distance between the fractured edges of the tibia to create an approximate 1 cm gap. Radiographic analysis of the repair process was used to determine bone regeneration after two weeks in the distraction sites injected with TP508 as compared to saline controls (41). In the group receiving a 300 µg injection of TP508 into the distraction gap, bone growth had united the fracture in 4 of the 8 of the animals, as compared to 2 out of 7 in the saline control group. Radiographic scoring of the percentage of bone filling the gap was significantly higher in the TP508-treated group. The tibial segments were also isolated at the end of the two-week repair period and assessed for bone density using peripheral quantitative computed tomography (pQCT). This analysis showed that the bone mineral densities of the TP508-treated group were higher than those of the saline group ($p=0.045$). This demonstrated that TP508 had potential therapeutic applications in enhancing bone repair. Additional studies have verified TP508 enhances bone repair in high energy fractures (29), and stimulates healing of critical size ulnar defects (42). Several studies have also involved the use of TP508 formulated into various biodegradable scaffolds to either reduce the necessary dosage of TP508 or enhance its osteogenic effects (43, 44).

D. CARDIOVASCULAR EFFECTS OF TP508

The numerous demonstrations that TP508 accelerated tissue revascularization suggested that it could also be beneficial in treating cardiovascular indications. A major cardiovascular problem occurs when vascular supply to the left ventricle is gradually disrupted causing chronic myocardial ischemia. It was thought that injection of growth factors into ischemic regions of the heart could induce therapeutic angiogenesis to restore

cardiac function. Because of the regenerative properties of TP508, a study was initiated at Texas A&M using a porcine model of chronic myocardial ischemia to determine whether TP508 could improve blood perfusion, reduce endothelial dysfunction in the affected tissue, and improve left ventricular cardiac function in the affected tissue (22). In this model, an ameroid constrictor placed on the left circumflex coronary artery gradually restricts blood flow, resulting in left ventricular ischemia by Day 28. In this model, a pluronic gel with empty PLGA microspheres, or microspheres containing 150 μ g TP508, was injected into 15 different sites within the ischemic tissue on Day 28. Day 60 angiograms revealed a qualitative increase in blood vessel formation and filling in the affected area in the TP508 analysis. Analysis of blood flow in tissue isolated at Day 60 showed up to an 8 fold increase in myocardial perfusion, with a mean value of 0.1629 mL/kg/min for the TP508 microsphere injected treatment group vs. 0.02 mL/kg/min for placebo empty PLGA microspheres ($p=0.04$). Moreover, TP508 increased cardiac output and restored endothelial function (nitric oxide production) in isolated microvessels (17). This study suggested that TP508 could have potential benefit to a great many individuals suffering from chronic myocardial ischemia, but a number of questions regarding delivery of TP508 in PLGA microspheres made moving forward with this indication difficult.

Building on results with TP508 reversing effects of chronic myocardial ischemia, it was decided to determine whether TP508 systemic injection could reverse effects of acute myocardial infarct reperfusion injury (45). This injury occurs when an area of the heart becomes ischemic due to an acute blockage of blood causing an ischemic infarct, followed by additional vascular and cardiac cell damage due to the sudden influx of blood

once the infarct has been removed. In this study, male Yucatan minipigs were used as an animal model of myocardial infarct reperfusion injury by occluding their mid-left anterior descending coronary artery for 60 minutes, followed by 2 hours of reperfusion. Sterile saline or 0.5 mg/kg TP508 were administered i.v. as a bolus into the cardiac artery 50 min into reperfusion. Due to the circulation and short biological half-life of TP508, an additional infusion of 1.25 mg/kg/h of TP508 was necessary to keep the concentration of TP508 relatively constant during the course of the experiment. Note that for this systemic application of TP508, substantially more TP508 was necessary (~ 2 mg/kg total) than normally used in topical applications (0.1 – 1.0 µg for full thickness wounds ~1 – 30 cm² in area) for therapeutic effect. Treatment with TP508 reduced the area of infarction from a mean of 40% of the left ventricular area to ~20% (p<0.05). Additional characterization of the tissue found greater phosphorylated endothelial nitric oxide synthase (eNOS) and a higher expression of anti-apoptotic Bcl-2 in the TP508 treated tissue as compared to the saline control. These findings indicate that TP508 improves microvascular function and promotes cells survival in ischemic tissue.

While these results are promising, the population of young, healthy swine may not mimic the clinical population at risk for myocardial infarct, which is generally elderly and hypercholesterolemic or diabetic. A second study used hypercholesterolemic Yucatan swine, who received a diet high in fat and cholesterol (46). In this study, TP508 administration reduced infarct size by over 50%. In addition, it was shown to improve microvascular function. Interestingly, in the hypercholesterolemic swine, TP508 was most effective at double the dosage used in the normal swine (1 mg/kg bolus + 2.5 mg/kg/h

infusion). Other findings in this study were that TP508 treatment caused an increase in HSP90, and decreases in Caspase-3 and PARP in the ischemic tissue, thus confirming that TP508 promotes pro-survival and anti-apoptotic pathways *in vivo*. Similar results were seen in a model of diabetes mellitus type I induced in male Yucatan swine (47).

An additional study investigated the effectiveness of TP508 dimer in the hypercholesterolemic swine model (48). One of the issues with using TP508 as a therapeutic peptide is that the monomer rapidly homodimerizes through formation of a disulfide bridge at the Cys14 residue between two TP508 monomers when the lyophilized powder is reconstituted in aqueous buffers at room temperature and near-neutral pH. This is particularly pertinent when TP508 is administered as an infusion for longer than an hour, as the purity of the TP508 monomer drops below USP specifications for purity as it dimerizes. Several methods are available to limit this dimerization, such as modification of the Cys14 residue to a serine (abbreviated as TP508S), buffer formulation including methionine and EDTA to inhibit disulfide bridge formation. However, as *in vitro* studies indicate that the dimer form of TP508 is also biologically active, allowing the monomer to completely dimerize prior to lyophilization is an elegant method of ensuring that the drug substance maintains a single molecular identity hours after reconstitution. Results from this study demonstrated that the dimer had similar effects on reduction in infarct size and induction of anti-apoptotic and cytoprotective pathways as the TP508 monomer in the affected tissue.

E. CLINICAL TRIALS WITH TP508

Based on preclinical results, TP508 has been evaluated in clinical trials for both accelerated closure of diabetic lower extremity ulcers and distal radius fracture repair (37). For diabetic ulcer treatment, a 60-patient, randomized, placebo-controlled double-blind phase I/II study was performed to determine if topical applications of TP508 enhanced either rate of wound closure or chance to complete closure within a 20 week time period. This study was comprised of 3 arms, with patients receiving either 1 µg of TP508, 10 µg of TP508, or saline alone in a 100 µL volume, applied immediately after the twice-weekly debridement and wound irrigation process, and prior to bandaging. Inclusion criteria included lower extremity ulcers ≥ 0.9 cm² which had been present for at least 8 weeks, and had been classified as Wagner Grade I, II, or early Grade III. This includes ischemic ulcers that have exposed bone or tendon, but in the physician's opinion have not yet eroded bone or tendon.

Due to the severe nature of the diabetic ulcers and common co-morbidities occurring in diabetic patients, adverse events were reported in all three treatment groups. Incidence of adverse events was similar for all three groups with 76% for saline treatment, 75% for 1 µg TP508 treatment, and 78% for 10 µg TP508 treatment. Analysis of the ulcerated region showed similar incidence of edema (2-3 patients per group), erythema (3-4 patients per group) and worsened local pain after treatment (2 patients per group), indicating no local reactions to the TP508 treatment. No adverse reactions to TP508 were observed in hematology or blood chemistry analyses. In all safety analyses, no statistical difference was seen between treatment groups for adverse events, serious adverse events,

or discontinuations. In summary, topical application of TP508 displayed excellent safety in humans during this trial.

Efficacy analysis for accelerated closure of diabetic ulcers by TP508 included percentage of population achieving complete wound closure by 20 weeks as its primary variable and time to closure events as a secondary efficacy endpoint. The primary efficacy variable was further broken down into two populations. In the Intent-to-Treat (ITT) population, any study members withdrawn from the study for any reason were treated as failed closures. This results in ITT group sizes of n=21 for saline control, n=20 for 1 µg TP508 treatment, and n=18 for 10 µg TP508 treatment. The “Per Protocol” (PP) population excluded both discontinuations and study members in the ITT population whose ulcers did not meet study inclusion criteria. This included patients whose ulcers had been present for less than 8 weeks, or had ulcer areas less than 0.9 cm². This reduces the PP population sizes to n=15 for saline control, n=11 for 1 µg TP508 treatment, and n=14 for 10 µg TP508 treatment. Both groups showed a dose dependent response to TP508 treatment. In the ITT group, percentage of wounds closed by 20 weeks were 48% for saline control, 52% for 1 µg TP508 treatment, and 61% for 10 µg TP508 treatment. This trend was more prominent in the PP population, with percentage of wounds closed by 20 weeks were 33% for saline control, 45% for 1 µg TP508 treatment, and 57% for 10 µg TP508 treatment.

For the second efficacy endpoint, time to closure, only the PP population was analyzed. 100% closure was not reached for the saline control group, indicating a mean time to closure of greater than 140 days (20 weeks) set as the clinical trial duration. This was reduced to 112 days for the 1 µg TP508 group, and 87 days for the 10 µg TP508 group.

Because DFU closure rates slow as they near completion, time to 80% closure was also analyzed. These results were 57 days for the saline control group, reducing to 47 days for the 1 μ g TP508 group and 32 days for the 10 μ g TP508 group.

Due to the sample sizes involved and the inherent variability of diabetic ulcer rate of closure, results of this Phase I/II clinical trial were insufficiently powered to show statistically significant differences between the TP508 treatment groups and placebo for either the primary or secondary efficacy endpoints. However, a subset analyses of diabetic ulcers located on the foot (DFU) showed that both 1 μ g TP508 and 10 μ g TP508 significantly increased in complete wound closure ($p=0.045$ and $p=0.032$, respectively). TP508 also significantly reduced time to closure of DFU in both the 1 μ g ($p=0.040$) and 10 μ g ($p=0.033$) groups. Of particular interest in the subset analysis was for DFU located on the heel, a notoriously difficult area to heal completely due to hyperkeratinization at the wound edges, and because of pressure applied to the heel when patients are weight bearing or on their backs. Heel DFUs showed a 165% increase in wound healing rate when 10 μ g TP508 was applied, as compared to placebo ($p=0.02$). In addition, six of the seven heel DFUs treated with either 1 or 10 μ g TP508 attained complete closure in the 20 week surveillance period, compared to 0 of 5 heel DFUs attaining complete closure in the placebo group. These promising efficacy results, along with the strong safety data from this phase I/II clinical trial, shows that TP508 warrants further investigation as a therapeutic for the closure of diabetic foot ulcers.

F. PHYSICO-CHEMICAL PROPERTIES OF TP508

With 6 glycine residues, 5 acidic residues and 3 basic residues, along with negligible hydrophobic character, TP508 is extremely soluble in aqueous solutions. It is listed with solubility specifications of >50 mg/ml, however, we have determined that it is soluble in excess of 200 mg/mL in 0.9% sterile saline used for injection of the peptide (McVicar and Carney, unpublished). Its high glycine content contributes to a low molecular weight of only 2.3 kDa for this 23-amino acid peptide. It possesses an acidic isoelectric point of 4.2, making it negatively charged under normal physiological conditions. These properties are summarized in Figure 1.3.

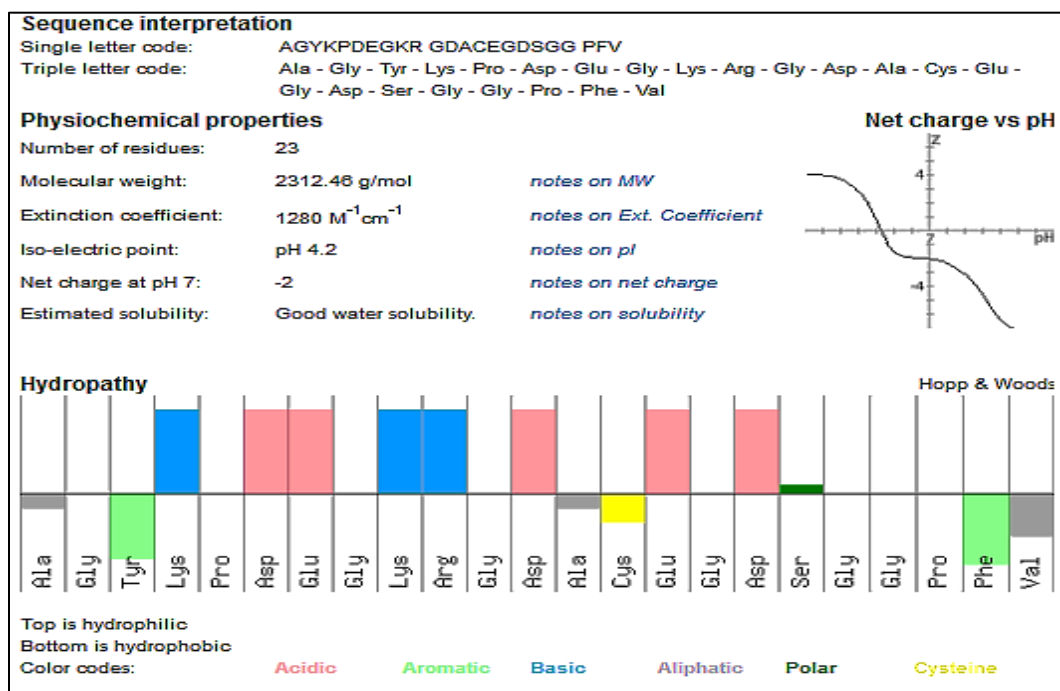


Figure 1.3 – Physico-chemical summary of TP508 properties.

As indicated previously, TP508 naturally forms a homodimer at neutral pH by forming a disulfide bridge between the Cys14 residues of two TP508 monomers. This dimerized version of TP508 retains the tissue repair activity of the TP508 monomer, as

evidenced by the cytoprotective and antiapoptotic activity in a model of myocardial ischemia reperfusion injury in hypercholesterolemic swine (48).

Figure 1.4 illustrates the lack of secondary structure of TP508, both in its conformation within prothrombin (Figure 1.4A, from PDB crystal structure 5EDK) (49) and in predicted conformations of TP508 alone in aqueous solution from most to least likely using PEP FOLD 2.0 peptide prediction software (50). Images are presented using a cartoon main chain with stick side chain data, spectrum coloration from N-terminus (blue) to C-terminus (red) using EduPyMol version 1.7.4.5 (64 bit). Table 1.1 summarizes the color coding of corresponding amino acid residues, along with their relative amino acid position in TP508, human prothrombin and thrombin. All predicted structures are primarily random coil, with only a partial α -helix consistently predicted in the Pro-Asp-Glu portion of the sequence. This lack of secondary structure has also been confirmed by circular dichroism analysis of the peptide (McVicar and Carney, unpublished).

This lack of secondary structure represents a major technical challenge in isolation and identification of a receptor for TP508. TP508 has minimal constraints on its conformation, making computational prediction of protein-protein interactions with known receptor structures not possible at the current state of the art. This is also a complicating factor in interpreting results of modified versions of the TP508 molecule for investigational purposes. For example, it has been reported that R-G-D amino acid motif within TP508 interacts with $\alpha_v\beta_3$ integrin to mediate HUVEC cell adhesion (51). However, this evidence uses surface plasmon resonance with TP508 covalently bound to the chip using thiol chemistry at its Cys14 residue, creating a constraint in the TP508 molecule immediately adjacent to the RGD motif. This may have artificially increased the binding affinity of

TP508 to the integrin, explaining why these results have not been observed when TP508 is unbound in solution.

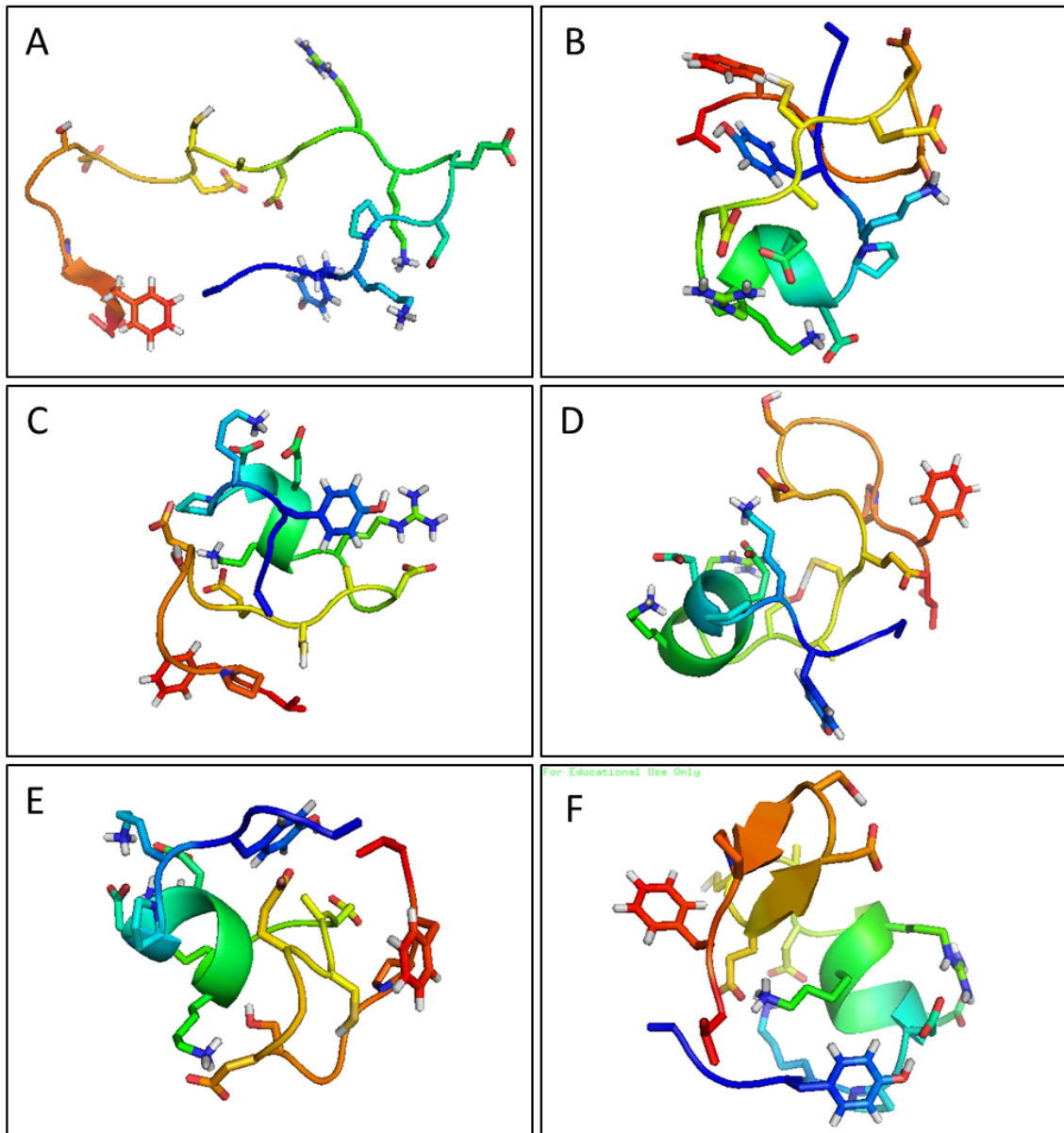


Figure 1.4 – Conformation of TP508 within human prothrombin, and ensemble of predicted TP508 conformations in aqueous solution. Cartoons are colored from red (N-terminus) to blue (C-terminus).

Residue	A	G	Y	K	P	D	E	G	K	R	G	D	A	C	E	G	S	D	G	G	P	F	V
TP508	1	2	3	4	5	6	7	8	9	10	11	12	13	14	15	16	17	18	19	20	21	22	23
Prothrombin	508	509	510	511	512	513	514	515	516	517	518	519	520	521	522	523	524	525	526	527	528	529	530
Thrombin	12	13	14	15	16	17	18	19	20	21	22	23	24	25	26	27	28	29	30	31	32	33	34

Table 1.1 – Color coding of TP508 residues and relative amino acid positions in human prothrombin and thrombin. Amino acid residues are colored according to their relative position in Figure 1.4. Below, each amino acid is listed at its relative position in TP508, and the corresponding position in full length prothrombin and in the cleaved, proteolytically active thrombin molecule.

TP508 presents several other bioanalytical challenges that make its analysis difficult. It possesses a single tyrosine residue for measurement of extinction coefficient, which can lead to complications in spectrophotometric analyses under conditions where the tyrosine may be modified. Its molecular weight of 2.3 kDa places it above the size threshold for a number of techniques used for examining small molecules (usually less than 500 Da), but below that of many protein manipulation methodologies. For example, most concentration techniques have molecular weight cutoffs of at least 10 kDa, making sample concentration difficult. For gel electrophoresis techniques, highly crosslinked acrylamide gels ($\geq 16\%$) are necessary to distinguish TP508 from the dye front. Western blotting transfers require reduced transfer time to prevent TP508 migrating through the filter. This complicates or prevents direct comparison to higher molecular weight proteins on the same blot, which would have only partial transfer.

The TP508 sequence represents a highly conserved region in thrombin that is present in vertebrates and invertebrate species making it essentially non-immunogenic. This is an advantage of using the TP508 peptide as a drug, but creates challenges for quality high-affinity antibody creation. Antibodies raised to TP508 may have reduced specificity due to its short sequence and lack of secondary structure. In addition, they may have limited reactivity towards TP508 depending on whether it is in solution, adsorbed or covalently linked to surfaces, or interacting with cell receptors or other molecules in a biological matrix.

Common methods of tagging proteins for analysis in biological systems also have limited application with regard to TP508. Large protein tags such as the ubiquitous GFP

would substantially change diffusion and binding characteristics of TP508. Even smaller tags such as the highly charged FLAG tag (DYKDDDDK) can cause substantial shifts in the mass and pI of the peptide. As a result, the bulk of research on TP508 localization and binding to date has involved radioisotopic labeling. Additional assay development that employs fluorophores directly attached to TP508, such as TAMRA-TP508 (see Section 4A) and LC/MS techniques are currently being investigated.

Chapter 2: Modifying TP508 for improved efficacy through PEGylation

A. PEGYLATION AS A MEANS TO INCREASE BIOLOGICAL HALF-LIFE

Peptides represent an attractive class of therapeutic drugs due to their natural roles as growth factors, hormones, cytokines, and as effector molecules in roles such as host immunity. Their short amino acid sequences allow for production through both synthetic and recombinant expression routes with high fidelity and purity, making them amenable to the traditional screening tools used for drug discovery. They also cover the gap in size between traditional small molecule drugs, which are usually less than 500 Daltons in size, and therapeutic proteins of >15 kDa, while possessing elements of both classes in relation to mechanism of action. Peptides are less prone to bioaccumulation than small molecule drugs, while having generally greater bioavailability than large proteins.

One of the main disadvantages of peptides as drug products, however, is their rapid degradation and clearance by the body once administered. Oral administration requires that the therapeutic peptide be protected from acid hydrolysis by the stomach, further digestion within the GI tract, and that the peptide is able to cross from the GI tract into the bloodstream. Injection of peptides directly into the bloodstream avoids several of these issues, but peptides also face challenges of enzymatic degradation within the blood, as well as direct clearance by the kidneys. Polypeptides of less than 15 kDa are not subject to retention by the glomeruli, allowing them to pass intact into the urine. This results in a concentration-independent reduction in administered peptide over time known as biological half-life. Peptide biological half-lives range from minutes to a few hours, drastically limiting the amount of time an administered peptide falls inside the

concentration range required for therapeutic effect. This can result in limited efficacy of the peptide, as well as substantially increase dosage requirements for therapeutic effect.

Intense interest from both the pharmaceutical industry and medical researchers in increasing the half-life of peptides within the body has resulted in the development of a number of technologies for addressing this issue. These techniques vary from embedding the peptide in a biocompatible polymer for timed release, to cyclizing or otherwise modifying peptides to limit susceptibility to degradation, to bonding the peptide to molecules found natively within the host, such as albumin or antibody fragments, and to other non-native biocompatible molecules. The oldest and most mature of these technologies are based on increasing the peptide size beyond the glomerular filtration limit by covalent attachment to a biocompatible molecule such as polyethylene glycol (PEG, shown in Figure 2.1), a process known as PEGylation.

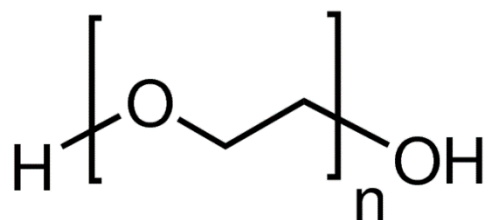


Figure 2.1 – Chemical structure of polyethylene glycol.

As a polymer, polyethylene glycol possesses a number of desirable properties for covalent attachment to peptides. It possesses high solubility and uptake into the bloodstream through the GI tract, but is not digested or degraded. This places it in the dietary category of soluble fiber, which is in fact one of its uses as a food additive. PEG demonstrates minimal toxicity and low immunogenicity, and has even been demonstrated

to reduce immunogenicity of attached proteins (52-54). Due to its wide use in everything from paint to cough syrup, it is commercially available in food grade purities in a variety of sizes. In addition, it bulks to a large hydrodynamic volume in solution per unit weight. This is particularly desirable both from the perspective of preventing clearance of a bound peptide through the kidneys, as well as in steric hindrance of enzymatic degradation of the peptide by limiting access due to its bulk. Finally, it has an FDA designation of GRAS (Generally recognized as safe) as an inactive ingredient in drug formulation, facilitating its approvability in conjugation with therapeutic polypeptides.

B. POLYPEPTIDE MODIFICATION WITH POLYETHYLENE GLYCOL FOR IMPROVED THERAPEUTIC EFFICACY

The simplest form of PEGylation is the addition of a single unbranched chain of polyethylene glycol to a specific site on the peptide. During the drug discovery and early development stages, where the effects of attaching PEG of different sizes to targeted locations on the polypeptide on parameters such as solubility and biological activity are evaluated, this is most easily performed using commercially available PEGs synthesized with various functional groups for targeted attachment at one end. The other end of the PEG molecule is synthesized with a monomethoxy group (often denoted by the abbreviation mPEG) to render it inert to polymerization and side reactions.

There are a wide variety of functionalized PEGs developed for targeting both N- and C-terminus of a polypeptide for attachment, as well as chemistries for covalent attachment of PEG to various sidechains. For targeted PEGylation at the N-terminus of a polypeptide, polyethylene glycol n-hydroxysuccinimide ester (PEG-NHS) may be used to

create a bond with the primary amine (Figure 2.2). PEG-NHS can also create covalent amide bonds with primary amine-containing sidechains such as arginine, histidine and lysine. This can be convenient if multiple PEG moieties joined to a single polypeptide is desired, but can also create unwanted polydispersity where a single molecular form is not easily purified. In some instances, however, buffer pH can be manipulated to cause the reaction to preferentially target the N-terminus (pH 5), or internal lysines (pH 8 – 9) by taking advantage of the differences in pKa of the lysine sidechain ϵ -amine vs. the terminal α -amine (55).

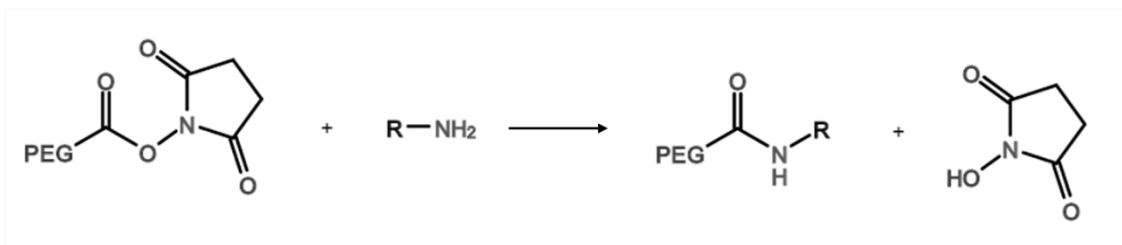


Figure 2.2 – Reaction scheme for covalent attachment of PEG-NHS to primary amine on protein.

Another functionalized PEG, which has excellent site specificity, is the thiol-reactive PEG-maleimide. PEG-maleimide is used to form a covalent thioether bond with the sulfhydryl sidechain of a free cysteine residue present or engineered into a peptide or protein (Figure 2.3).

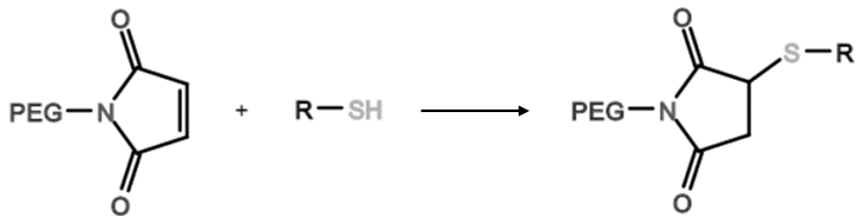


Figure 2.3 – Reaction scheme for covalent bond formation between PEG-maleimide and thiol sidechain of cysteine residue in protein.

There are several carboxyl-reactive functionalized PEGs such as mPEG-Amine and mPEG-hydrazide commercially available for covalent modification of polypeptides as well. Because TP508 has previously been demonstrated to lose biological activity when modified near its C-terminus, carboxyl-reactive functionalized PEGs were not examined in this project. Thus the reaction schemes for C-terminal PEGylation are not discussed here, though they have been extensively reviewed elsewhere (56, 57).

Bifunctional and multifunctional PEGs have also been developed for polypeptide PEGylation research. Homobifunctional PEGs, such as maleimide-PEG-maleimide, are intended to bind two copies of a polypeptide at the same region. This can be useful, for example, to create bivalent ligand for investigating receptor dimers (58). Heterobifunctional PEGs, such as NHS-PEG-hydrazide, are used when binding to different sites on the same polypeptides results in useful topologies. They can also be useful in the production of peptide drug conjugates (59).

Multifunctional PEGs present several advantages in modifying polypeptides for therapeutic use. For small (<5 kDa) polypeptides, a multifunctional PEG which can bind four or more polypeptide moieties to a single core results in a substantially larger molecule,

increasing its biological half-life by slowing direct clearance by the kidneys. A second advantage of combining multiple copies of the polypeptide of interest on a multi-arm PEG backbone is that it results in increased binding avidity. As illustrated in Figure 2.4, when one of the polypeptide moieties of a multivalent compound is receptor-bound (Fig. 2.4 (i)) then dissociates from the receptor (Fig. 2.4 (ii)), another polypeptide moiety on the multivalent molecule is nearby and can bind to the receptor (Fig. 2.4 (iii)). This, in effect, increases the apparent local concentration of the peptide around the receptor (Figure 2.5). As a result, even though the binding affinity of the polypeptide does not change, the percentage of time that the receptor is occupied may be increased when multiple ligand moieties are bound to a single flexible core (Figure 2.5A) as compared to the same concentration of free monomeric ligand (Figure 2.5B). This is the same phenomenon as seen in IgM, where the pentameric antibody binds tightly to multiple epitope regions on a viral or bacterial surface, resulting in strong binding despite the low affinity of any one subunit (60).

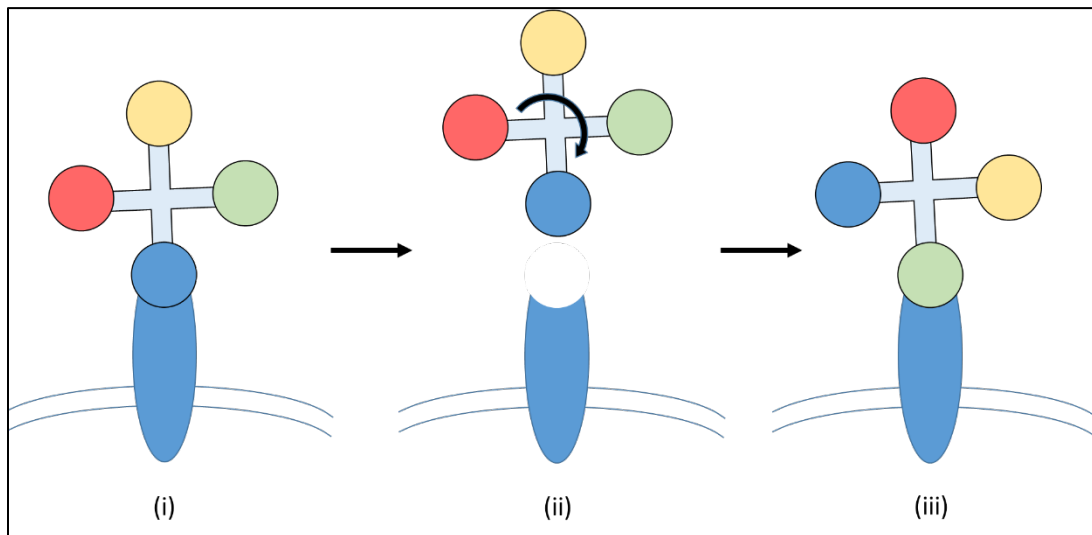


Figure 2.4 – Illustration of binding avidity of a multivalent PEGylated polypeptide.

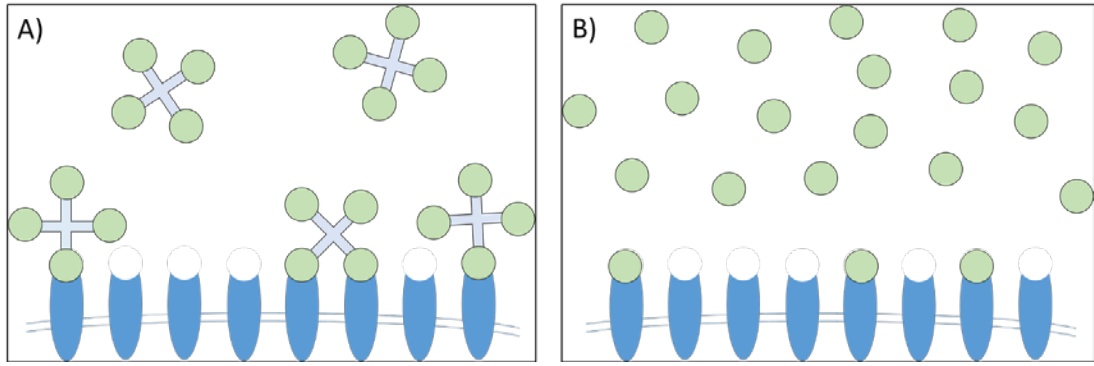


Figure 2.5 – Receptor occupancy of multivalent PEGylated polypeptides and free monomeric peptide at the same concentration.

C. HYPOTHESIS AND AIMS

My hypothesis is that the radioprotective efficacy of systemically-administered TP508 is diminished by its short biological half-life. Increasing the peptide's size through site-specific PEGylation will increase its efficacy. This hypothesis will be evaluated through 3 aims:

Aim 1: Verify that PEGylation of TP508 increases its biological half-life.

Aim 2: Confirm that bioactive TP508 derivatives have increased efficacy in radiomitigation and/or wound healing in an *in vivo* murine model.

Aim 3: Determine the relative specific activity of the PEGylated TP508 derivatives compared to the TP508 monomer *in vitro*.

SECTION 2: RESULTS

Chapter 3: Characterization of PEGylated TP508 Derivatives

A. IDENTITY AND PURITY OF PEGYLATED TP508 DERIVATIVES

A total of 10 TP508 derivatives were designed for these studies to cover a variety of PEG sizes and conjugation sites. These peptides were subsequently synthesized and purified by American Peptide Company (Vista, CA). These comprised TP508 PEGylated at the N-terminus with PEG5k- (PEG5k-TP508, Product #363808), PEG20k- (PEG20k-TP508, Product #363806), and PEG 30k- (PEG30k-TP508, Product #357438) using PEG-NHS attachment chemistry (Figure 5); TP508 PEGylated at its internal cysteine (PEG20k-Cys14-TP508, Product #363898) using PEG-maleimide attachment chemistry (see Figure 6); fluorescent variants of these 4 compounds; a tetravalent TP508 derivative (Product #363901) prepared by reacting a 4-arm PEG-maleimide of 2000 MW with TP508 moieties attached by their internal cysteine sidechains; and finally a truncated variant of TP508 which is missing the first 7 TP508 residues and has been demonstrated to show chemotactic activity for neutrophils, but not to enhance healing of incisional wounds (61).

Certificates of analysis for these peptides showed purities of >95.0% by reversed-phase high performance liquid chromatography (HPLC). However, separation by this technique is by a combination of peptide size and hydrophobicity, and was not optimized for PEG-peptide conjugates. Thus, a combination of sodium dodecyl sulfate – polyacrylamide gel electrophoresis (SDS-PAGE) and Western Blotting was used to verify purity and determine whether the TP508 moiety of the PEGylated TP508 derivatives was still available for binding to a polyclonal rabbit antibody raised to the last 14 residues of TP508 (anti-TP508b ab Rb411). PEG-conjugated peptides migrate more slowly than proteins of equivalent size because PEG does not bind SDS at the same ratio or linearize

in the fashion of polypeptides. PEGylated peptides also form a characteristic inverted teardrop shape due to small variations in length of the PEG polymer (purification of PEG is generally performed using size-based approaches, and as a result the PEG is polydisperse, with molecular weights $\pm 10\%$ of their average value). Instead of a single major band, the tetravalent TP508 derivative displays 3 bands of roughly equivalent intensity at migrations of 16, 14.1, and 12.6 kDa, and an elongated smear at above 16 kDa (Figure 3.1, Lane 7). The roughly 2 kDa difference between each band suggested that the lower bands might be incompletely reacted 4-arm PEG species containing only 3, 2, or 1 TP508 moieties, respectively. This was verified by the Western Blot of these samples, where all bands plus the smeared region bound the anti-TP508b Rb411 antibody (Figure 3.2).

This mixture of molecular species complicates any subsequent analysis of a multivalent PEGylated TP508 derivative. Each partially filled tetravalent species would potentially have different binding avidity, circulating half-life, concentration displaying a therapeutic effect, etc. Discussions were initiated with the American Peptide Company about further purification of the tetravalent TP508 derivative. It was determined that generating a more highly purified version of the PEG-peptide conjugate, with all 4 arms of the PEG containing a TP508 moiety, would be highly challenging technically. Therefore, the derivative studies conducted in this project were limited to monomeric PEGylated TP508 derivatives.

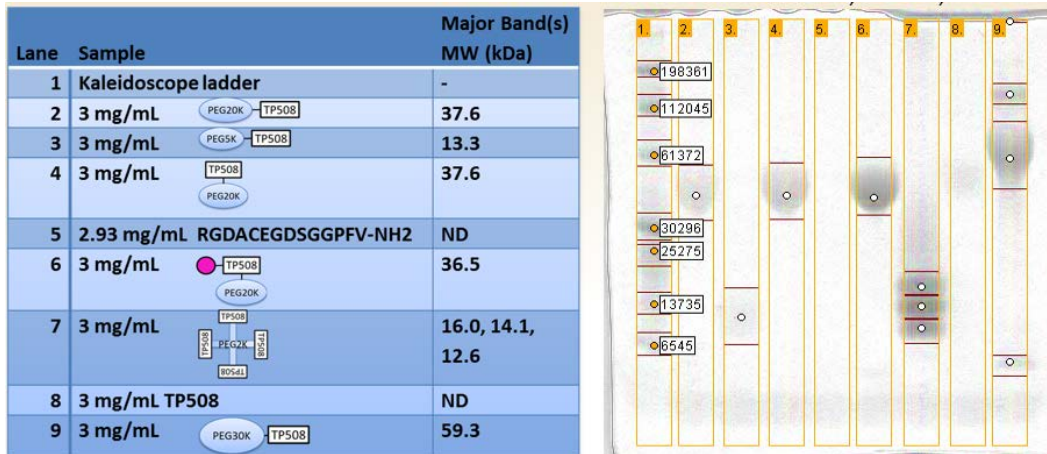


Figure 3.1 – SDS-PAGE of TP508 derivatives. Lane loading legend (right) along with analyzed gel (left). Numbers in lane 1 of analyzed gel are the molecular weights of ladder proteins (in Daltons).

The anti-TP508B Rb411 polyclonal antibody was able to detect all monovalent TP508 derivatives in the Western blot. Because all of the derivatives were loaded at a concentration of 3 mg/mL, it would be expected that the higher molecular weight bands would bind less anti-TP508B antibody, since the fraction of TP508 would be smaller as the MW of the TP508 derivative increases, and the antibody binds only to the TP508 moiety. This was the case with the N-terminal PEGylated TP508 derivatives, with PEG5k-TP508 (Figure 3.2, lane 3) being more intense than PEG20k-TP508 (Figure 3.2, lane 2), and PEG30k-TP508 being the faintest of the 3 (Figure 3.2, lane 9). It is interesting, however, that the PEG20k-Cys14-TP508 derivative (Figure 3.2, lane 4) and its fluorescent TAMRA-labeled variant (Figure 3.2, lane 6) were much fainter than their N-terminally bound counterpart, despite being no less intense on the SDS-PAGE gel. This suggests that PEGylation of the internal cysteine creates greater steric hindrance for antibody binding to TP508 than does PEGylation of the terminal amine, and suggests that PEG20k-Cys14-TP508 may also be less bioactive.

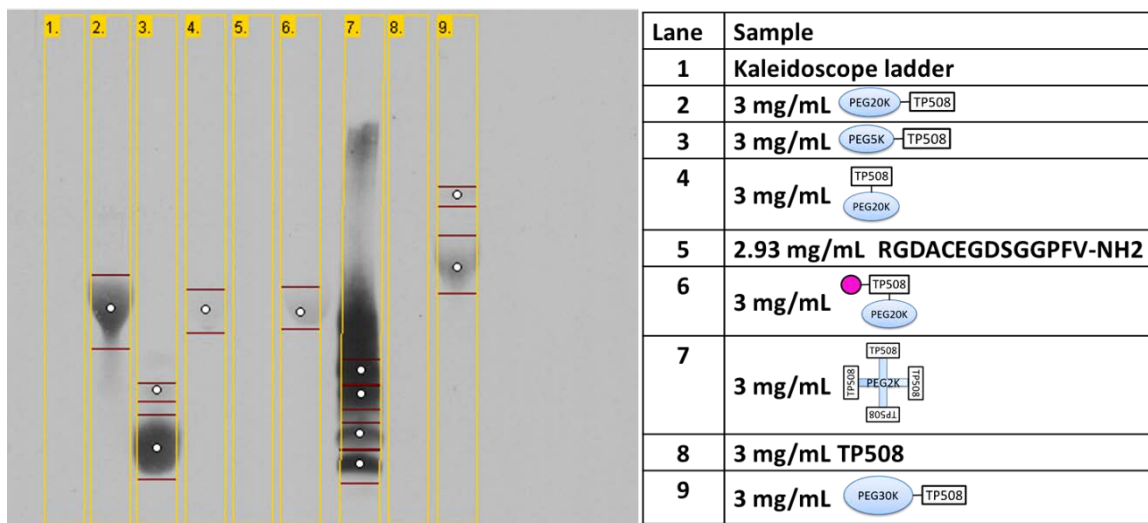


Figure 3.2 – Western Blotting of TP508 derivatives using anti-TP508B Rb411 polyclonal antibody.

Also of note is the fact that TP508 and the truncated TP508 14-mer appear absent in their respective lanes by both SDS-PAGE and Western blot. An 8-12% Bis-Tris gel was chosen for the initial SDS-PAGE of the PEGylated TP508 derivatives because of their anticipated slow migration. This would result in the <2.5 kDa peptides coming out in the solvent front. Interestingly, with regards to Western Blotting of TP508 even in higher percentage acrylamide crosslinked gels, TP508 does not generally appear as a band on either nitrocellulose or PVDF membranes, even when reducing transfer times to minimize loss due to peptide migrating through the filter. This is likely because when TP508 is driven by electromotive force onto the membrane, where neutral and hydrophobic regions attach to the membrane, the conformation necessary for binding to the Rb411 antibody is lost. However, when performing dot blotting, where the protein is directly applied to the membrane and adsorbs to it, which results in attachment at a variety of sites and results in

a broader variety of conformations available for attachment, the anti-TP508B Rb411 antibody regains its ability to bind TP508.

An additional note on the anti-TP508B Rb411 antibody: A series of polyclonal antibodies raised to either the first 14 (anti-TP508A) or last 14 residues of TP508 (anti-TP508B) were produced in rabbits by Covance, with the antiserum from Rb411 having the most consistent binding to TP508 when performing IP assays for receptor pulldown. However, in use with Western blot, this antibody also shows non-specific activity towards serum albumin, present in low molecular weight standard ladder (Bio-Rad #161-0304). This may complicate future receptor purification approaches where serum is present in cell growth media, and either a different monoclonal antibody or TP508-specific aptamer is recommended.

B. PLASMA HALF-LIFE OF TP508 AND TP508 DERIVATIVES

To determine if PEGylation of TP508 did indeed extend the duration that TP508 is detectable in the blood stream after injection, fluorescently-labeled variants of TP508 monomer, TP508 dimer, PEG5k-TP508, PEG20k-TP508, PEG20k-Cys14-TP508 and PEG30k-TP508 were all examined for increased plasma half-life (see Section 4B for method). Mice were injected intravenously with 500 μg TAMRA-TP508 or the molar equivalent of each of the derivatives, or with TAMRA-PEG30k-TP508 at the molar equivalent of 100 μg TAMRA-TP508 due to quantity available and solubility concerns. Figure 12 shows the results for 3 separate time courses per treatment, presented as mean \pm SD, with the decay curve calculated using the GraphPad Prism 7.01 nonlinear regression – one phase exponential decay function. TP508 monomer (Figure 3.3A) clearly follows a standard one-phase decay rate, likely due to clearance occurring much faster than any proteolytic degradation can occur. The TP508 calculated half-life is 13.70 minutes (95% CI: 11.8 – 16.4 minutes, $R^2 = 0.9801$), which is in agreement with the serum half-life

previously reported as 10 to 14 minutes in Yucatan swine (47). The PEG5k-TP508 derivative (Figure 3.3B) has the same plasma half-life, within error, as TP508, with a calculated value of 11.5 minutes (95% CI: 9.8 to 13.7 minutes, $R^2 = 0.9835$). This was to be expected since PEG5k-TP508 has a molar weight of 7.3 kDa, well below the size filtration limit of the kidneys for proteins. Note that, although the half-life is the same, the initial TP508 concentration in the blood for this derivative is on the order of 5-fold higher at $T = 5$ minutes after injection. This may indicate that PEG5k-TP508 has less diffusion out of the tail vein into the tail collagen than TP508 monomer under the pressurized conditions at the base of the tail during IV injection. This could be seen as a bright pink band under the skin at the base of the tail due to the presence of the fluorescent TAMRA molecule, which is dark purple in the lyophilized powder and a dark pink on reconstitution in 0.9% saline or DPBS at the concentrations tested.

The larger PEGylated derivatives show a size-dependent increase in plasma half-life, as expected. PEG20k-Cys14-TP508 has a calculated half-life of 70 minutes (Figure 3.3D), a roughly 5-fold increase over that of TP508. The PEG20k-TP508 and PEG30k-TP508 derivatives have even flatter curves, suggesting further enhanced half-lives on the order of 7-fold for PEG20k-TP508 and 20-fold for PEG30k-TP508, but precise determinations could not be determined due to sample variability and the low R^2 values for these derivatives. Note that as the plasma half-lives increase, R^2 values decrease, indicating less goodness of fit with the one-phase decay model (Table 2). The loss of fidelity to the one-phase decay curve may in part be due to a second-phase component, such as TP508 proteolysis, becoming a larger factor at later time points.

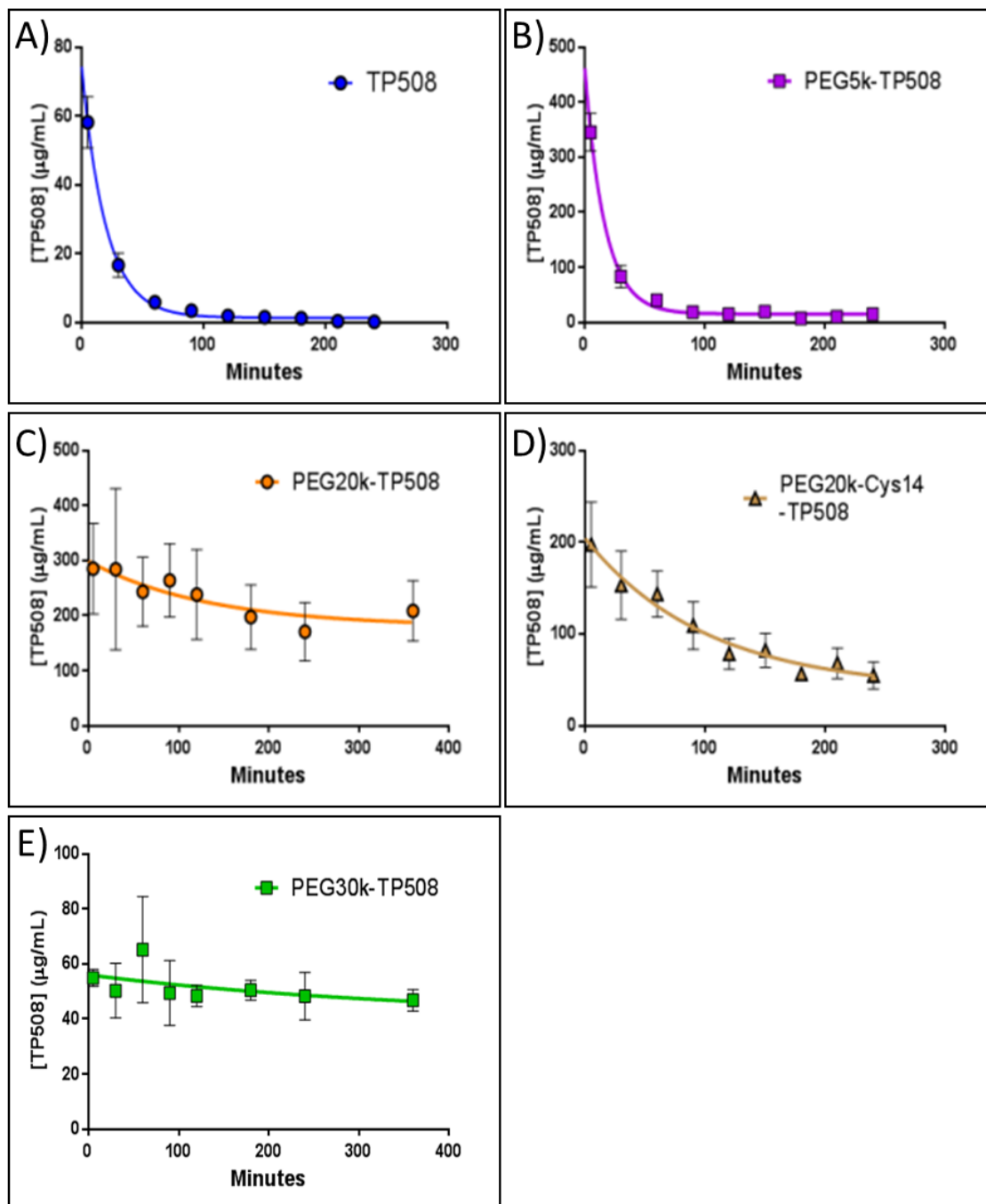


Figure 3.3 – Decay curves for TAMRA fluorescently-labeled TP508 & TP508 derivatives. A) Decay curve for TP508 (blue); B) Decay curve for PEG5k-TP508 (purple); C) Decay curve for PEG20k-TP508 (orange); D) Decay curve for PEG20k-Cys14-TP508 (brown); E) Decay curve for PEG30k-TP508. Data presented as mean \pm SD.

	TP508 Monomer	PEG5k- TP508	PEG20k- C14-TP508	PEG20k- TP508	PEG30k- TP508
Best-fit values					
Half Life (minutes)	13.7	11.5	70	*nd	*nd
95% Confidence Intervals					
Half Life (minutes)	11.8 to 16.4	9.9 to 13.7	40 to 280	24 to +infinity	23 to +infinity
Degrees of Freedom	24	24	24	21	21
R square	0.98	0.98	0.81	0.21	0.10
Number of points analyzed	27	27	27	24	24

Table 3.1 – Plasma half-life and attendant statistics for TP508 and PEGylated TP508 derivatives. *nd – not determined due to low R² values.

The fluorescent TAMRA tag is located on the N-terminus of the peptide, and occurs on a linker between the peptide and PEG in the N-terminal PEGylated derivatives. As a result, it is possible that the plasma fluorescence of the samples could represent partially degraded forms of TP508, in addition to full length TP508. To determine if this was the case, an in-gel fluorescence assay (Section 6C) was used with plasma samples from the first TAMRA-TP508 plasma half-life time course (Figure 3.4). In this assay, SDS-PAGE gel migration is reduced by the 5-tetramethylrhodamine fluorescent tag, which is a zwitterion and neutrally-charged at near neutral pH, instead of having the uniformly negative charge to mass ratio of the protein moiety. This causes partially degraded TAMRA TP508 to migrate slower through the gel, rather than faster. As can be seen in Figure 3.4, by the 90 minute timepoint, substantial amounts of the protein are migrating more slowly, and by 120 minutes, only degraded species are visible. Total protein

concentration from the in-gel assay closely matches that of the original plate-based fluorescence assay (Figure 3.5).

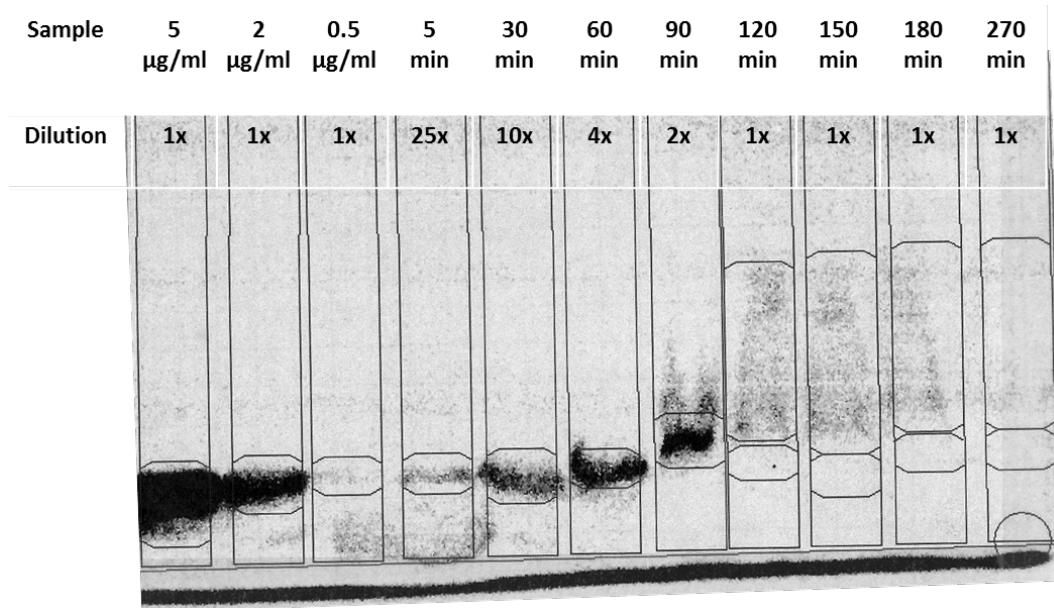


Figure 3.4 – In-gel fluorescence of TAMRA-TP508 biological half-life samples.

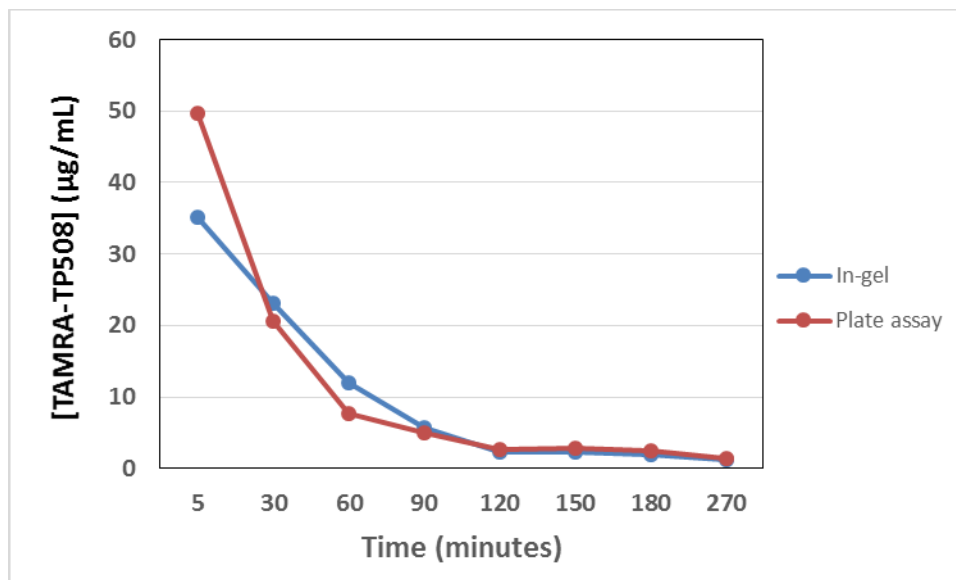


Figure 3.5 – Total TAMRA-TP508 concentration determined from the in-gel fluorescence assay as compared to the plate-based fluorescence assay.

Chapter 4: Biological activity of TP508 Derivatives

A. INITIAL WORK TO ESTABLISH A SIMPLE *IN-VITRO* ASSAY FOR TP508 ACTIVITY USING WI-38 FIBROBLASTS

I proposed to develop an *in vitro* biological activity assay based on the response of WI-38 human fetal lung fibroblasts to TP508 and TP508 derivatives. Previous studies demonstrated that TP508 binds specifically to these cells (62). Moreover, specific gene products were upregulated in response to TP508 in pilot studies carried out by Chrysalis BioTechnology, Inc. in 2001 (Keherly and Carney, unpublished). These studies were performed using Clontech PhosphoImager cDNA expression library technology, which used ^{32}P -radiolabeled dATP to evaluate differences in transcription (see Figure 4.1 for original PhosphoImager workflow). Thus, a strategy evolved for us to confirm the upregulation of specific gene products by TP508 using RT-qPCR and then use the gene product up-regulation as a marker of TP508 activity.

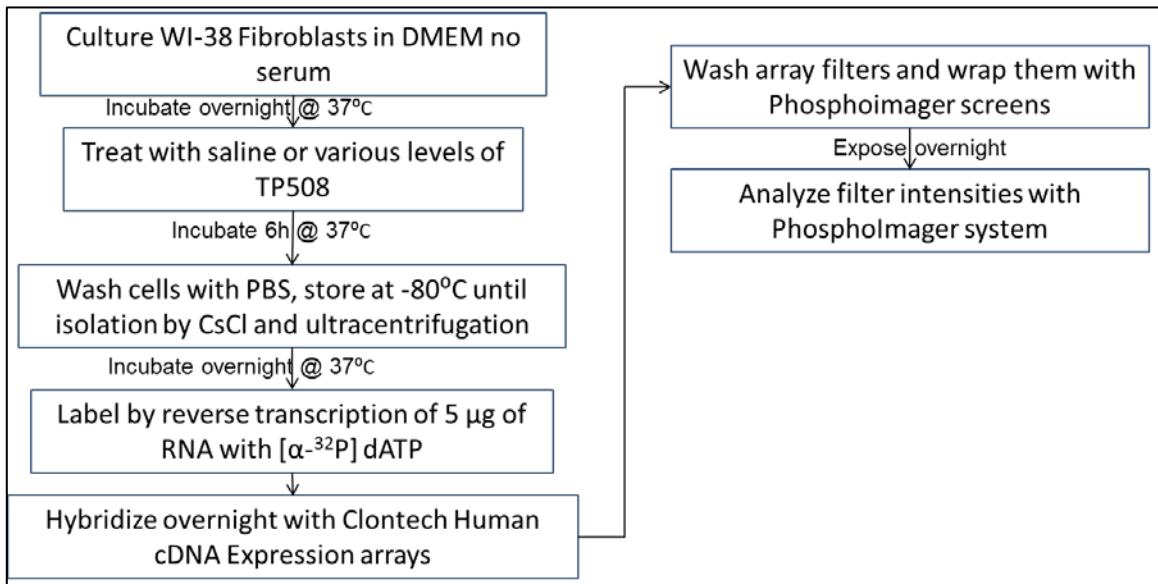


Figure 4.1 – PhosphoImager workflow for analysis of transcriptional response of WI-38 fibroblasts to TP508

Of 400 genes assayed, 8 genes displayed 1.2 – 4 fold upregulation in mRNA levels with TP508 treatment as compared to saline controls. Therefore, we prepared PCR primers for these genes and analyze their expression in WI-38 cells with RT-qPCR. In addition to these eight genes identified by the PhosphoImager studies, a ninth candidate, annexin V, was added to the list due to its reported upregulation in response to TP508 treatment (63). The nine gene candidates chosen to be assayed for a quantitative, dose dependent TP508 biological activity assay using RT-qPCR are listed in Table 4.1.

Gene	RefSeq mRNA Accession #	Description	Activity
NR2F6	NM_005234.3	Human v-erbA related ear2 gene	transcription factor http://www.uniprot.org/uniprot/P10588
NR2F1	NM_005654.4	Human v-erbA related ear-3 gene	COUP transcription factor 1 http://www.uniprot.org/uniprot/P10589
AXL	NM_001699.4	Human tyrosine kinase receptor (axl aka UFO)	Transduces signals from GAS6, activates Akt pathway http://www.uniprot.org/uniprot/P30530
ILK	NM_001014794.1	Human integrin-linked kinase	Acts with integrin beta 1 subunit, may also interact with beta 2, 3 & 5, can phosphorylate AKT1 http://www.uniprot.org/uniprot/Q13418
BCL2L1	NM_138578.1	<i>H. sapiens</i> bcl-xL	Apoptosis inhibitor, part of the Bcl-2 family http://www.uniprot.org/uniprot/Q07817
MAP2K3	NM_002756.4	<i>H. sapiens</i> MAP kinase kinase 3 (MKK3)	Activated by cytokines, environmental stress http://www.uniprot.org/uniprot/P46734
EGR1	NM_001964.2	Early growth response protein 1 gene	Transcriptional regulator of mitogenesis and differentiation http://www.uniprot.org/uniprot/P18146
ETV6	NM_001987.4	transcription factor ETV6 (aka TEL, TEL1)	Gene knockout studies in mice suggest it is required for hematopoiesis and maintenance of the developing vascular network http://www.ncbi.nlm.nih.gov/gene/2120
ANXA5	NM_001154.3	<i>H. sapiens</i> Annexin V (aka A5)	anticoagulant protein http://www.uniprot.org/uniprot/P08758

Table 4.1 – Gene candidates for RT-qPCR method development for a quantitative dose dependent assay for TP508 biological activity.

WI-38 cells that had been archived from stocks believed to be identical to those used in 2001 were cultured, and RNA isolated as described in Section 4D & 4E. RT-qPCR primer design and analysis were performed by the UTMB Molecular Genomics core. Triplicate data with 3 independent replicates per treatment were prepared using a 24h period of serum-free culture for the cells, in the same manner as the 2001 PhosphoImager analysis. Despite using the same periods of serum-free incubation followed by TP508 treatment, none of the 9 genes showed upregulation by TP508 beyond a 1.2 fold increase over saline control when assayed by RT-qPCR (Figure 4.2). There are several possible interpretations of these results. The original PhosphoImager results, like later microarray technology, were prone to occasional false positives which would then not replicate using RT-qPCR. It is also possible that the WI-38 cells, which were assayed from passage 10-14 for the RT-qPCR investigation, may have lost responsiveness to TP508 due to culture and serum adaptation. For example, receptor expression of the putative TP508 NPAR may have been reduced as cells were grown to full confluence multiple times in high serum conditions.

To further investigate the hypothesis that the WI-38 cells may have lost their responsiveness to TP508 after multiple passages of the cells in DMEM/F-12 growth media, the RT-qPCR replicate results were analyzed based on the passage at which the TP508 RT-qPCR response was analyzed. No difference in TP508 response between passage 10 and passage 14 was observed (Figure 4.2), suggesting that if the lack of response was due to a passaging issue, it occurred before passage 10, or that the WI-38 cells were not the same as those used in prior studies.

We further evaluated the responsiveness of these WI-38 fibroblasts to TP508 by analyzing their proliferative response using the MTT assay (Section 4F) since prior studies reported that TP508 stimulated cell proliferation in combination with low concentrations of thrombin (64). WI-38 cells seeded into 24-well plates at a concentration of 1×10^5 cells per well were incubated for 24h in DMEM/F-12 growth media with various concentrations of TP508 or thrombin. The MTT cell viability assay was then used to determine differences in the number of viable cells between groups. Only the wells treated with 125 ng/mL thrombin showed increased proliferation, indicated by a higher absorbance value (Figure 4.3). No response was seen to TP508 at the concentrations tested, nor was there any significant difference between 125 ng/mL of thrombin alone, or in conjunction with the various levels of TP508 tested. Figure 4.3 presents this data as mean \pm SD. These data show that TP508 alone did not enhance proliferation while 125 ng/mL thrombin did. It also shows that TP508 has no additive or synergistic effect in enhancing proliferation combination at the lower concentration of thrombin (62.5 ng/mL). Thus, it appears that under the culture conditions used, these WI-38 cells do not respond to TP508

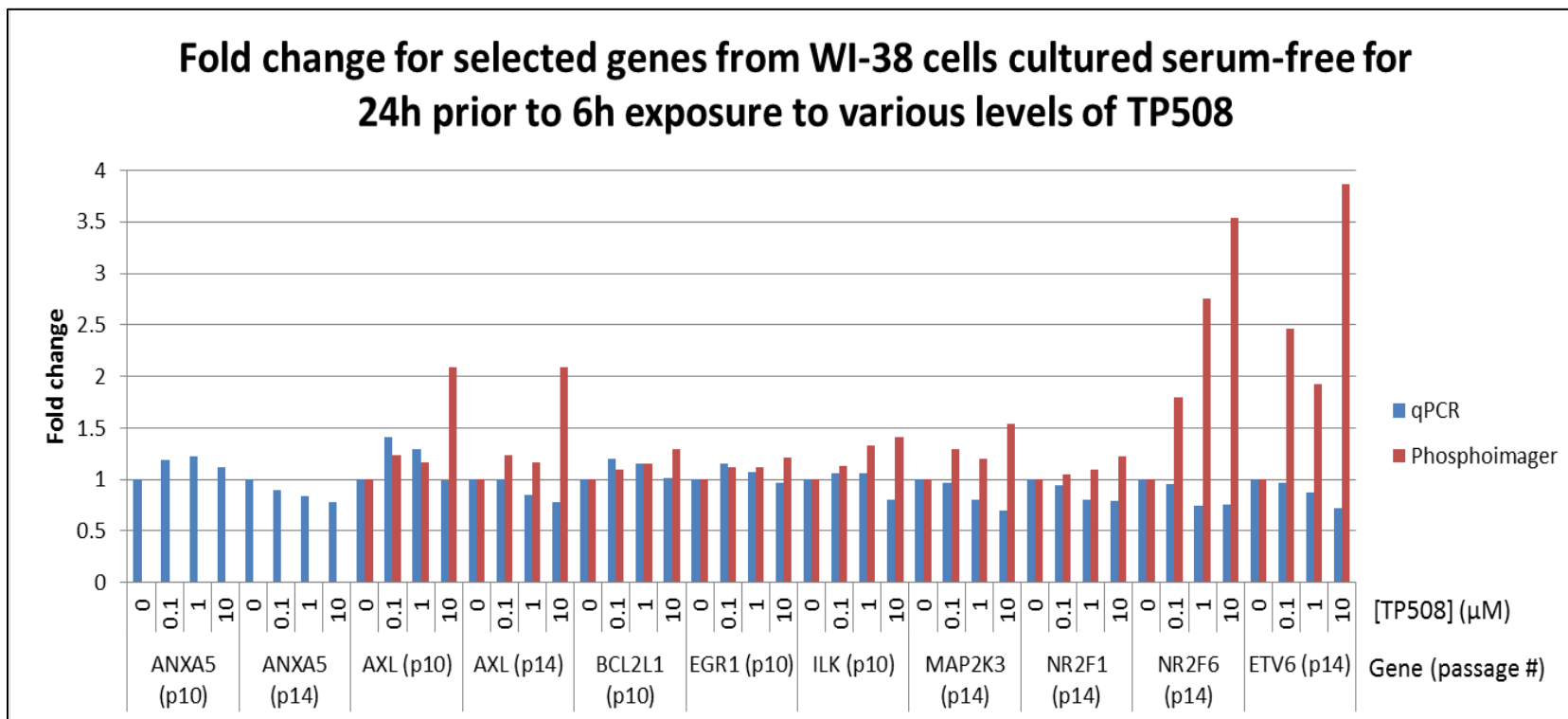


Figure 4.2 – Comparison of WI-38 fibroblast transcriptional response for selected genes in response to TP508 stimulation by qPCR and PhosphoImager analysis.

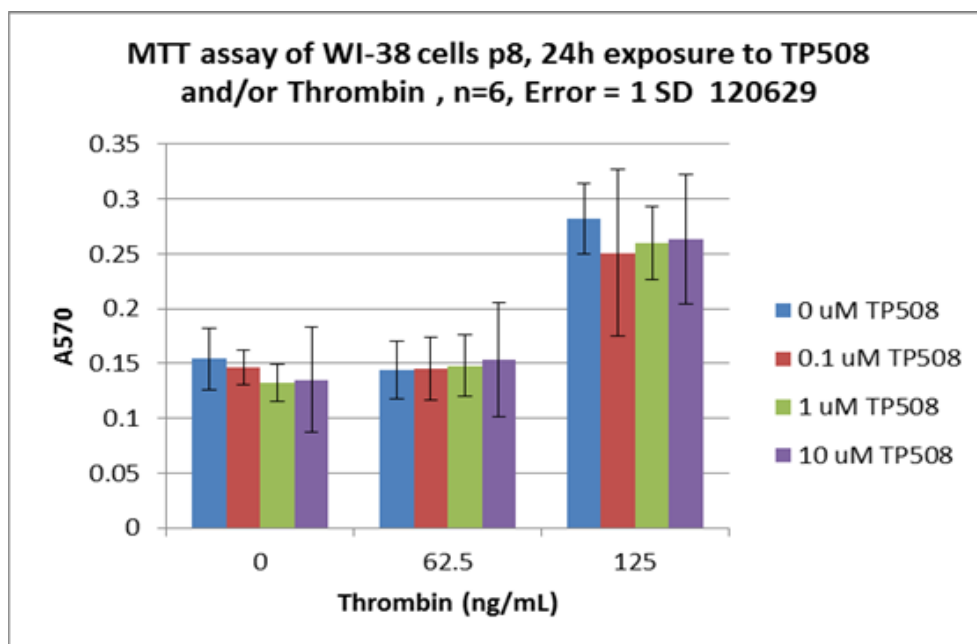


Figure 4.3 – MTT cell viability results for WI-38 cell proliferation after 24h treatment with TP508 and thrombin. Data presented as mean +/- SD.

Another possibility for lack of response to TP508 in these WI-38 cells was that they may no longer express TP508 receptor binding sites. A fluorescent competition binding assay was attempted to evaluate the binding of TP508 to these cells (Section 4G, Figure 4.4). In this assay, a static amount of fluorescently-labeled TAMRA-TP508 was added to each well of WI-38 fibroblasts, along with various concentrations of unlabeled TP508. If specific binding is present, the unlabeled TP508 is expected to reduce the fluorescence in a sigmoidal curve as unlabeled TP508 concentration increases and displaces specifically bound TAMRA-TP508, but not any that is nonspecifically bound to the cells.

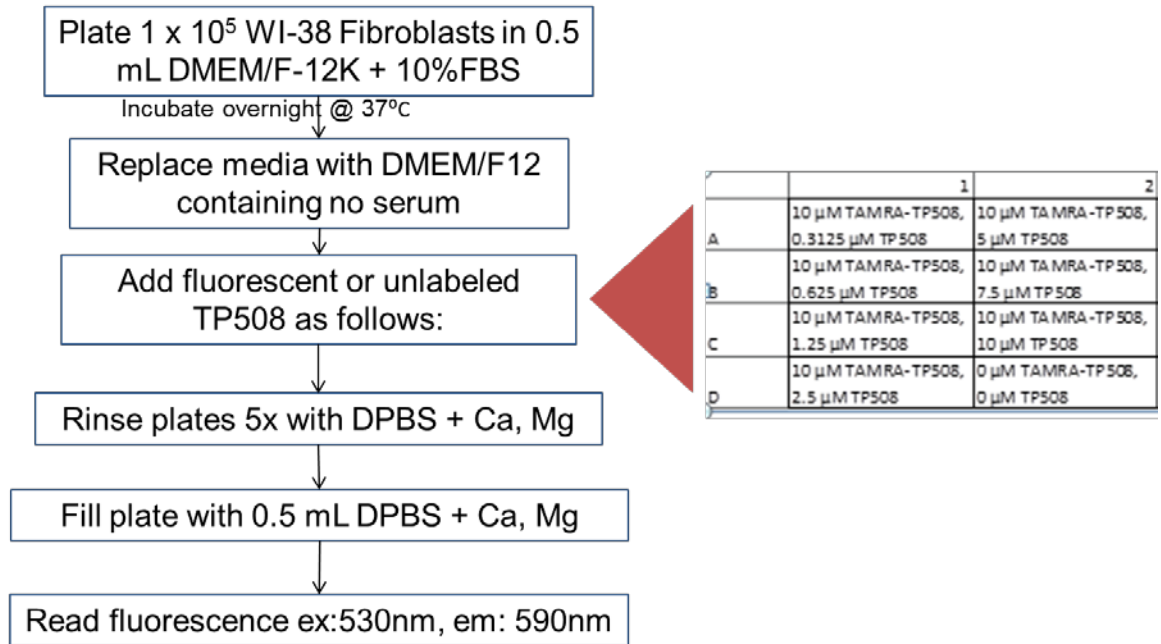


Figure 4.4 – Fluorescent competition assay workflow.

10 μM TAMRA-TP508 produced a signal of 49,000 ± 3000 units prior to washing the fibroblasts. Figure 4.5 summarizes the fluorescent intensity of 10 μM TAMRA-TP508 competing with 0 – 10 μM unlabeled TP508 for binding to WI-38 fibroblasts. After incubation for 45, 60, or 110 minutes, however, washing removed essentially all fluorescence from these cells, with the maximum fluorescent intensity being less than 100 units (less than 0.2% of original signal), an intensity similar to blank wells containing no TAMRA-TP508. Thus there was no detectable binding of TAMRA-TP508 to the cells with or without addition of unlabeled TP508. Therefore, with this assay it was impossible to discern whether or not the cells had TP508 binding sites. This may indicate that either TAMRA-TP508 interferes with specific binding, that the fluorescent marker is not sensitive enough to detect specific binding, or that the archived WI-38 cells had lost specific binding to TP508.

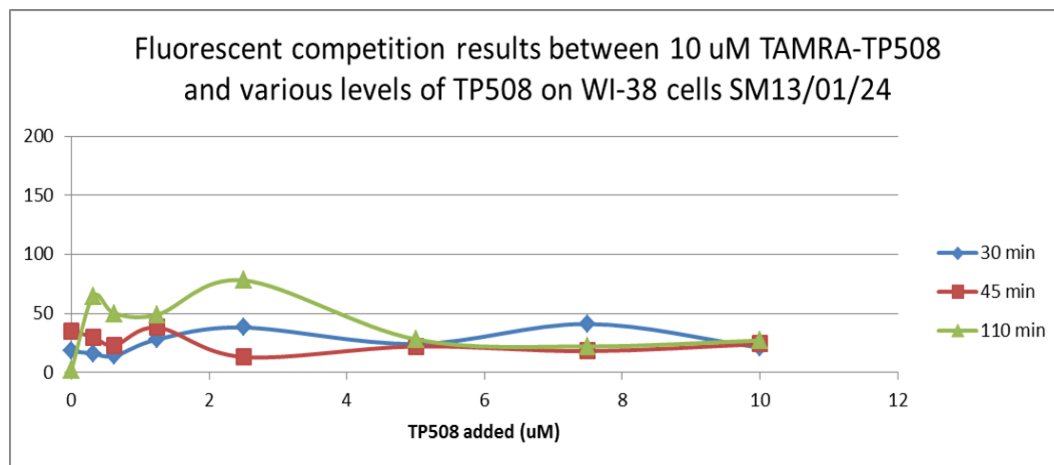


Figure 4.5 – Fluorescent competition assay of TAMRA-TP508.

In summary, we were unable to confirm a significant upregulation of selected genes with RT-PCR in WI-38 cells following TP508 treatment. Moreover, we were unable to confirm either a proliferative response in these cells to TP508 using the MTT assay, or specific binding using a fluorescently-labeled TP508 molecule. Therefore, the biological activity of PEGylated TP508 derivatives could not be assessed with WI-38 cells. This necessitated a change in strategy to an alternate cell population or alternative method of analysis to assess the biological activity of the PEGylated TP508-derivatives.

B. USE OF A MOUSE AORTIC RING ASSAY FOR ANGIOGENIC ACTIVITY OF TP508 ADMINISTERED *IN VIVO*

Due to the lack of response of the archived WI-38 cells to TP508 *in vitro*, it became necessary to move from what we had hoped to be a simple *in vitro* cellular assay to more complex *ex vivo* and *in vivo* methods where the biological activity of TP508 was currently being studied with a high degree of reproducibility. Kantara et.al. (65) recently showed that a single injection of TP508 into CD-1 mice 24h post-irradiation mitigated effects of the radiation on gastrointestinal crypts and significantly increased animal survival. Additional studies showed that TP508 systemic injection post-irradiation had protective effects on aortic endothelial cells which could be measured by analyzing endothelial sprouting from aortic segments isolated 24 hours after injection (66). Therefore, the decision was made to test the TP508 derivatives in CD-1 using the aortic explant angiogenesis assay, as described (66), but to modify the assay to automate analysis to allow better quantification, less operator dependence, and ability to process larger numbers of samples.

The rationale for using CD-1 outbred mice as opposed to more common inbred strains like C57Bl/6 mice, which might have a less variable response to ionizing radiation, is that mature outbred mice are anticipated to better represent a theoretical human population exposed to ionizing radiation by a nuclear incident. This is an essential requirement for the development of TP508 as an FDA-approvable therapeutic for radiomitigation, as clinical trials must be performed under the FDA “Animal Rule.” Since the efficacy and safety of TP508 administration after lethal or near-lethal levels of ionizing radiation can only be assessed in animal models, these models must be as representative of the response of a human population as possible. For this project to identify potentially

promising TP508 derivatives, the use of CD-1 mice from the same background and vendor as those being used in nuclear countermeasure studies greatly simplifies go/no go decisions related to switching to a new TP508 derivative for future systemic applications.

The aortic ring endothelial sprouting assay is commonly used to examine the impact of growth factors, inhibitors, and siRNAs on angiogenesis and development of the microvasculature (60). In this assay, an aorta is dissected, cleaned and sectioned into rings that are then cultured on extracellular matrix for up to 10 days (67). During this time, tube-like formations of vascular endothelial cells sprout from the aortic ring, which can then be qualitatively or quantitatively analyzed to determine positive and negative effects on angiogenesis (67). Factors that can affect the variability of this assay include the choice of extracellular matrices and the contribution of different cells populations that accompany the explanted aortic rings.

A number of extracellular matrices are available for culture of the aortic rings, including collagen and fibrin gels. In these culture conditions, thick, tube-like structures with low to moderate branching are observed. An alternative matrix, Matrigel®, allows for thin, highly branched and connected vessels more similar to capillary networks *in vivo* (68). This matrix, purified from Engelbreth-Holm-Swarm mouse sarcoma cells, is composed primarily of laminin and collagen IV in a 2:1 ratio, along with numerous low abundance proteins including multiple growth factors. This Matrigel environment enables persistence of stem and progenitor cell phenotypes and other cells including pericytes, fibroblasts, and smooth muscle cells present in addition to the vascular endothelial cells contained in the aortic tissue, enhancing the biological relevance of sprouting from these rings (68, 69).

A major goal of this project was to determine whether the PEGylation of TP508 that increased its half-life in plasma (Section 2, Chapter 3B) also increased its biological activity. Therefore, we used the aortic ring assay as an endpoint to evaluate the bioactivity of these derivatives. In prior studies, it was shown that injection of TP508 24h prior to sacrifice and aortic isolation stimulated aortic endothelial sprouting from explanted aortic segments (70). It was observed, however, that the amount of sprouting on individual segments varied considerably, therefore the procedure was modified and standardized for this project.

CD-1 mice were pretreated with TP508 or TP508 derivatives 24 hours prior to isolation of the aortas (see Section 4H), to capture priming effects of the TP508 treatment *in vivo* which translate into enhanced endothelial sprouting when exposed to the pro-angiogenic environment within the Matrigel *ex vivo*. This model differed from prior models not only in having the test agent injected prior to aortic isolation, but also in the use of rings where only the cut edge of the aorta is in contact with the Matrigel. This provides for more consistency between samples and sprouting that is more single dimensional to allow for better quantitation. The workflow for this modified aortic ring assay is summarized in Figure 4.6.

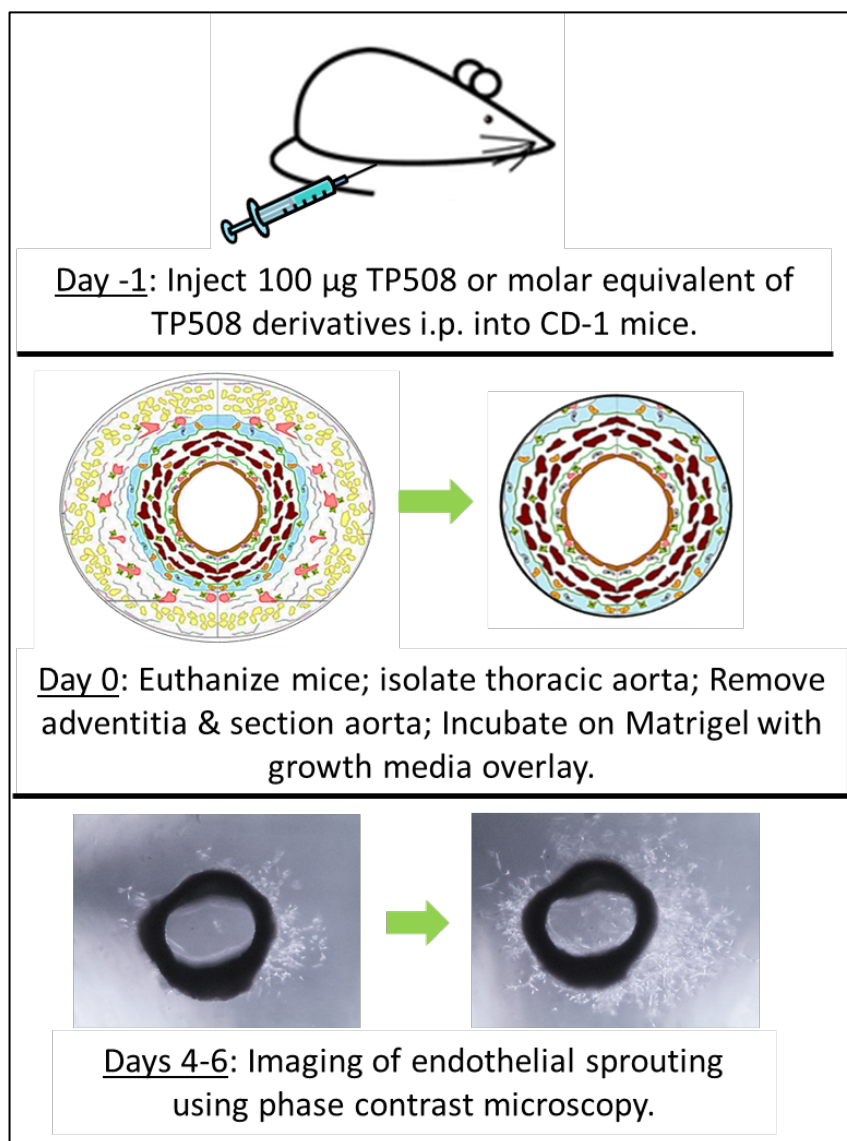


Figure 4.6 – Workflow for aortic ring assay with *in vivo* pre-treatment with TP508.

Male CD-1 mice aged 14-22 weeks were injected i.p. with either 100 μL 0.9% saline, 100 μL of 1 mg/mL TP508, or 100 μL of the equimolar equivalent for each TP508 derivative 24h prior to isolation of the thoracic aortas. The dose of 100 μg TP508 was selected based on the result that this was the minimum effective dose in promoting survival in CD-1 mice receiving an LD_{70} dose of ionizing radiation, and based on previous results for endothelial sprouting in segments of irradiated aortic tissue (66). The aortic rings began

to display endothelial sprouting by the third day of incubation in Matrigel. This was followed by an exponential increase in endothelial sprouting over Days 4-6. Representative images of endothelial sprouting at Day 5 are shown in Figure 4.7. By Day 6, the extent of sprouting from some of the rings exceeds the field of imaging for the phase contrast microscope at the lowest magnification (4x objective).

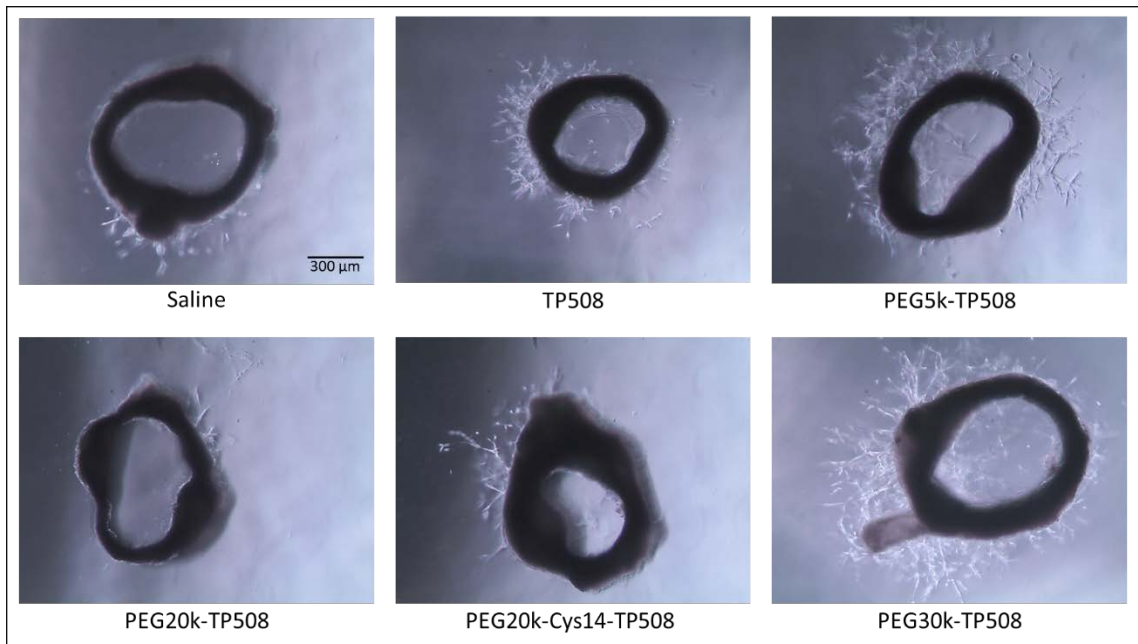


Figure 4.7 – Phase contrast microscopy of aortic rings with *in vivo* pretreatment at Day 5.

This experiment used three full biological replicates per treatment, using a different mouse per replicate of each treatment, culturing 8-12 rings per mouse. Despite this large sample set, substantial variability in the number of endothelial sprouts from ring to ring was observed. A number of rings did not show any sprouting from Days 4 – 6, while others produced in excess of over 300 sprouts by Day 6. When analyzing the percentage of rings sprouting for each treatment, these treatments fell into two groups with similar viabilities. In the first group, PEG20k-TP508 (orange, Figure 4.8), PEG20k-Cys14-TP508 (brown)

and the 14-mer of TP508 (pink) all show a percentage of rings sprouting similar to the saline control (red), ranging from 45 – 54% by Day 6. The second group, which includes the TP508 (blue), PEG5k-TP508 (purple), and PEG30k-TP508 (green) treatments, have a greater percentage of aortic rings sprouting, ranging from 78 – 86% of rings sprouting by Day 6. These data indicate that the biologically active TP508 derivatives have a protective effect in maintaining the angiogenic potential of the tissue against damage incurred during dissection and processing, similar to its protective effects in ischemic tissue (34, 40, 45, 47, 71).

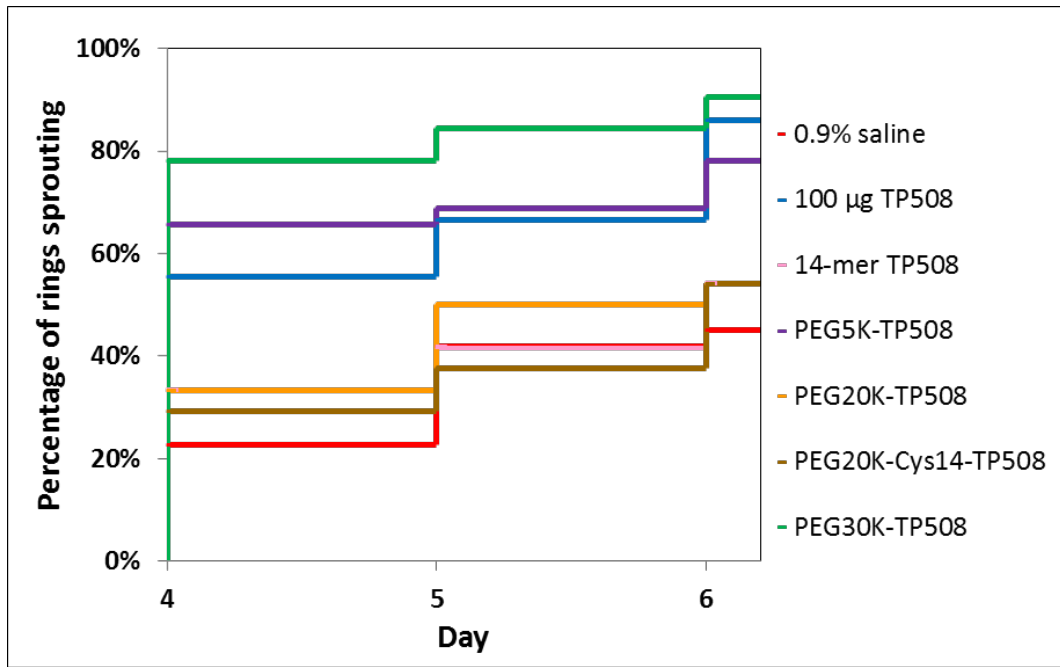


Figure 4.8 – Percentage of aortic rings displaying endothelial sprouting at Days 4-6 after *in vivo* pretreatment.

This difference in number of rings showing endothelial sprouting is also reflected in the mean and maximal sprouting for each treatment. Figure 4.9 summarizes the endothelial sprouting data for each treatment at Day 4, 5 and 6 post-embedding in Matrigel.

The data are presented as mean \pm SEM. The 14-mer TP508, PEG20k-TP508 and PEG20k-Cys14-TP508 show no significant difference in sprouting from saline control from Days 4-6. TP508 (blue bars, Fig. 4.9) shows a consistent trend of increased sprouting over saline control (red bars, Fig. 4.9), with a 29% increase in sprouting at Day 4, a 98% increase in sprouting on Day 5, and a 93% increase in sprouting on Day 6. However, due to the large amount of ring-to-ring variability in number of sprouts, this difference between saline and 100 μ g TP508 treatment did not reach statistical significance for the number of samples tested. PEG5k-TP508 administered at the same molar concentration (purple bars, Fig. 23), however, produced statistically significant increases in sprouting over saline control on Days 4, 5 and 6. PEG5k-TP508 increased sprouting by 262% on Day 4 ($p=0.023$), 277% on Day 5 ($p=0.017$), and 209% on Day 6 ($p=0.013$). The PEG30k-TP508 derivative treatment also resulted in significantly enhanced endothelial sprouting over saline control, with a 240% increase on Day 5 ($p=0.038$) and a 168% increase on Day 6 ($p=0.021$). These results indicate that PEGylation can enhance the pro-angiogenic activity of TP508 administered systemically, but that the activity of the PEGylated TP508 derivatives does not have a simple correlation with the length of PEG attached to the TP508 molecule.

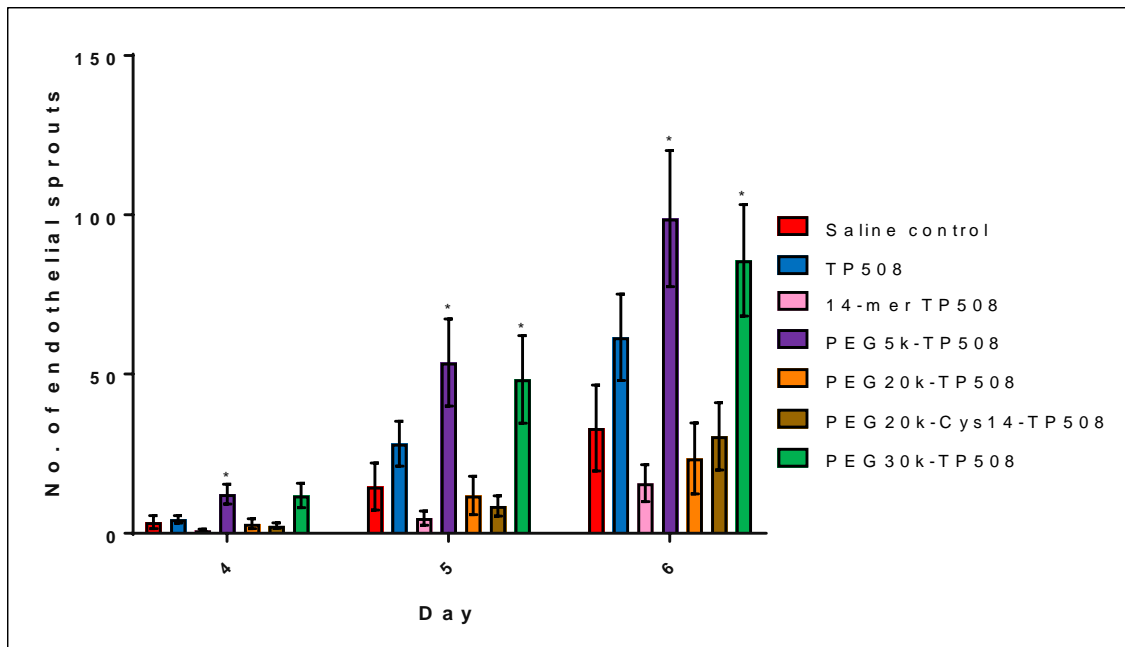


Figure 4.9 – Number of endothelial sprouts at Days 4-6 after *in vivo* pretreatment. Data presented as mean ± SEM, * $p < 0.05$.

At the completion of these experiments, representative rings from the saline, TP508, PEG5k-TP508 and PEG30k-TP508 treatments were fixed for immunofluorescent imaging on Day 7 post-embedding in Matrigel® as per Section 4H. Samples were immunolabeled with anti-CD31 to verify that sprouting cells were of endothelial lineage, with NG2 chondroitin sulfate to identify pericytes recruited to the sprouting network, and counterstained with DAPI. Figure 4.10 shows the phase contrast image of each ring prior to fixation in column 1 and the merged immunofluorescent image taken at 2.5x objective in column 2 (anti-CD31 in green, NG2 chondroitin sulfate in red, DAPI in blue). White boxes in Fig 4.10 column 2 define the boundaries of the inset images taken using 10x objective in columns 3 to 5. Note that the endothelial networks are much more extensive in the PEG5k-TP508 and PEG30k-TP508-treated samples. Pericyte recruitment, which is known to stabilize endothelial sprout networks by bridging across multiple endothelial cells

and provide growth factors and a supply of endothelial progenitor cells (72) was only detected in the PEG5k-TP508 and PEG30k-TP508 samples.

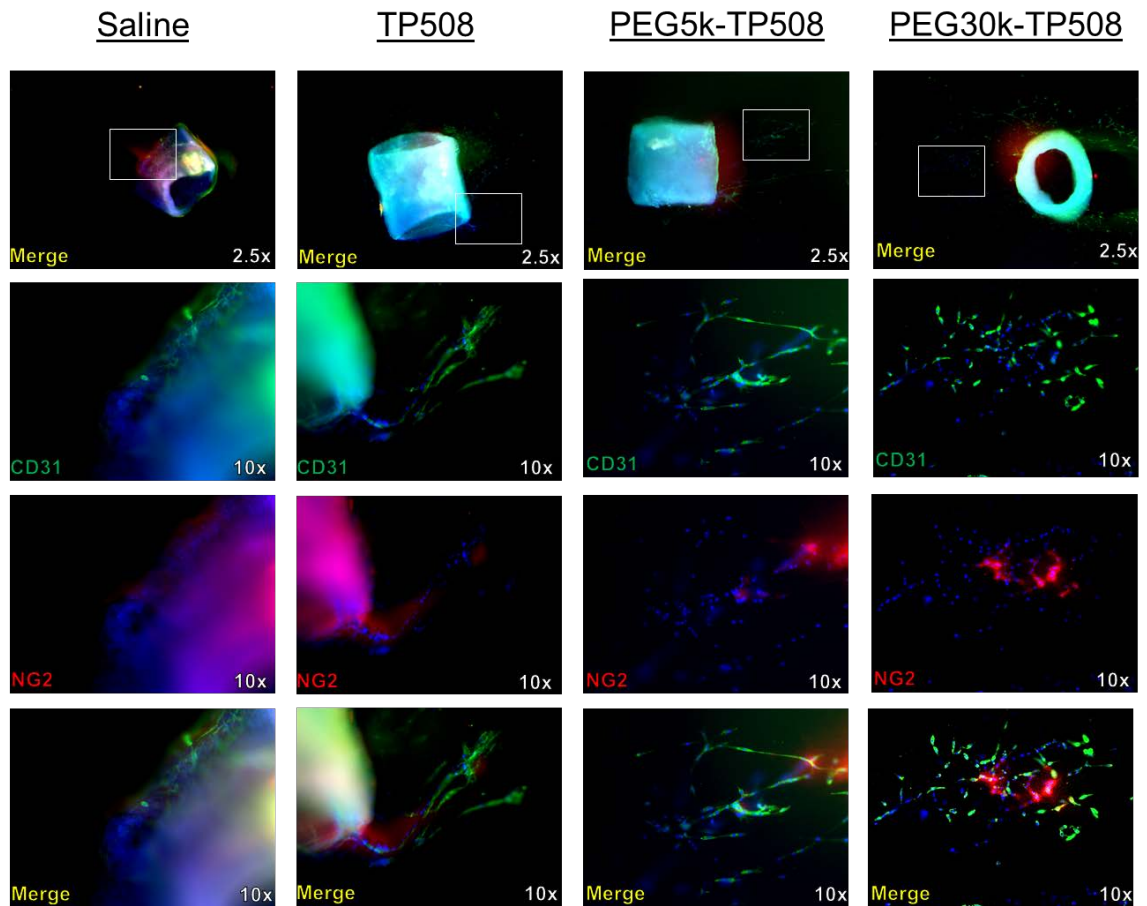


Figure 4.10 – Phase contrast and immunofluorescent images of aortic rings with *in vivo* TP508 treatment. White box in 2.5x objective images represents the portion of the image shown at 10x objective. Aortas were labeled with anti-CD31 (green) to identify endothelial cells, NG2 chondroitin sulfate proteoglycan (red) to identify endothelial cells, and DAPI to identify cell nuclei (blue).

C. BONE MARROW CELL PROLIFERATION IN RESPONSE TO TP508

In addition to the aortic rings harvested 24h post-IP injection with TP508 or the TP508 derivatives, femurs were also harvested from two of the mice in each treatment group. Bone marrow contains niches of stem cells of both hematopoietic and mesenchymal lineage, and their preservation and proliferation post-irradiation are key to recovery and prevention of both acute and delayed radiation effects. As a baseline, we wished to determine the proliferative effects, if any, of TP508 and the bioactive TP508 derivatives on normal bone marrow. The femurs isolated from the CD-1 mice 24h post injection were fixed and prepared as per Section 4I for various tissue staining techniques. H & E staining of sections adjacent to sections used for immunofluorescence were used to identify key structures such as the red bone marrow (which contains large concentrations of hematopoietic cells and blood cells) and bone marrow sinuses. The bone marrow sinuses are of particular interest as they are the route by which new blood cells and endothelial progenitor cells connect with the capillary network inside the bone for uptake into the blood stream.

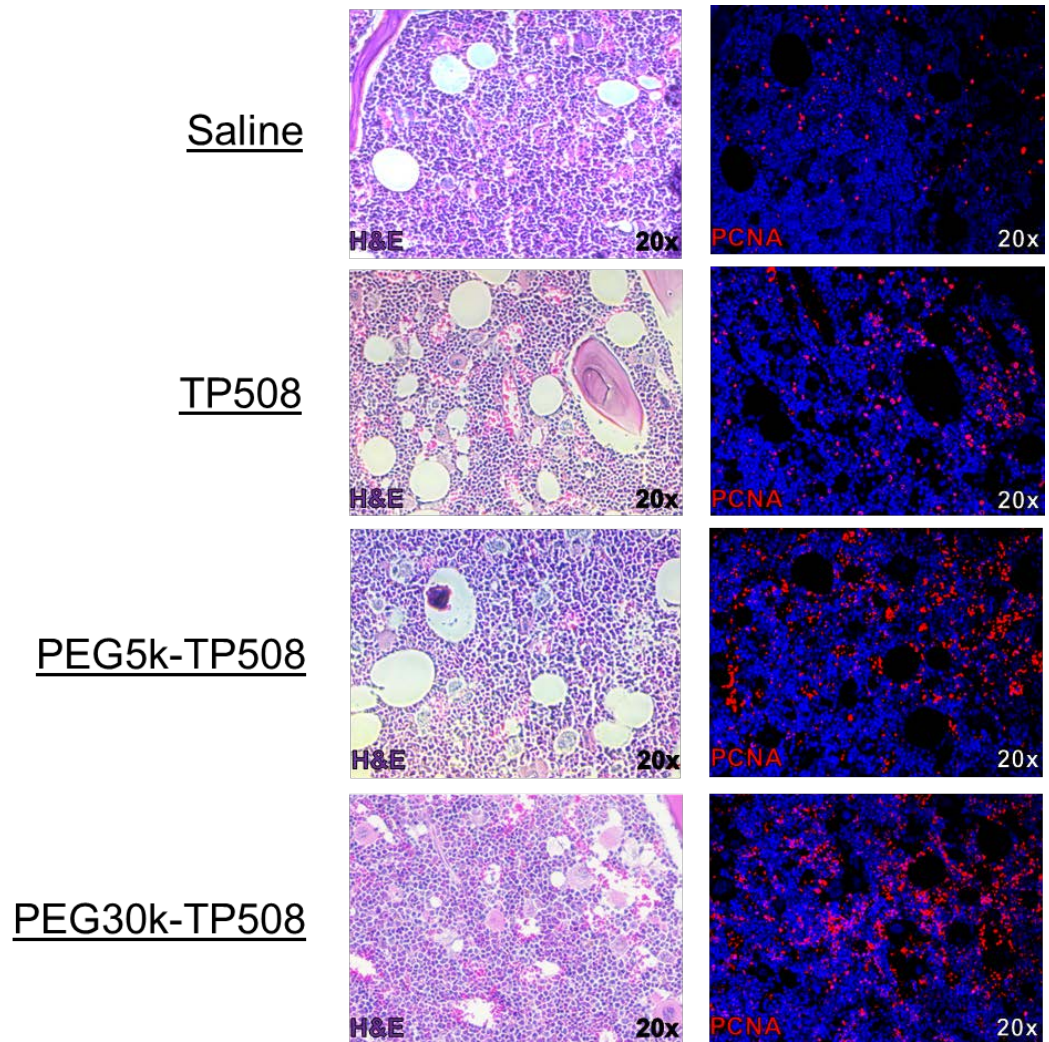


Figure 4.11 – H&E staining and PCNA immunofluorescent staining of longitudinal bone marrow sections from naïve CD-1 mice 24h after TP508 pretreatment. Hematoxylin and eosin staining (right) taken using a 20x objective with phase contrast imaging. Immunofluorescent samples (left) taken using a 20x objective with anti-PCNA (red) used to identify proliferating cells and DAPI (blue) to identify cell nuclei.

Figure 4.11 displays representative bone marrow sections after H&E staining (left) and immunofluorescent staining for PCNA (red) and DAPI (blue). The round, white areas in H&E stained sections are the bone marrow sinuses. In the immunofluorescent sections, PCNA+ cells indicate actively proliferating cells. In the saline control, these cells are randomly distributed throughout the section. In the TP508-treated sections, a greater number of PCNA+ cells were visible, with some clustering near the bone marrow sinuses. This clustering effect was even more pronounced in the PEG5k-TP508- and PEG30k-TP508- treated samples.

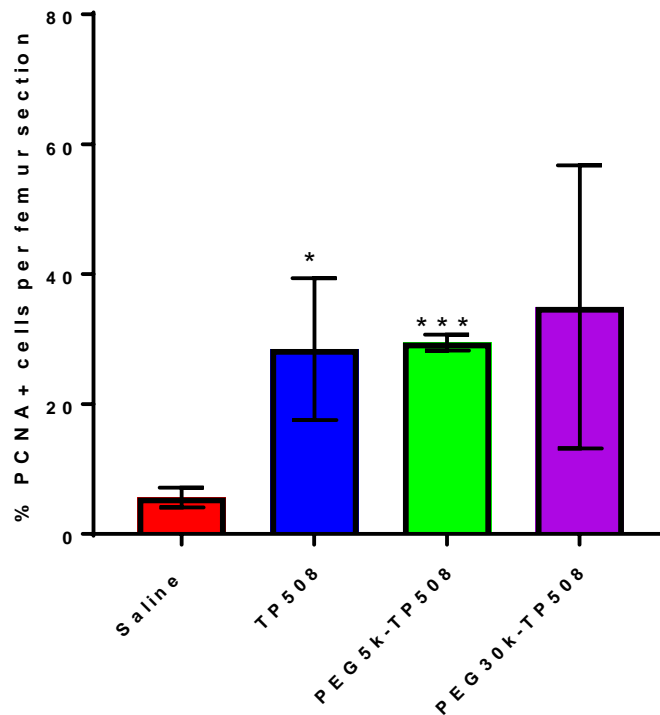


Figure 4.12 – Quantitation of PCNA+ cells in bone marrow sections from CD-1 mice 24h after TP508 pretreatment. Data presented as mean ± SD, * p<0.05, *** p<0.001.

Quantitation of these marrow samples was performed using ImageJ to determine percentage of PCNA+ cells in each field (n = 2 slides, 3 fields per slide). Figure 4.12 summarizes the quantitation results, presented as mean \pm SD. Red marrow from the saline control treatment had a mean of 5.6% PCNA+ cells. Actively proliferating cells in the TP508-treated samples was significantly increased to 28.5% (p=0.05, indicated by “*” in Fig. 4.12), an approximate 5-fold increase over saline control. The PEG5k-TP508-treated cells also displayed a significant increase in PCNA+ cells at 29.5% (p=0.002, indicated by “***” in Fig. 4.12). PEG30k-TP508-treated samples had a mean of 35% PCNA positive cells, but did not attain significance (p=0.099) with the small number of samples. The clustering around the bone marrow sinuses may indicate that these actively proliferating cells are migrating toward the sinuses for transport into the blood stream. Another hypothesis is that the bone marrow sinuses are the location where TP508 that has been administered systemically diffuses into the bone marrow, and thus the strongest proliferative effect is seen immediately surrounding the sinuses. These results are consistent with the hypothesis that TP508 represents the minimal sequence for a natural signal in wound healing which causes bone marrow stem cells to proliferate and mobilize cells for tissue repair.

D. EFFECT OF TP508 AND PEGYLATED TP508 DERIVATIVES ON HEALING OF WOUNDS IN IRRADIATED MICE

The results of the aortic ring assay after TP508 derivative administration in vivo offer compelling evidence that PEGylation enhances the biological activity of TP508 as an injectable drug in naïve mice. The next step in confirming the enhanced biological activity of the TP508 derivatives was to examine their effect on tissue repair in the radiation combined injury (RCI) mouse model that had been established in the Carney Laboratory. Ionizing radiation impairs cutaneous wound healing through a variety of mechanisms. Acute effects of ionizing radiation that impair wound healing include slowed proliferation of stem cells and fibroblasts (73-75), inflammation which is slow to resolve (76), and damage to the basement membrane (77). This phenomenon is highly clinically relevant, as both acute and delayed effects of ionizing radiation can affect surgical outcomes and overall health of patients undergoing radiation therapy.

This experiment used an established model of radiation combined with injury (RCI) summarized in Section 4I and Figure 4.13 (Olszewska-Pazdrak and Carney, Unpublished). Experiments using this model have demonstrated that 8 Gy irradiation of male CD-1 mice (LD50/30) followed by a full thickness 1.2 x 1.2 cm dorsal excision two days later significantly impairs the repair of full thickness excisional wounds relative to unirradiated sham controls. A single 100 µg TP508 injection (the same dosage as used for the aortic ring assay) administered 1 day post-irradiation restores about half of the wound healing rate lost by irradiation. This TP508 response is approximately half-maximal since injection of TP508 at doses of 500µg can fully restore normal rates of healing in this model

(Ozslowska-Pazdrak and Carney, unpublished). Use of TP508 at this half-maximal concentration provides a useful benchmark for comparison of the relative effectiveness of the TP508 derivatives in this model, as it allows for increased activity beyond that of the TP508 monomer in restoring wound healing. Therefore, 10 mice per treatment group were injected i.p. 24h after 8 Gy irradiation with either 100 μ L of 0.9% saline or saline containing 100 μ g (43.4 nmol) TP508 or 43.4 nmol of each of the TP508 derivatives. This was followed 24h later by surgical excision of a 1.2 x 1.2 cm dorsal full thickness section of skin. Wound areas were then imaged immediately after wounding (Day 0). An occlusive dressing was applied to cover the wound and prevent infection. The dressings were removed on Day 3 post-wounding, and images taken on Day 3, 5, 7, 10, 13 and 15 post-wounding. By Day 15, wounds in the sham irradiated animals near closure, setting the upper limit for useful data collection on wound healing rate.

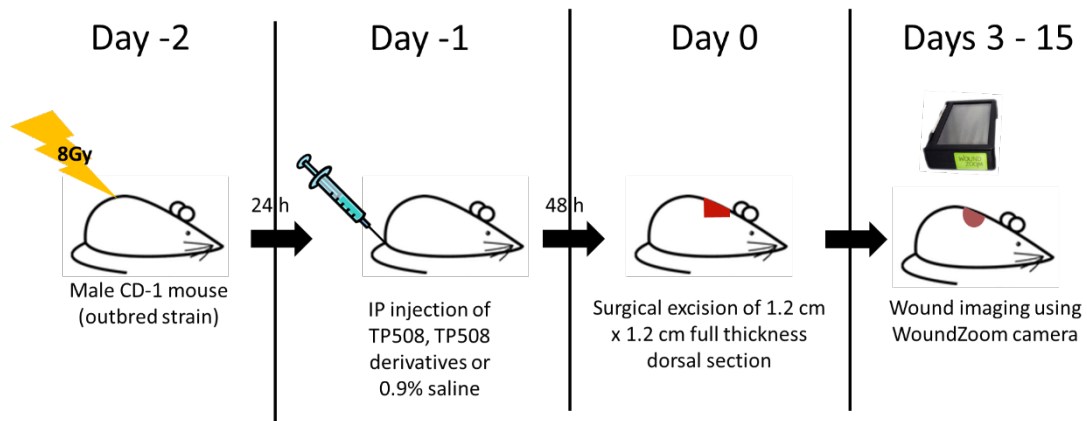


Figure 4.13 – Workflow for assessing wound closure rates in murine RCI model.

Representative images of wounds at Day 0, Day 5, Day 10 and Day 15 for each treatment are displayed in Figure 4.14. Wounds are nearly closed in the sham irradiated (0 Gy) saline control by Day 15, while the 8 Gy saline control wound is still approximately

half the size of the original wound. Note that substantial rounding from the original square defect is seen at Day 5 in the 8 Gy saline control, while the borders of the sham irradiated control are squarer, similar to the original wound shape. This is also the case with the TP508 and PEG5k-TP508 treatments, while the PEG20k-TP508 treatment has rounding similar to the 8 Gy saline control.

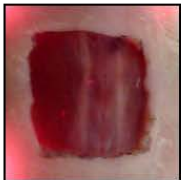
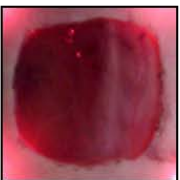
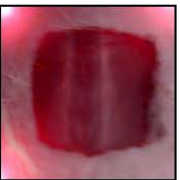
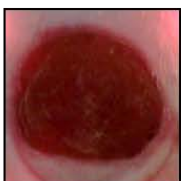
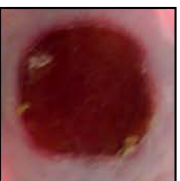
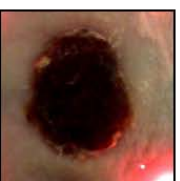
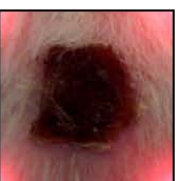
Treatment	Saline	Saline	TP508	PEG5k-TP508	PEG20k-TP508	PEG20k-C14-TP508	PEG30k-TP508
8 Gy Radiation	-	+	+	+	+	+	+
Day 0							
Day 5							
Day 10							
Day 15							

Figure 4.14 – WoundZoom images of from Day 0 – Day 15 in RCI model.

Wound areas calculated from WoundZoom images showed a slight increase from 1.44 cm² at Day 0 to ~ 1.6 cm² at Day 3 in the irradiated mice as the wound retracted and became rounder in response to surrounding muscular contraction and reduced tissue tension at the site of injury. From Day 3 – 15, however, mean wound areas reduced in a linear fashion (Figure 4.15). By Day 15, clustering of treatment results is once again visible, with PEG5k-TP508 and PEG30k-TP508 being similar to the TP508 treatment, while the PEG20k-TP508 and PEG20k-Cys14-TP508 treatments display wound closure similar to the 8 Gy saline control.

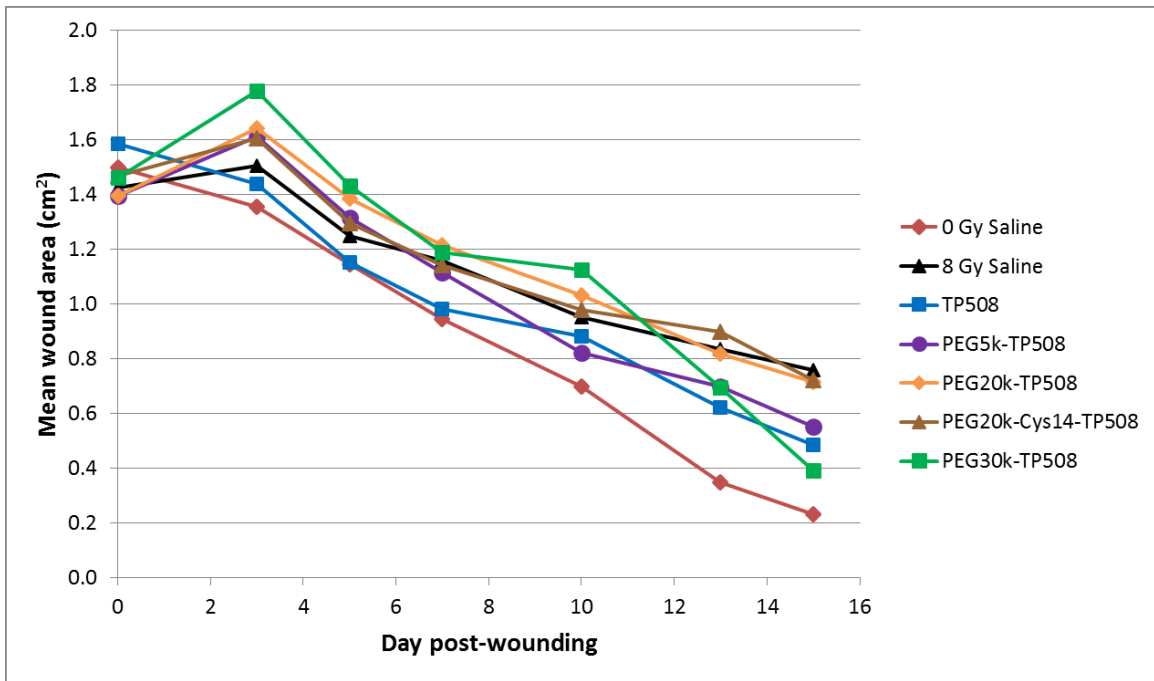


Figure 4.15 – Mean wound areas in RCI model at various days post-wounding. Male CD-1 were mice exposed to either sham (red) or 8Gy ionizing radiation followed by injection 24h later with 100 µL saline, 100 µg TP508 (blue) or the molar equivalent of each TP508 derivative. Mice received a 1.2 x 1.2 cm full thickness dorsal wound 48h after irradiation or sham irradiation. Wound areas for Day 0, 3, 5, 7, 10, 13 & 15 were determined using a WoundZoom camera and software.

Further investigation of the wound healing rate per day during the linear portion of wound closure from Day 3 -15 was performed using the linear regression function in SigmaPlot 12 to determine the wound closure rate per day. These results are summarized in Figure 4.16 as mean \pm SEM.

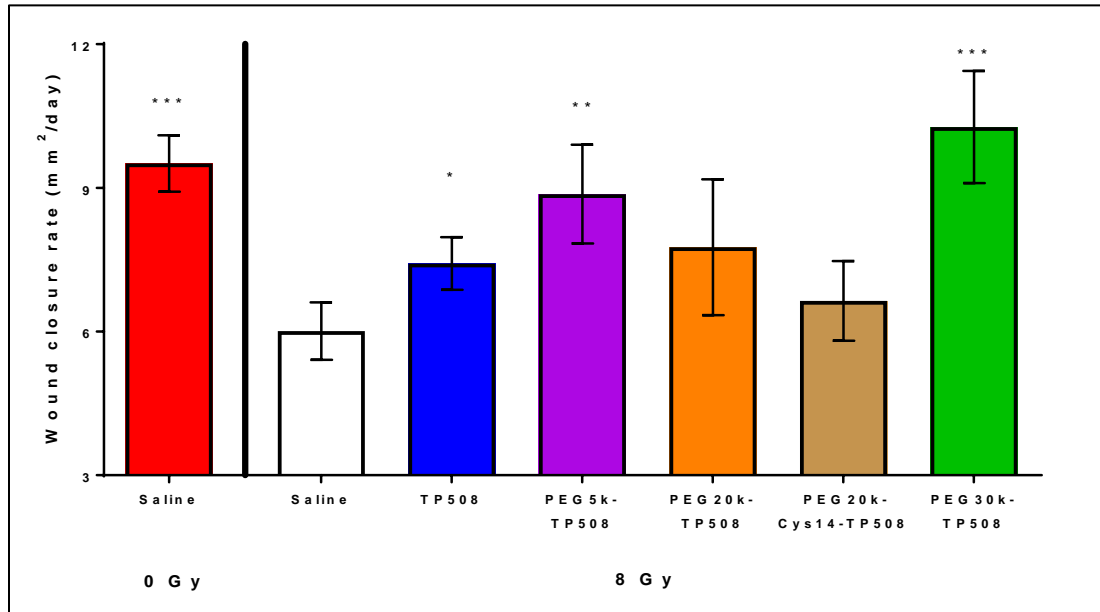


Figure 4.16 – Mean rate of wound closure per day in RCI model. Male CD-1 mice treated with sham irradiation (red) or 8 Gy ionizing radiation prior to injection 24h later with 100 μ L saline, 100 μ g TP508 (blue) or the molar equivalent of each TP508 derivative. Mice received a 1.2 x 1.2 cm full thickness dorsal wound 48h after irradiation or sham irradiation. Wound closure rate is calculated using linear regression of Wound areas calculated with WoundZoom imaging and software from images taken at Day 3, 5, 7, 10, 13 & 15 post-wounding. Wound closure rate presented as mean \pm SEM, * $p < 0.05$, ** $p < 0.01$, *** $p < 0.001$.

In the sham-irradiated control (0 Gy Saline, red bar), the mean rate of wound closure is 9.5 ± 0.6 mm²/day. This is significantly faster ($p < 0.001$) than the rate in the 8 Gy saline control, which has a mean wound closure rate of 6.0 ± 0.6 mm²/day, or 63% of the rate in the 0 Gy saline control. The 100 μ g TP508 treatment group increased wound

closure above the 8 Gy saline control to a rate of 7.4 ± 0.6 mm²/day ($p=0.043$). This is equivalent to restoring 40% of the wound closure rate that was impaired by 8 Gy ionizing radiation. Neither the PEG20k-TP508 derivative at 7.8 ± 1.4 mm²/day nor the PEG20k-Cys14-TP508 derivative at 6.6 ± 0.8 mm²/day had wound closure rates that were statistically different from the 8 Gy saline control. The PEG5k-TP508 and PEG30k-TP508 derivatives both accelerated wound healing above the 8 Gy saline control, with wound closure rates of 9 ± 1 mm²/day ($p=0.009$) and 10 ± 1 mm²/day ($p<0.001$), respectively. Thus, the wound closure rates in PEG5k-TP508 and PEG30k-TP508 groups was similar to that of the 0 Gy saline control. Note, however, that due to the greater retraction of wounds in the irradiated animals from Day 0 to Day 3 as compared to the sham irradiated animals, the sham irradiated animals had smaller wounds at Day 15 than any of the treatment groups in the 8 Gy irradiated animals.

In addition to the PEGylated TP508 derivatives, the 14-mer variant of TP508 (RGDACEGDSGGPFV) was also assessed for accelerated wound healing in 8 Gy irradiated CD-1 mice. It resulted in a 5 ± 1 mm²/day wound healing rate, similar to control, at the concentration equimolar to 100 μ g TP508. This variant was primarily evaluated to determine whether it could be used interchangeably with TP508 in systemic injection. This was of interest from a drug development standpoint because the shorter form can be manufactured by peptide synthesis more economically than full-length TP508. This would allow stockpiling of a greater number of doses of TP508 against nuclear incident. With the lack of activity above saline control in this assay, further development of the 14-mer was halted.

These wound closure results support those of the aortic ring assay for the *in vivo* biological activity of the TP508 derivatives after IP injection (Section 2, Chapter 4B). 43.4 nmol PEG5k-TP508 and PEG30k-TP508 (the molar equivalent of 100 µg TP508) both result in enhanced biological activity at levels similar to or better than TP508 at the same dosage, while the PEG20k-TP508 and PEG20k-Cys14-TP508 derivatives were not statistically different from saline control. These results indicate that increased PEG length and the resulting increase in biological half-life described earlier (Section 2 Chapter 3B) does not have a direct correlation with increased biological activity of TP508 demonstrated in this model. In the case of the PEG20k-Cys14-TP508 derivative, it may be that the covalent attachment to the Cys14 residue, located in the middle of the peptide sequence, causes the hydrodynamic volume of the PEG to sterically hinder access to the binding site of TP508, or causes a conformational change that drastically reduces the binding affinity of TP508. The PEG20k-TP508 derivative, on the other hand, has PEG attached to the same site as the PEG5k-TP508 and PEG30k-TP508 derivatives, which are both active. The question then becomes whether the steric hindrance and reduced binding affinity of PEG20k-TP508 is greater than the advantage conferred by its 6.8-fold increase in biological half-life, resulting in lower *in vivo* activity. Alternatively, the PEG20k-TP508 derivative might be even more active than the PEG30k-TP508 derivative, causing the dosage tested *in vivo* to be above the therapeutic window of TP508.

E. USE OF *IN VITRO* ASSAYS TO BETTER UNDERSTAND HOW STERIC HINDRANCE OF TP508 DERIVATIVES MAY EFFECT THEIR BIOLOGICAL ACTIVITY OR LACK THEREOF

To further investigate how conformational changes or steric hindrance of derivatives might affect activity, it is essential to develop an *in vitro* assay where plasma half-life is removed as a variable in assessing the biological activity of TP508 derivatives. Because of the successful utilization of the aortic sprouting *in vivo* assay, we chose to evaluate three types of assays that involved endothelial cells to identify an assay that demonstrated a significant TP508 dose response with sufficient magnitude of response to analyze the difference between activities of the various TP508 derivatives compared to native TP508. The three assays evaluated were: (1) an *in vitro* version of the aortic ring assay with automated quantification; (2) a quantifiable tube formation assay; and (3) an endothelial cell activation assay based on repair of radiation-induced DNA double strand breaks (DSB). The following sections describe the work leading to potential selection of one of these assays and its use in determining the *in vitro* activity of PEGylated TP508 derivatives.

E (1). DEVELOPMENT OF A QUANTITATIVE SEMI-AUTOMATIC *IN VITRO* AORTIC RING ASSAY

Initial assay development began with modifying the aortic ring assay for improved imaging and endothelial sprout quantitation. A key modification involved the use of Angiogenesis μ Slides from iBidi that use only 10 μ L of Matrigel in an inner chamber located at the bottom of each well to create a flat, thin section of extracellular matrix. When aortic rings are placed on top of the Matrigel and the upper chamber is filled with culture media, endothelial sprouting only occurs within the thin Matrigel layer, which allows the

entire sprouting network to be visualized in a single, phase contrast image. This, in turn, allows for automated counting of the sprouts using commercial programs or freeware developed at academic institutions.

Aortic rings were prepared as described in Section 4K. Because TP508 or the TP508 derivatives were added after ring preparation, rather than before, it was possible to add an overnight serum-starvation step to sync growth and reduce variability. Optimization experiments using iBidi Angiogenesis μ Plates were used to examine factors including whether ring position within the thoracic aorta or plating order affected sprouting results, as well as to determine whether there was a linear dose response to TP508. For both optimization and dose response experiments, TP508 was diluted in EGM2 media to achieve indicated concentrations, 50 μ L was added to each well prior to ring addition, and plates were incubated for 30 minutes at 37°C, 5% CO₂. After ring addition, plates were incubated for 48 hours prior to media change and then incubated for up to 10 days. It should be noted, however, that TP508 is anticipated to only be at therapeutically effective concentrations for a few hours before being degraded within the media (66).

Endothelial sprouting was delayed by 1 to 2 days using the *in vitro* treatment in the iBidi μ Plates as compared to the *in vivo* assay described previously (Section 2, Chapter 4B), with the exponential sprouting phase occurring between days 6 - 8. (See Figure 4.17 for *in vitro* and *in vivo* assay comparison). This may be due to a number of factors, including the serum starvation step in the *in vitro* assay used to sync cell growth, the reduced quantity of Matrigel, the single contact surface between Matrigel and the base of the aortic ring, which lessens the surface area from which sprouting may occur from aortic

tissue, and the delayed application of TP508 from 1 day prior to aorta isolation to 1 day post-isolation. Nevertheless, the sprouting appeared sufficient to work toward optimization.

One other item of note in evaluating the sprouting is that *in vitro* treatment with TP508 produces substantially thinner sprouts than are present with after *in vivo* dosing. Figure 4.23 compares sprouting from a ring treated with 100 μg TP508 *in vivo* (Fig. 4.17A), and one that has been treated with 1 $\mu\text{g}/\text{mL}$ TP508 *in vitro* (Fig. 4.17B) after 7 days incubation in the iBidi μSlides . The tube-like structures created with *in vivo* TP508 treatment are thicker and have several layers of cells, may have a visible lumen, and exhibit thickening at several junctions in the sprouting network. In contrast, the sprouts generated after *in vitro* treatment are generally only a single cell thick, with no layering at junctions in the sprouting network. This difference may be in part due to the serum starvation step incorporated in the *in vitro* assay, but might also be the result of enhanced pro-angiogenic priming of endothelial cells and/or pericytes.

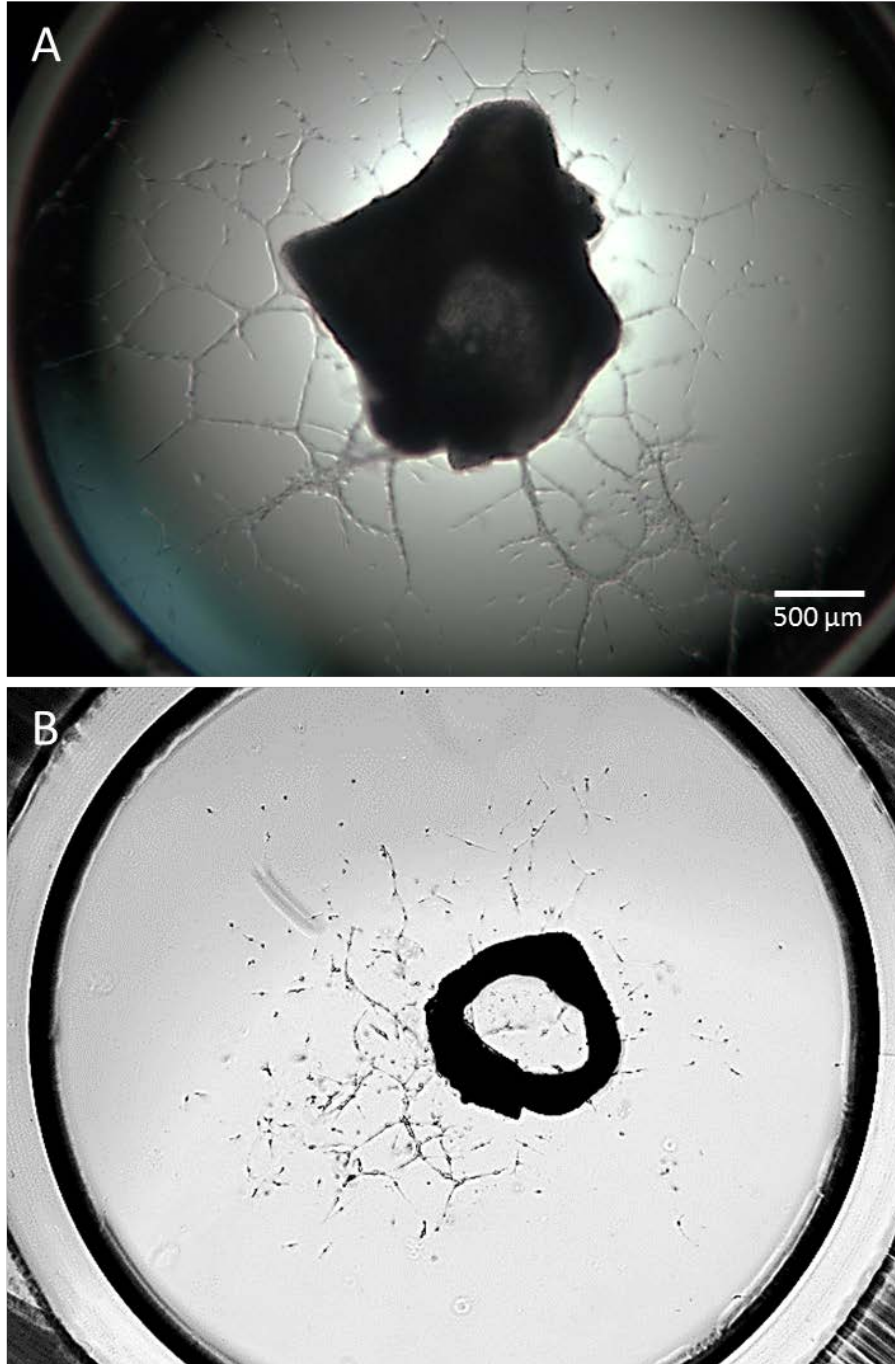
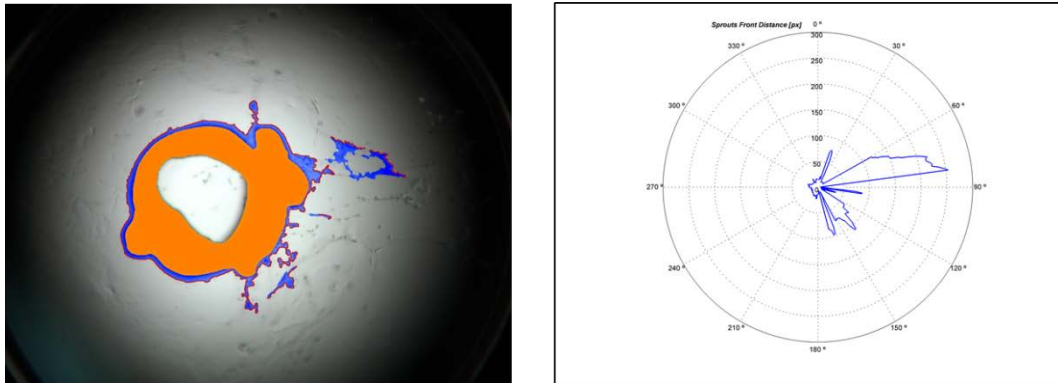


Figure 4.17 – Comparative aortic sprouting with *in vivo* and *in vitro* TP508 treatment. A) Aortic ring from male CD-1 mouse receiving i.p. injection of 100 µg TP508 24h prior to aorta harvest, after 7 days incubation in EGM2 media; B) Aortic ring from male CD-1 mouse treated with 1 µg/mL TP508 *in vitro*, after 7 days incubation in EGM2 media.

With the entire sprouting network visible in a single microscope image, several image analysis programs were evaluated for semi-automated analysis that would allow faster and more accurate processing of samples, as well as generating additional information such as total sprouting length for each image. Several programs exist for this analysis of endothelial tube networks, such as the Angiogenesis Analyzer plugin for ImageJ (78, 79), and the AngioTool program developed by the National Cancer Institute (80). These programs, however, were incapable of masking the aortic ring in the image and excluding it from the network analysis, leading to errors in identification of the endothelial sprouts. WimSprout software from Wimasis (Cordoba, Spain), which was developed specifically for evaluating endothelial networks sprouting from aortic tissue (81, 82) was also evaluated. For this analysis, images are uploaded to a server and then evaluated automatically by the WimSprout software. Figure 4.18 shows representative results from a test analysis of saline-treated (top) and 100 μ g TP508-treated (bottom) aortic rings using WimSprout. The images on the right of Fig. 4.18 show the images with color overlay of the portions of the image designated aortic ring (orange), endothelial sprouting area (blue) and endothelial sprouting perimeter (red). Images on the left of Fig. 4.18 illustrate the sprouting distance from the aortic ring and area of sprouting in a 360° plot. It can be seen in the overlay images on the right of Figure 4.18 that multiple endothelial sprouts (grey lines) have not been designated as such by the program, making it unsuitable for our assay.

Well B7 (saline), Day 7



Well E8 (TP508), Day 7

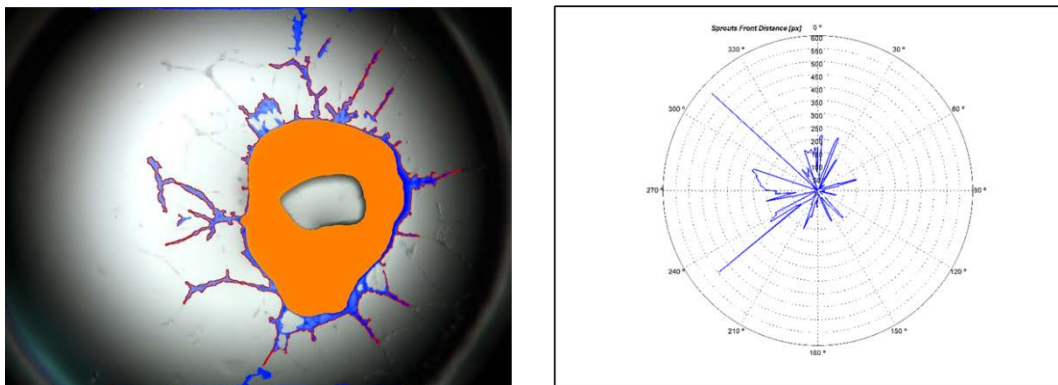


Figure 4.18 – WimSprout analysis of endothelial sprouting.

I next evaluated a macro written to utilize a program that had previously been used in our laboratory. ImagePro Plus 7.0 from Media Cybernetics (Rockville, MD) contains a macro for analysis of angiogenic sprouting submitted by Rebecca Blatt of the University of Virginia (83). This macro allows for automated analysis of the sprouting network after several manual user-defined steps, as illustrated in Figure 4.19. The first key step, shown in Figure 4.19A, is to manually trace the outline of the aortic ring in the phase contrast image (tracing in red), which then removes it from subsequent analysis. Figure 4.19B shows the subtraction mask of the phase contrast image, with the traced ring removed. In

this step, the sprouting area for analysis is user defined (red trace, Fig. 4.19B), allowing the user to exclude visual artefacts such as bubbles or debris from analysis. Figure 4.19C shows the resulting analysis of the subtraction mask for the sprouting network. The area of analysis is outlined in light green (same outline traced in red in Fig. 4.19B). Various diameter vessels are split into 4 classes, from small to large, colored in red, teal, dark green, and purple. Classification data for each image is exported in comma separated value (.csv) file format for analysis in Microsoft Excel. While this analysis provided a reasonable first pass, several inaccuracies were observed. The macro was developed for a higher magnification, and this resulted in multiple sprouts being excluded by analysis. The program also had a tendency to split a single branch into several sections rather than designating it as a single branch. In addition, vessel classes 2-4 had a tendency to overestimate vessel area, identify imperfections in the Matrigel as large vessels, and complicate Excel analysis by having 4 subclasses per image. Therefore, this macro was optimized for more accurate and simplified analysis by: 1) reducing the number of vessel classes to 2, incorporating class 3 & 4 vessel sizes into class 2; 2) decreasing the minimum area setting by 30% to identify smaller branches; 3) increasing the smoothing function to prevent intensity changes from causing a single branch to be split into multiple parts by analysis; and 4) incorporating a minimum major (long) axis requirement for analysis, also to ensure that single branches were not split into multiple parts. (See Appendix A & B for macro optimization). Figure 4.19D shows the image analysis with the optimized macro with identification of small endothelial branches and reduced sprouting area estimation.

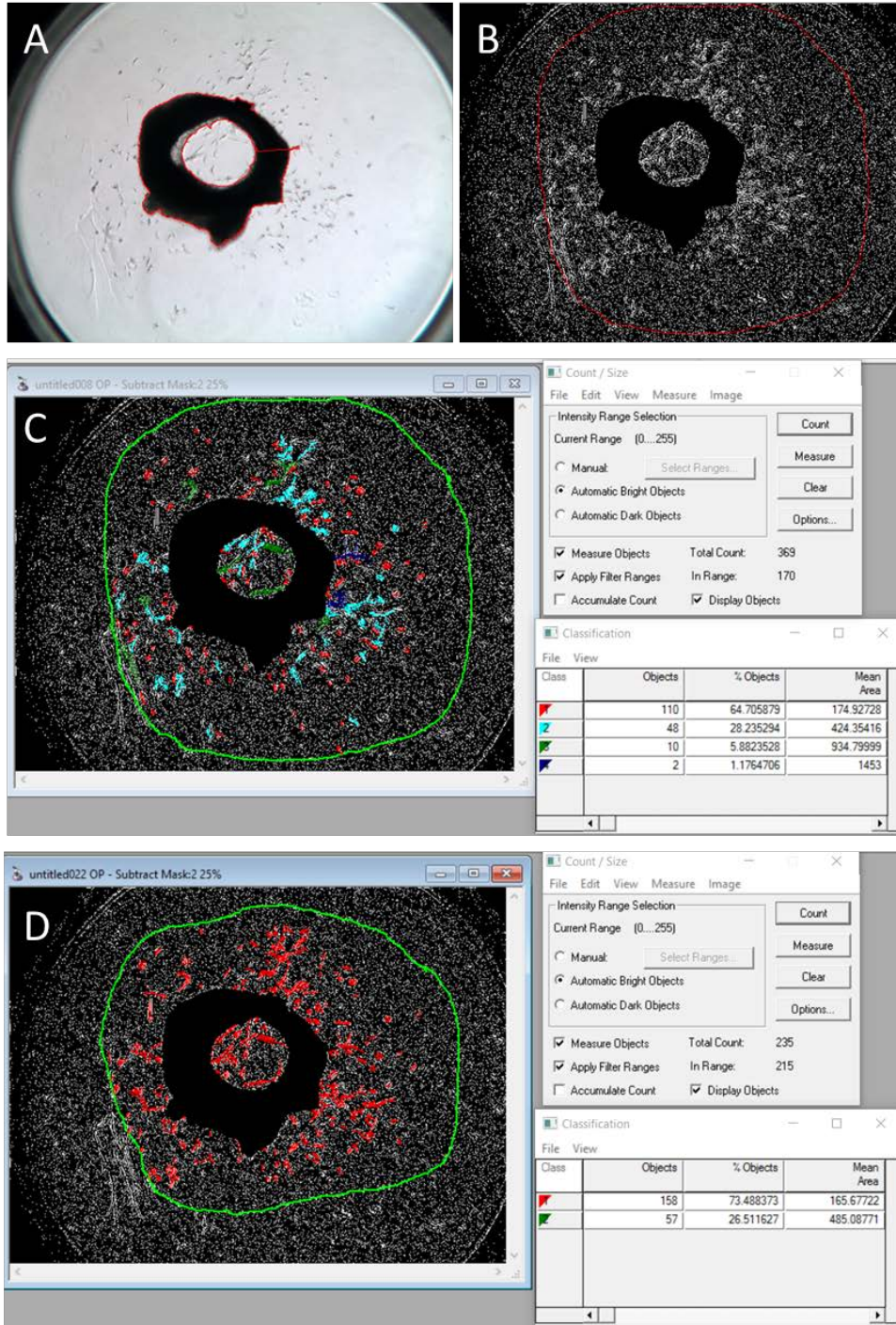


Figure 4.19 – Endothelial sprouting analysis using angiogenesis macro in ImagePro Plus 7.0. A) Aortic ring is traced (red line) for masking; B) Region of interest is defined on subtraction mask; C) Endothelial spots defined using original macro; D) Endothelial sprouts defined using optimized macro.

After endothelial sprouting quantitation, analysis of the various plating factors was performed. The first factor evaluated was ring position within the thoracic aorta, since variations in tissue thickness and composition might cause ring-to-ring variability in sprouting. Ring 1 position was standardized as the most proximal ring to the heart after the aortic arch had been completely removed from each thoracic aorta. Treatment was removed as a factor from this analysis by normalizing ring sprouting at Day 8 for each treatment. This was done by dividing the number of sprouts from each ring by the maximum number of sprouts seen for that treatment. Results are summarized in Figure 4.20. There is no strong positional trend effect on sprouting, with positions of maximal and minimal sprouting from each mouse aorta occurring at random ring positions. This indicates that, as long as the aortic arch is completely trimmed from the thoracic aorta before sectioning the aorta into rings for plating on Matrigel, no positional bias in sprouting should occur between rings.

The next factor evaluated was plating order. Plating each aortic ring to ensure that it is upright, contacting the Matrigel surface, and centered within the well can take up to 2 minutes per aortic ring, particularly as hydrophobic and electrostatic effects attract the ring to the sides of the well. This means that the rings can have a period of up to 30 minutes per mouse where they are at room temperature between 37°C incubation of the rings and incubation of the slide or plate. After plating the aortic rings from one mouse, the μ Plates were returned to the incubator for at least 10 minutes before plating rings from the next mouse. As seen in Figure 4.21, plating order had a strong effect on endothelial sprouting, with virtually all of the samples in Plate 1 having reduced sprouting as compared to Plate

2, which was only at room temperature twice for plating. This verifies that prolonged duration at room temperature has a deleterious effect on the sprouting potential of the aortic tissue.

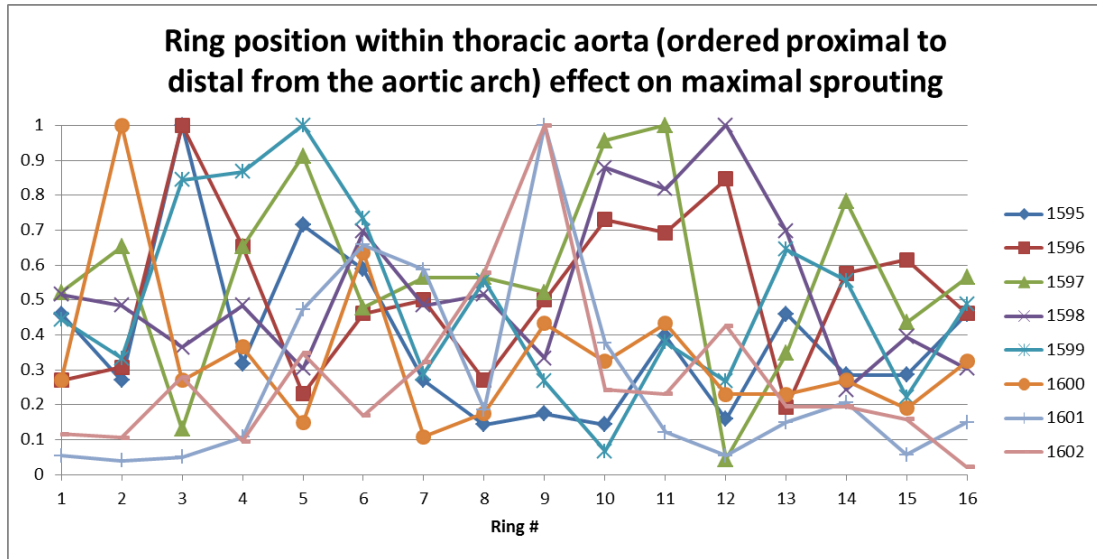


Figure 4.20 – Effect of aortic ring position within thoracic aorta on endothelial sprouting.

Aortic rings from mouse # 1595 and mouse # 1600 are the only ones within Plate # 1 that have sprouting above 50 sprouts per well. Since aortic rings for mouse #1595 were in column 1 & 2 of the 96-well plate, while those of mouse # 1600 were in column 11 & 12, these results are likely due to edge effects of the 96-well plate format. These edge wells are more prone to evaporation of media, particularly with long incubation times at elevated temperatures, and adjust to temperature changes more quickly than internal wells going between room temperature and 37°C incubation (84). Due to these effects, all future studies were carried out in 15-well μ Slides, to ensure that rings were never at room temperature for more than 30 minutes.

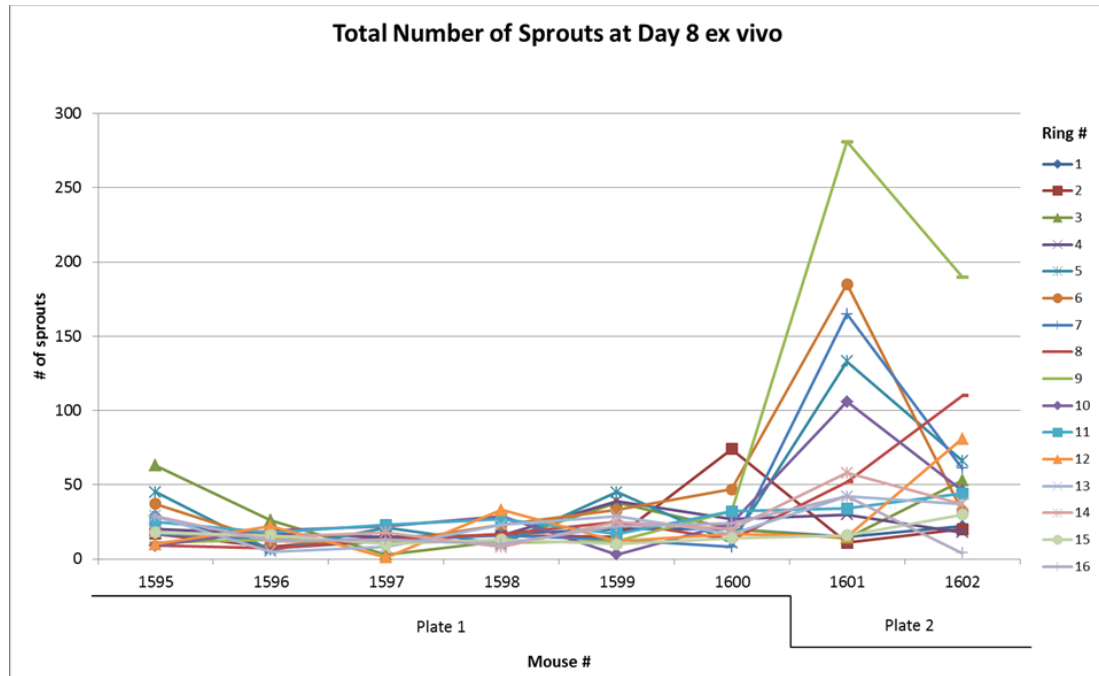


Figure 4.21 – Plating order effect on endothelial sprouting in the *in vitro* aortic ring assay.

Despite reduced sprouting activity due to plating order, the pro-angiogenic activity of TP508 was still evident. Figure 4.23 displays the number of endothelial sprouts per ring for each treatment at Day 6, 7 and 8, presented as mean \pm SEM. The 1 μ g/mL TP508 dose showed a statistically significant increase in sprouting on Day 6 ($p=0.006$) and Day 7 ($p=0.033$), and the 5 μ g/mL TP508 dose showed a statistically significant difference on Day 7. The 10 μ g/mL TP508 dose also trended higher than the saline control, but the 20, 50 and 100 μ g/mL TP508 doses resulted in sprouting levels similar to saline controls on all days evaluated. This suggests that TP508 has a near optimal *in vitro* dose of 1 μ g/mL in the aortic ring assay.

VEGF (recombinant human VEGF derived from Sf21, R & D Systems cat # 293-VE), was also evaluated as a positive control. Since VEGF is already present in the culture

media, a high dose of 250 ng/mL was used in an attempt to elicit a statistically significant maximal increase in sprouting. As shown, the 250 ng/mL VEGF control trended higher than the saline control on Day 6, but did not attain significance ($p=0.061$). The VEGF control was similar to saline control on Day 7 & 8. As a result, it is not recommended as a positive control at this concentration.

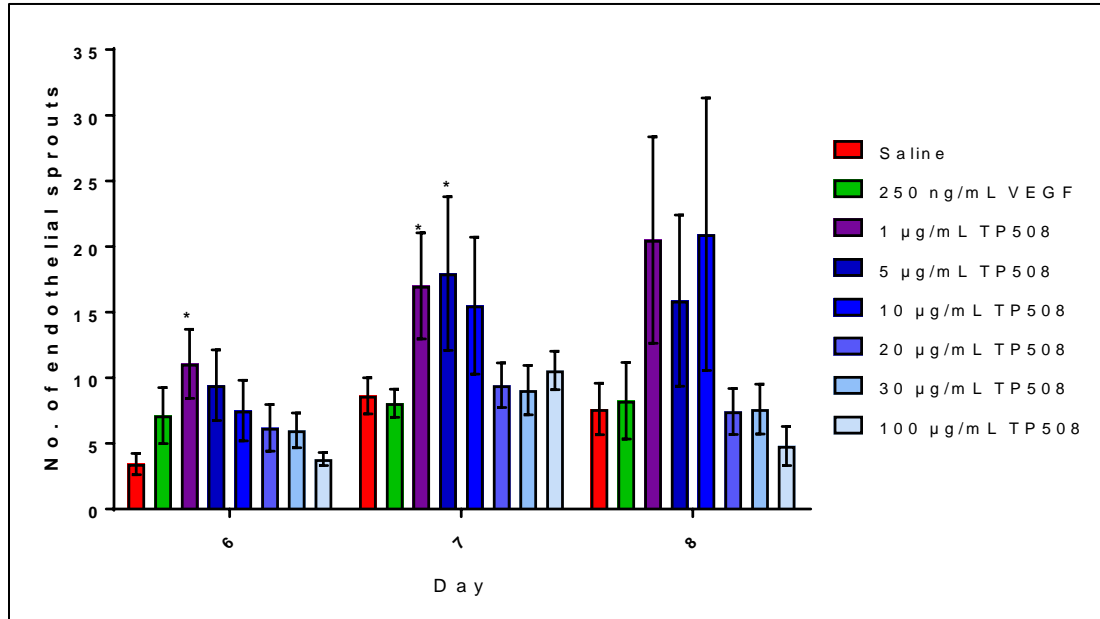


Figure 4.22 – Concentration dependent effect of TP508 dosage *in vitro* on endothelial sprouting in aortic ring assay. Aortic rings were prepared from naïve male CD-1 mice and serum starved overnight to sync growth. Rings were then cultured in iBidi μ Slides on growth factor reduced Matrigel with EGM2 media supplemented with 0.9% saline, 250 ng/mL VEGF, or various concentrations of TP508 for two days. Media was then exchanged for EGM2 alone and rings were cultured up to 8 days *in vitro*. Data presented as mean \pm SEM, $n = 16$, * $p < 0.05$.

Based on the significant increase in endothelial sprouting *in vitro* observed with TP508 concentrations of between 1 μ g/ml and 10 μ g/ml, this aortic ring assay was used to investigate optimal dosages for each of the TP508 derivatives. For each experimental

replicate, aortic rings from 7 mice were pooled for overnight serum starvation and then separated into $n = 3$ aortic rings for each concentration of TP508 or TP508 derivative tested ($n = 9$ aortic rings per treatment). Steric hindrance caused by PEGylation of the derivatives was expected to lower their specific activity compared to TP508. To cover the anticipated optimal dosage for each of the derivatives, a range equivalent to one order of magnitude below the optimal molar concentration of TP508 *in vitro* ($1 \mu\text{g/mL}$) through two orders of magnitude above the optimal concentration was selected for screening the activity of the TP508 derivatives.

Figure 4.23A summarizes the endothelial sprouting results at Day 7 for the mouse aortic ring assay of the TP508 derivatives based on the molar equivalent concentration of TP508 in $\mu\text{g/mL}$. Figures 4.23B – 4.23F show the results for TP508 and each derivative separately, presented as mean \pm SEM. Two-way ANOVA analysis of the data set was performed in GraphPad Prism 7.01, comparing endothelial sprouting results at each concentration to the saline control ($0 \mu\text{g/mL}$ TP508), using Dunnett's multiple comparison test to correct p-values for the multiple comparisons performed in this analysis.

The saline control (red circle, Fig. 4.23A) had a mean of 40 ± 7 sprouts by Day 7. TP508 (blue line, Fig. 4.23A, B) was used as a positive control, and assayed at concentrations of 0.1, 1, 5 and $10 \mu\text{g/mL}$. With these TP508 concentrations, only $1 \mu\text{g/mL}$ significantly increased endothelial sprouting with a mean of 87 ± 14 sprouts ($p = 0.015$). PEG5k-TP508 treatment (purple line, Fig. 4.23A, C) resulted in elevated (but not significant) sprouting across a range equivalent to $1 - 50 \mu\text{g/mL}$ TP508, with maximal sprouting at a molar equivalent of $50 \mu\text{g/mL}$ TP508. PEG20k-TP508 treatment (orange

line, Fig. 4.23A, D) resulted in elevated sprouting across a range equivalent to 5 – 100 $\mu\text{g/mL}$ TP508, with maximal sprouting at a molar equivalent of 50 $\mu\text{g/mL}$ TP508 (mean of 100 ± 30 sprouts, $p = 0.013$). PEG20k-Cys14-TP508 (brown line, Fig. 4.23A, E) treatment had only slightly elevated sprouting over saline control at the 30 and 50 $\mu\text{g/mL}$ TP508 equivalent concentrations, but none were statistically significant. PEG30k-TP508 treatment (green line, Fig. 4.23A, F) resulted in elevated sprouting across a range equivalent to 1 – 30 $\mu\text{g/mL}$ TP508. PEG30k-TP508 treatment resulted in maximal sprouting at the molar equivalent of 1 $\mu\text{g/mL}$ TP508, with a highly significant increase over saline control at a mean of 110 ± 30 sprouts (adjusted p -value of 0.0004).

Although TP508 and PEG30k-TP508 both showed significant stimulation of endothelial sprouting at molar equivalent concentrations of 1 $\mu\text{g/mL}$, the results with other derivatives did not agree with the *in vivo* wound healing or angiogenesis results. In addition, it appeared that PEG20K-TP508 had activity at high molar concentrations where it appeared to have no activity in previous *in vivo* assays. In addition, results showed only a 2-fold increase in endothelial sprouting and had a considerable amount of variability, making it difficult to interpret the dose responses. A potential weakness of this assay is that the media containing TP508 and the TP508 derivatives is incubated with the aortic tissue for two days before being changed. This step is necessary to minimize rings lifting off the Matrigel surface prior to endothelial sprouting into the Matrigel, but allows for potential confounding factors such as differences in degradation rate between the TP508 derivatives. The decision was therefore made that additional investigation into specific activity of the

TP508 derivatives *in vitro* was necessary using assays where TP508 effects could be measured more directly within hours of treatment rather than after seven days.

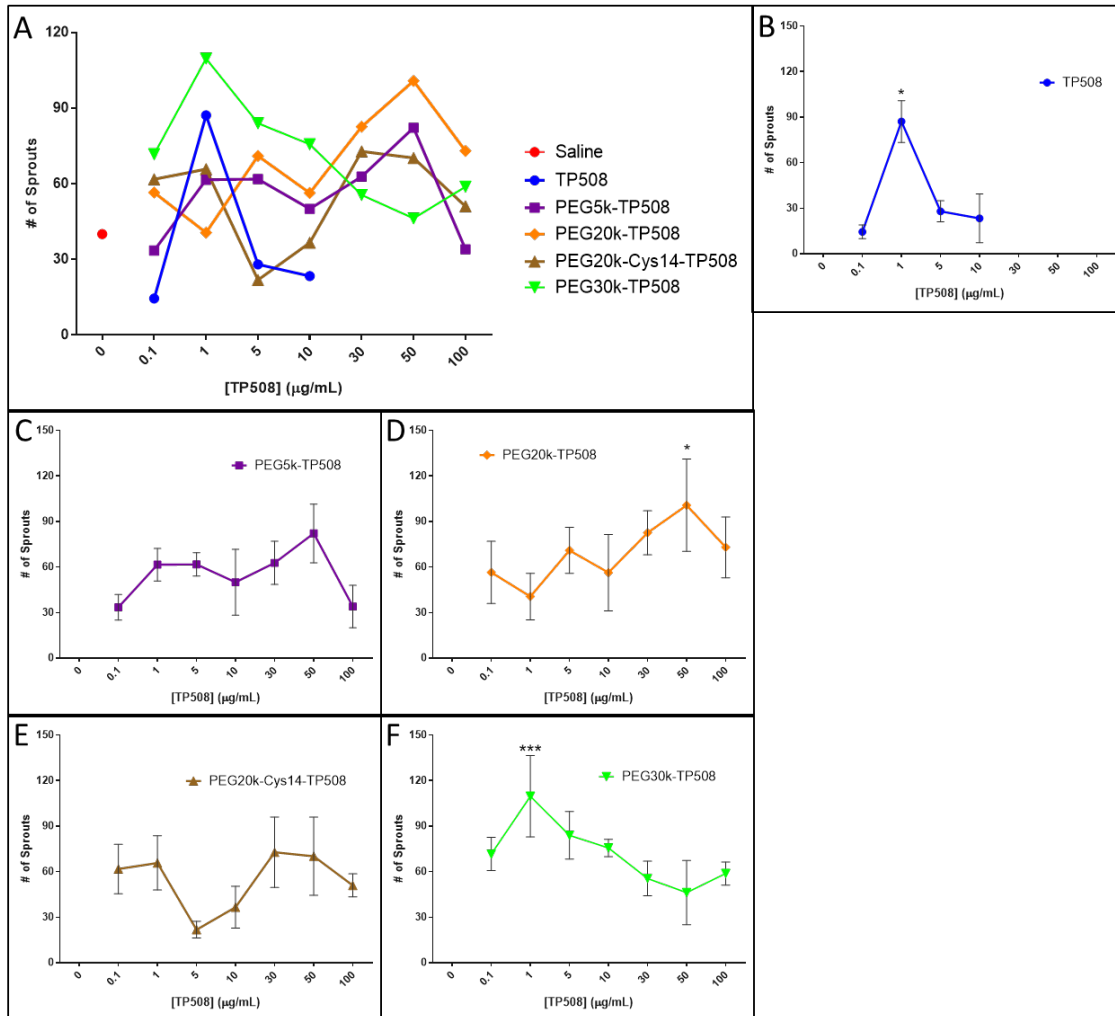


Figure 4.23 – Endothelial sprouting activity profile of TP508 and TP508 derivatives using *in vitro* dosing in the mouse aortic ring assay. Aortic rings were prepared from naïve male CD-1 mice and serum starved overnight to sync growth. Rings were then cultured in iBidi µSlides on growth factor reduced Matrigel with EGM2 media supplemented with 0.9% saline, or various concentrations of TP508 or TP508 derivatives for two days. Media was then exchanged for EGM2 alone and rings were cultured up to 8 days *in vitro*. A) Combined plot of mean number of sprouts at each concentration of TP508 and the TP508 derivatives; Endothelial sprouting profile presented as mean \pm SEM for B) TP508, C) PEG5k-TP508, D) PEG20k-TP508, E) PEG20k-Cys14-TP508, and F) PEG30k-TP508. $n = 9 - 15$ rings, * $p < 0.05$, *** $p < 0.001$.

E (2). DEVELOPMENT OF A QUANTITATIVE ENDOTHELIAL TUBE FORMATION ASSAY

The endothelial tube formation assay is similar to the aortic ring assay, but uses endothelial cells seeded onto Matrigel in place of the aortic rings. These cells begin to elongate and form endothelial tube networks after approximately 2h incubation, with the networks becoming more defined and extensive over a period of up to 16h (85). Thereafter the networks begin to fall apart, with network junctions separating and tube segments shortening. As a result, this assay possesses advantages over the aortic ring assay for studying various aspects of angiogenesis as it does not require the use of animals and pro-angiogenic effects may be observed in a shorter time period.

A number of studies have shown that pericytes function as support cells to enhance endothelial tube formation and stabilize the resulting endothelial network (86-88). Pericytes also share many of the characteristics of adipose-derived stem cells (89) that have previously been demonstrated to be stimulated by TP508 (23). We therefore decided to examine the effect of TP508 on primary human dermal microvascular endothelial cells (HDMECs) alone, and in pericyte:HDMEC co-cultures at ratios of 1:1, 1:10, and 1:100 (approximating those seen *in vivo* at the capillary level) (90-92). Microvascular endothelial cells were used in preference to other endothelial cell lines such as human umbilical vein endothelial cells (HUVECs) for biological relevance as angiogenesis and remodeling in response to wounding primarily occurs in the microvasculature (93).

Figure 4.24 contains representative images of untreated HDMEC alone beginning to group together and beginning to elongate at 2.5h, creating more elongated tubes and beginning to form endothelial tube networks by 4.5h, and then forming mature networks by 16h.

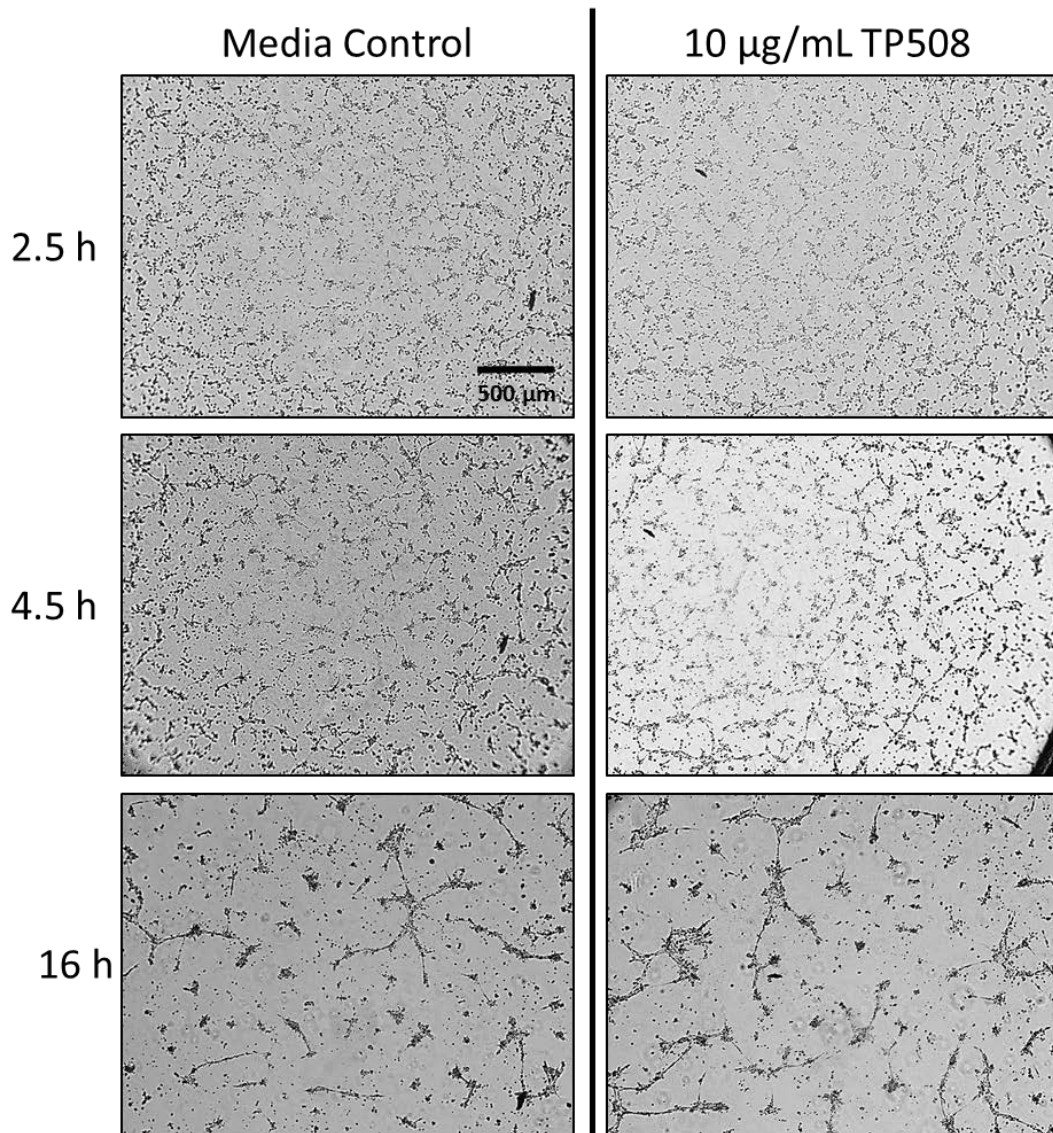


Figure 4.24 – Endothelial tube formation in HDMEC alone.

Of the various pericyte:HDMEC ratios tested, only the 1:100 ratio demonstrated enhanced tube formation in response to TP508. At this ratio, the morphology of the endothelial tube network at 16h, shown in Figure 4.25, is very similar to HDMEC alone. At the 1:10 pericyte:HDMEC ratio, clumps of cells begin to appear at the tube network junctions and tube network formation was somewhat reduced, while at the 1:1 pericyte:HDMEC ratio, extensive clustering of cells was observed, with little to no tube network formation.

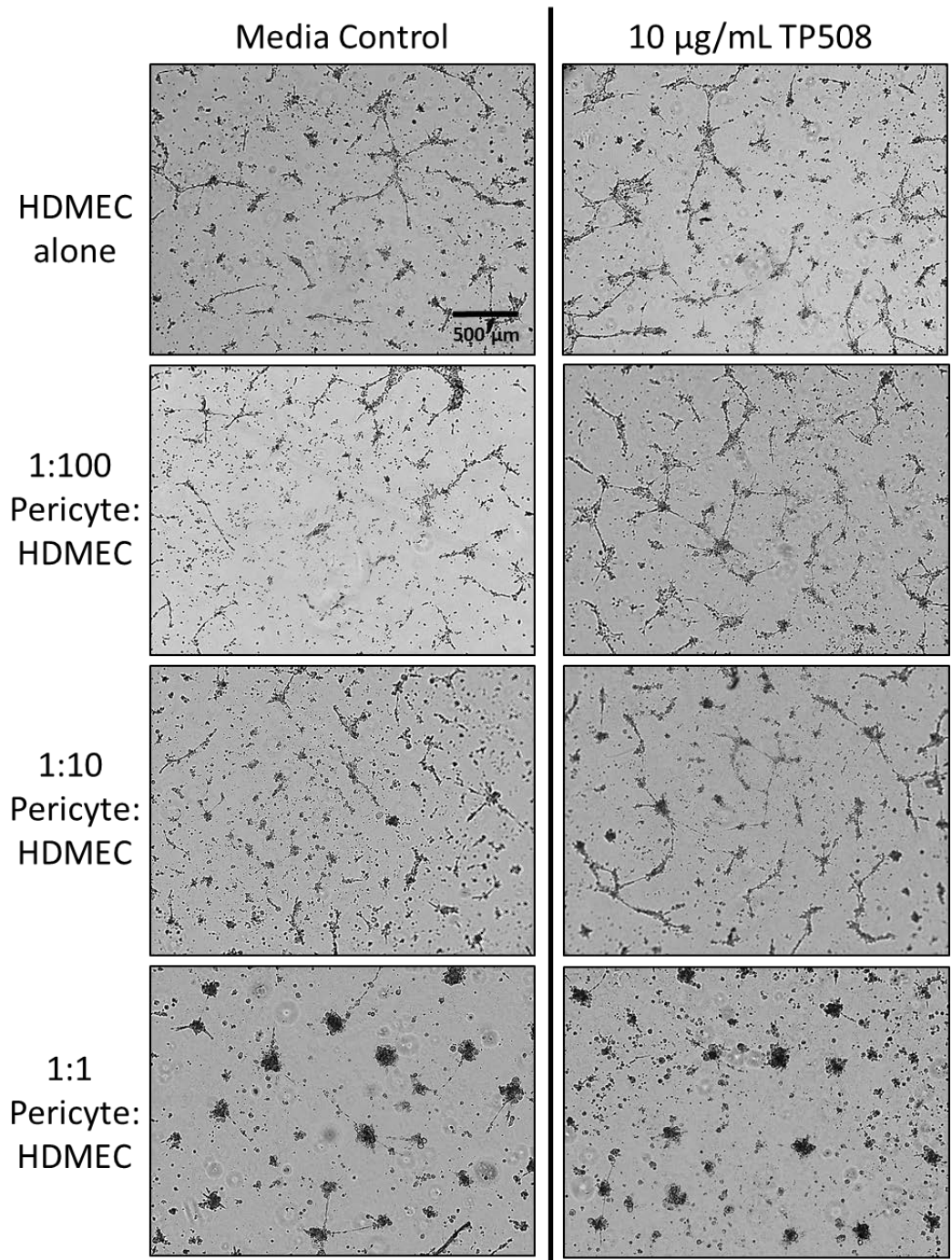


Figure 4.25 – Endothelial tube formation at 16h in HDMEC alone and in co-culture with pericytes at ratios of 1:100, 1:10 and 1:1 pericyte:HDMEC.

Quantitation of the total tube length formed at the 2.5, 4.5 and 16h time points is summarized in Figure 4.26 for experiments using a 1:100 pericyte:HDMEC co-culture. It is the summary of two separate experiments, n = 3 replicates per treatment per experiment, presented as the fold increase in tube formation over media control as mean \pm SD. Both 1 μ g/mL and 10 μ g/mL TP508 significantly increased endothelial tube formation at each time point. The 1 μ g/mL TP508 treatment increased tube formation 1.36 ± 0.07 fold over media control at 2.5h (p=0.004), 1.36 ± 0.02 at 4.5h (p<0.001), and 1.67 ± 0.07 fold at 16h (p=0.04). The 10 μ g/mL TP508 treatment had similar results, increasing tube formation 1.4 ± 0.1 fold over media control at 2.5h (p=0.012), 1.36 ± 0.02 at 4.5h (p<0.001), and 2.03 ± 0.03 fold at 16h (p=0.011). At the highest concentration of TP508 tested, 30 μ g/mL, no significant differences in tube formation from media control were observed, suggesting that this concentration is above the therapeutic window for the pro-angiogenic activity of TP508.

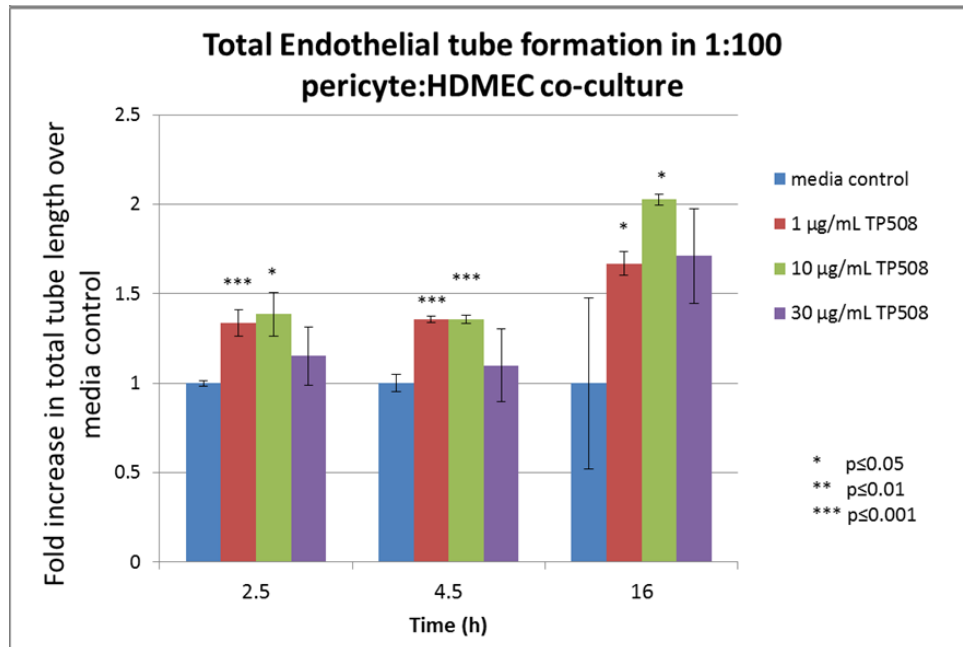


Figure 4.26 – Quantitation of fold increase in total tube length in 1:100 pericyte:HDMEC co-culture. Data presented as mean \pm SD, * $p < 0.05$, *** $p < 0.001$.

After establishing that TP508 enhances endothelial tube formation in 1:100 pericyte:HDMEC co-cultures in unirradiated cells, this assay was performed using cells exposed to 3 Gy ionizing radiation prior to plating on μ Slides to determine if the radiomitigation properties of TP508 extend to protecting the ability of these cells to form endothelial tubes after exposure to ionizing radiation. Figure 4.27 illustrates the differences in tube formation in unirradiated cells at 18h for saline control (Fig. 4.27A) and 10 μ g/mL TP508 treatment (Fig. 4.27B) versus cells exposed to 3 Gy ionizing radiation 1h before initiating the tube formation assay with saline control (Fig. 4.27C) and 10 μ g/mL TP508 treatment (Fig. 4.27D). Images show the entire well using phase contrast imaging with a 2.5x objective (25x magnification total). The 3 Gy ionizing radiation exposure almost completely prevents endothelial tube network formation in the saline control, with

mainly short segments with 2 – 3 branches visible. By contrast, the TP508-treated cells still form an endothelial tube network, though it is less extensive than in unirradiated cells, and contains larger clumps of cells that have not elongated in response to the culture conditions. Figure 4.27E compares the mean length of endothelial tube formation in the 3 Gy irradiated cells between the saline and 10 $\mu\text{g}/\text{mL}$ TP508 treated groups, presented as the mean \pm SD from two experiments with 2-3 replicates per experiment. The saline-treated cells only formed 3.63 ± 0.04 mm of endothelial tubes per well, as compared to 5.7 ± 0.2 mm for the 10 $\mu\text{g}/\text{mL}$ TP508 treatment, a significant increase ($p=0.0007$) of 57%.

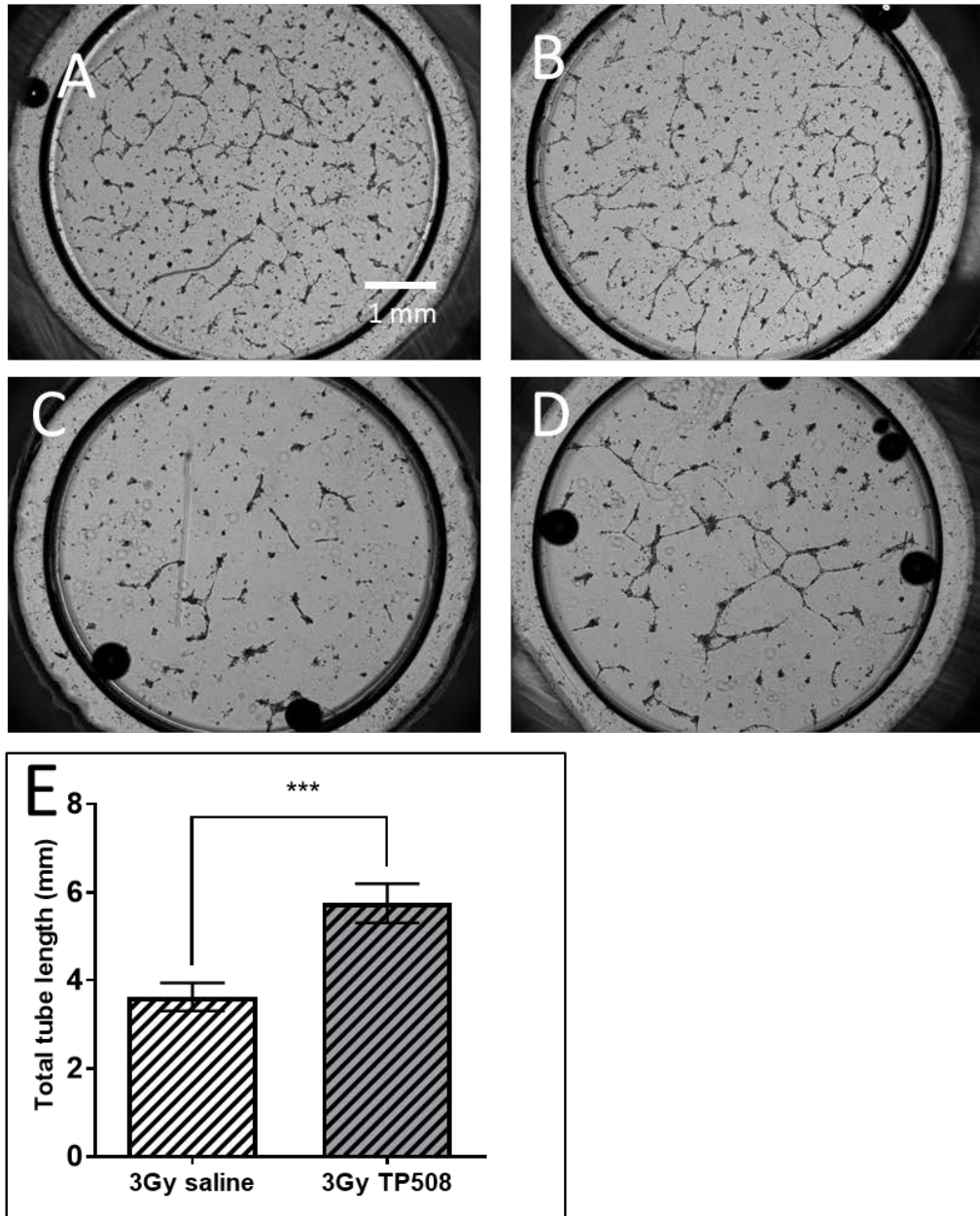


Figure 4.27 – TP508 treatment maintains the capacity of 1:100 pericyte:HDMEC co-cultures to form endothelial tube networks following 3 Gy ionizing radiation. Endothelial tube formation in 1:100 pericyte:HDMEC co-cultures at 18h A) Saline treatment, unirradiated cells; B) 10 µg/mL TP508 treatment, unirradiated cells; C) Saline treatment, 3 Gy ionizing radiation; D) 10 µg/mL TP508 treatment, 3 Gy ionizing radiation; E) Comparison of total tube length in 3 Gy irradiated co-cultures with saline or 10 µg/mL TP508 treatment, presented as mean ± SD, *** p < 0.001.

Although the data from the human microvascular endothelial cell tube assay confirmed that TP508 enhances angiogenic tube formation in pericyte:HDMEC co-cultures, the timing of the assay and necessity for pericyte co-culture make this a difficult assay to perform consistently. This makes the assay difficult to validate for use to evaluate differences between activities of TP508 derivatives or for future validation of commercial preparations. Therefore, we evaluated to a third type of endothelial assay that shows a rapid response to TP508 *in vitro* for these determinations.

E (3). DNA DOUBLE STRAND BREAK REPAIR

Recent studies conducted at Chrysalis BioTherapeutics showed that TP508 stimulates repair of radiation-induced DNA damage in primary cultures of human mesenchymal stem cells (hMSCs) (Rayavara, et. al., Manuscript in preparation). Ionizing radiation causes DNA double stranded breaks (DSBs) that must be repaired for cells to replicate and survive. These double strand breaks induce a number of events within cells leading to either repair or apoptosis of the cells. One of the early events in DNA DSB repair is the phosphorylation of histone H2AX (γ H2AX). γ H2AX localizes to DSB sites for recruitment of DNA repair proteins, causing foci which can be observed by immunofluorescence, as per Section 4M. These foci occur within minutes of exposure to ionizing radiation and their intensity and number decrease as DSBs are repaired.

The first goal in assessing the γ H2AX assay was to determine whether TP508 also accelerated repair of DNA DSB in HDMEC, and if so, if there was a dosage dependence that could be used to compare the relative specific activity of the various TP508 derivatives *in vitro*. HDMEC were pretreated with TP508 at doses of 0.05 and 0.2 mg/mL (doses chosen based on hMSC results) 1h prior to receiving 3 Gy ionizing radiation and were then

incubated at 37°C, 5% CO₂ until repair was halted by formalin fixation at 1, 5, 9 and 24h post-irradiation. This is the same radiation dosage which disrupted endothelial tube formation in Section 2, Chapter 4E (2).

The number of γ H2AX foci per nucleus were quantified using the CellProfiler program (94, 95) that determines nuclear outlines from DAPI channel images and then uses these outlines as a mask for the corresponding Alexa 488 channel immunofluorescent images of the γ H2AX foci. Representative images of the HDMEC nuclear outlines (blue) overlaid on the Alexa 488 channel images (γ H2AX foci outlined in green) at 1, 5, 9 and 24h post-3 Gy ionizing radiation are shown in Figure 4.28. From these images, it can be observed that the number of foci per nucleus is reduced at each timepoint as DSB are repaired. By 24h after 3 Gy ionizing radiation, the majority of the HDMEC have no γ H2AX foci, with a few cells still displaying a number of foci similar to 5 or 9h levels. From these images it also appears that TP508 accelerates DSB repair with fewer foci per cell nucleus after 5h, and 9h (Figure 4.30).

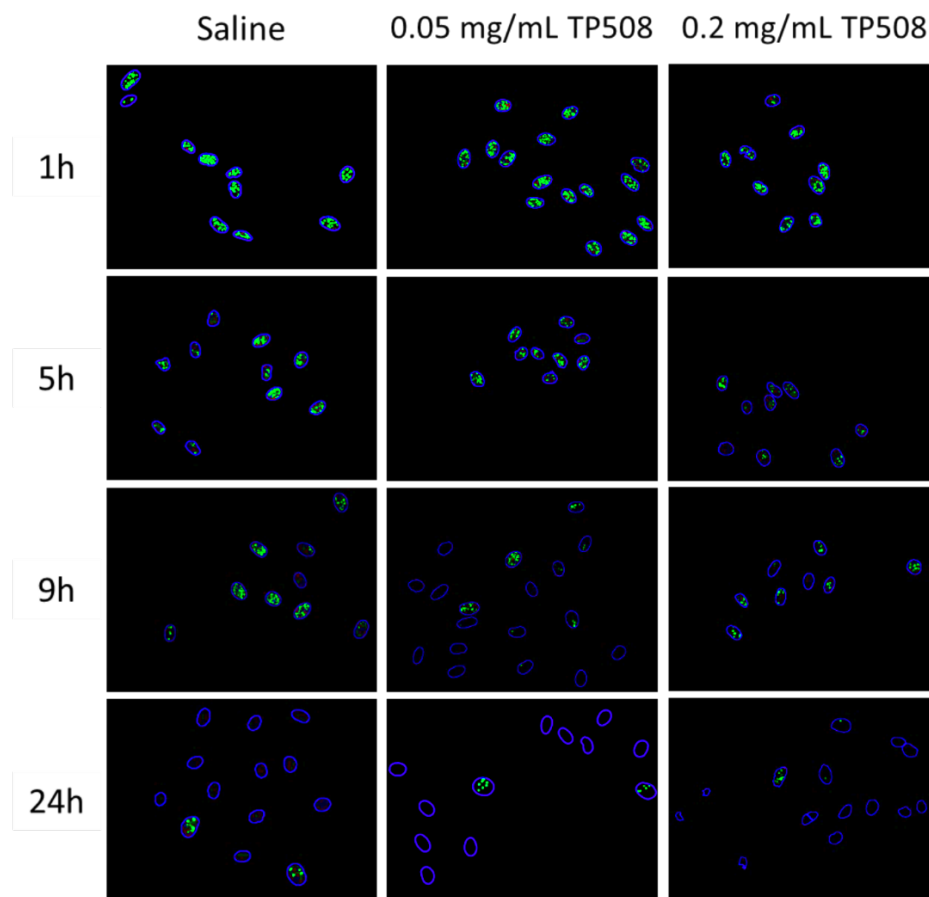


Figure 4.28 – CellProfiler overlay of nuclear outlines (blue) on images of γ H2AX foci (green) in HDMEC after 3 Gy ionizing radiation.

Imaging was performed on 3 replicates per condition, using 4 – 10 fields per replicate to provide 100 to 400 nuclei for quantitative analysis. Statistical analysis of these rigorous data sets was performed in GraphPad Prism 7.01, using 1-way ANOVA with Dunnet’s multiple comparisons test to adjust p-values for the multiple comparisons of each TP508 treatment to the saline control at the same timepoint. Figure 4.29 shows the number of γ H2AX foci per nucleus at each timepoint in HDMEC after 3 Gy ionizing radiation,

presented as mean \pm 95% confidence interval (CI). Using 95% CI error bars, any comparison between means where the error bars do not overlap represents a significant difference ($P=0.05$) between the means.

As shown in Figure 4.29, with the 0.05 mg/mL TP508 treatment 1h prior to 3 Gy irradiation, only the 1h timepoint had a significant reduction in the number of foci per nucleus with 11.1 foci/nucleus, as compared to 13.6 for the saline control (adjusted p-value of 0.022). The 0.2 mg/mL TP508 pretreatment, by comparison, had highly significant reductions in the number of foci per nucleus as compared to the saline control at 5h and 9h. At 5h, the 0.2 mg/mL TP508 pretreated HDMEC have a mean 2.6 foci/nucleus, compared to 7.0 foci per nucleus for the saline control (adjusted p-value <0.0001). This is equivalent to a reduction of 80% of the foci from the 1h timepoint, versus 49% for the saline control. At 9h, the 0.2 mg/mL TP508-pretreated HDMEC a mean 1.5 foci/nucleus, significantly reduced from the 6.5 foci/nucleus of the saline control at this timepoint (adjusted p-value <0.0001). By 24h, the saline control and both TP508 pretreatment concentrations all have similar means of ~ 1.5 foci/nucleus.

A residual level of γ H2AX foci persisting in human cells 24h or more after ionizing radiation, after DSB repair is complete, is regularly reported in literature (96-98). Since the 9h timepoint for 0.2 mg/mL TP508-pretreated HDMEC has the same number of foci per nucleus as the 24h timepoint, DSB repair may already be complete in these cells by the 9h timepoint.

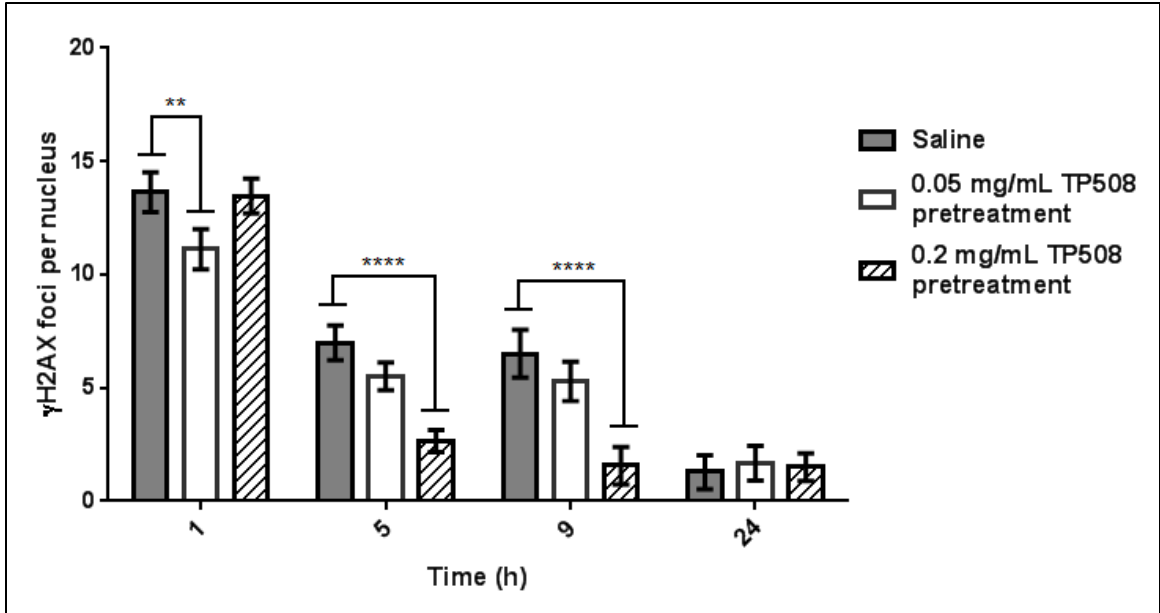


Figure 4.29 – Quantitation of γ H2AX foci per nucleus in HDMEC after 3 Gy ionizing radiation. HDMEC cultured on glass coverslips in EGM2 media were pre-treated with 0.9% saline or either 0.05 or 0.2 mg/mL TP508 1h prior to receiving 3 Gy ionizing radiation. Immunofluorescent imaging of samples fixed at 5h post-irradiation performed using anti- γ H2AX antibody to identify foci and DAPI to identify nuclei. Data presented as mean \pm 95% confidence interval, ** $p < 0.01$, **** $p < 0.0001$.

These experiments were repeated with HDMEC exposed to 6 Gy ionizing radiation. As radiation intensity is increased, the number of foci/nucleus increases in a linear relationship, generating a larger dynamic range to observe differences in DSB repair levels. Since DSB repair occurred so rapidly in the 3 Gy experiment, a 2.5h timepoint was added in place of the 24h analysis. Figure 4.30 shows representative images of the HDMEC nuclear outlines (blue) overlaid on the Alexa 488 channel images (γ H2AX foci outlined in green) at 1, 2.5, 5 and 9h post-6 Gy irradiation.

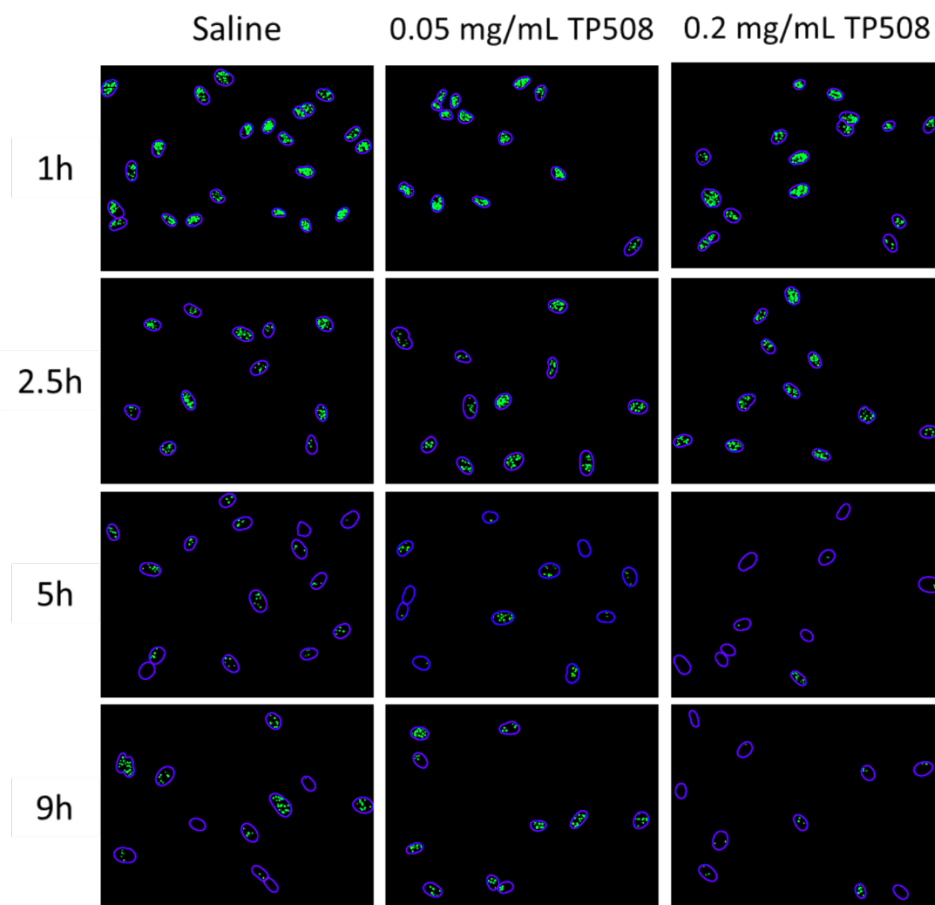


Figure 4.30 – CellProfiler overlay of nuclear outlines (blue) on images of γ H2AX foci (green) in HDMEC after 6 Gy ionizing radiation.

Quantitation of the number of γ H2AX foci per nucleus in HDMEC after 6 Gy of ionizing radiation exposure is shown in Figure 4.31. At 1h, the saline control HDMEC had a mean of 22.7 foci/nucleus, which is approximately 70% more foci per nucleus than observed at the same timepoint using 3 Gy IR. Both TP508 pretreatment doses had the same number of foci/nucleus as the saline control at the 1h timepoint. At the 0.05 mg/mL TP508 dose, the number of foci/nucleus at any of the later timepoints did not significantly differ from the saline control, indicating that this dose was insufficient to enhance DNA repair *in vitro*. The 0.2 mg/mL TP508 pretreatment, however, resulted in highly significant reductions in foci/nucleus at the 2.5, 5 and 9h timepoints. At 2.5h, 0.2 mg/mL TP508 pretreatment reduced the mean number of foci per nucleus to 11.4, versus 19.4 for saline control (adjusted p-value <0.0001). By 5h, 0.2 mg/mL TP508 pretreatment reduced the mean number of foci per nucleus to 7.0, versus 9.9 for saline control (adjusted p-value 0.0002). At the 9h timepoint, the 0.2 mg/mL TP508 pretreatment resulted in a mean of 2.1 foci/nucleus, suggesting nearly complete repair of DSBs, as compared to 6.0 foci/nucleus in the saline control.

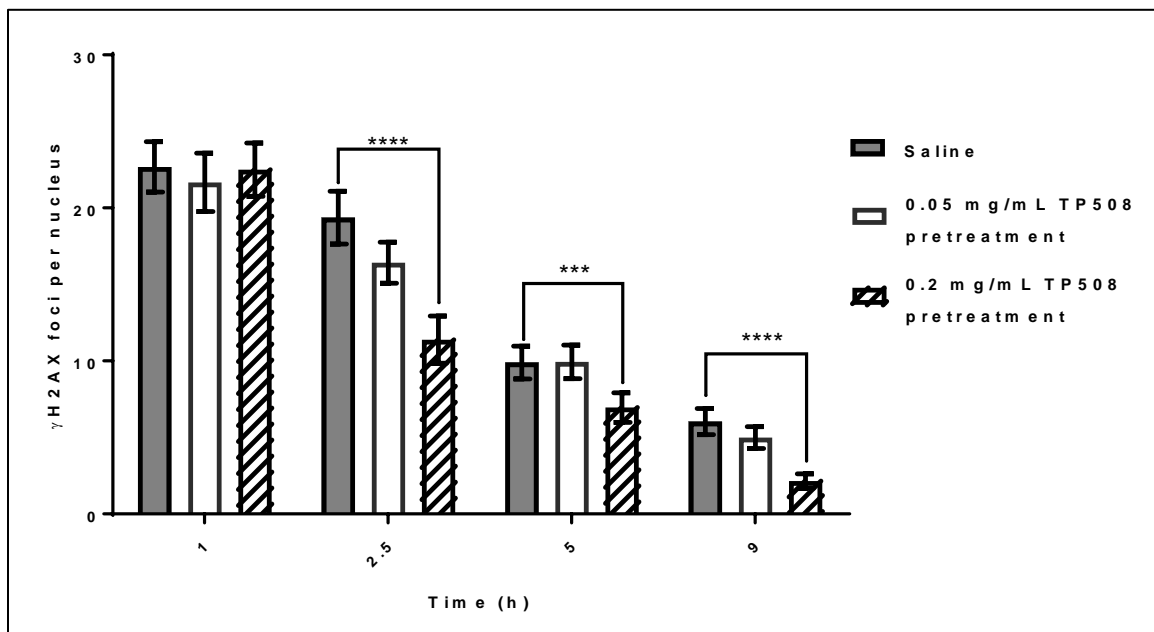


Figure 4.31 – Quantitation of γ H2AX foci per nucleus in HDMEC after 6 Gy ionizing radiation. HDMEC cultured on glass coverslips in EGM2 media were pre-treated with 0.9% saline or either 0.05 or 0.2 mg/mL TP508 1h prior to receiving 6 Gy ionizing radiation. Immunofluorescent imaging of samples fixed at 5h post-irradiation performed using anti- γ H2AX antibody to identify foci and DAPI to identify nuclei. Data presented as mean \pm 95% confidence interval, *** p<0.001, **** p<0.0001.

Based on these results, TP508 derivatives were assessed in HDMEC following 6 Gy irradiation for the ability of these derivatives to enhance DNA repair. The optimal concentration results for each derivative from the *in vitro* aortic ring assay (described in Section 2 Chapter 4E (1).) suggested that it might be necessary to use up to 50x the molar concentration of TP508 for the radiomitigation effect. Since the DNA repair assay required 0.2 mg/mL TP508 for efficacy in HDMEC, versus 1 – 5 μ g/mL TP508 for aortic sprouting, a 50x increase was anticipated to be beyond the solubility limit of at least some of the derivatives. As a result, concentrations of 86.5, 434 and 1080 μ M (equivalent to 1x, 5x

and 12.5x the effective dose of 0.2 mg/mL TP508) were tested for each derivative. This experiment was performed twice, with at least two replicates per experiment analyzed at 1 and 5h. 4 – 10 fields were imaged per replicate to generate at least 130 nuclei per condition for analysis.

Figure 4.32 summarizes the γ H2AX foci/nucleus results for the TP508 derivatives in HDMEC at 5h after 6 Gy IR, presented as mean \pm 95% CI. At 1h, as in the previous experiment with HDMEC exposed to 6 Gy IR, the number of foci/nucleus in all treatments agreed within error, with means ranging from 21.4 – 23.6 foci per nucleus. This was reduced to 18.2 foci/nucleus in the saline control at 5h. The 86.5 μ M TP508 positive control (equivalent to 0.2 mg/mL TP508) had 7.0 foci/nucleus at the 5h timepoint, a highly significant reduction compared to the saline control (adjusted p-value <0.0001, designated by “#” in Fig. 4.34). The PEG5k-TP508 also significantly reduced the number of foci/nucleus at 86.5 μ M, with 8.3 foci/nucleus (adjusted p-value <0.0001). None of the other derivatives significantly differed from the saline control at 86.5 μ M, indicating that only PEG5k-TP508 was effective in this assay at the same concentration as TP508. None of the TP508 derivatives displayed significant differences at the 434 μ M concentration, indicating that at this concentration PEG5k-TP508 is above its window for efficacy. At the 1080 μ M concentration, PEG20k-Cys14-TP508 showed its first confirmation of biological activity of any of the assays used in these studies. At this concentration, PEG20k-Cys14-TP508 pretreatment resulted in a mean of 5.9 foci/nucleus, a value equivalent to the effect of the TP508 positive control. This suggests that the optimal

concentration of PEG20k-Cys14-TP508 for biological activity in this assay is close to 12.5-fold that of TP508 monomer.

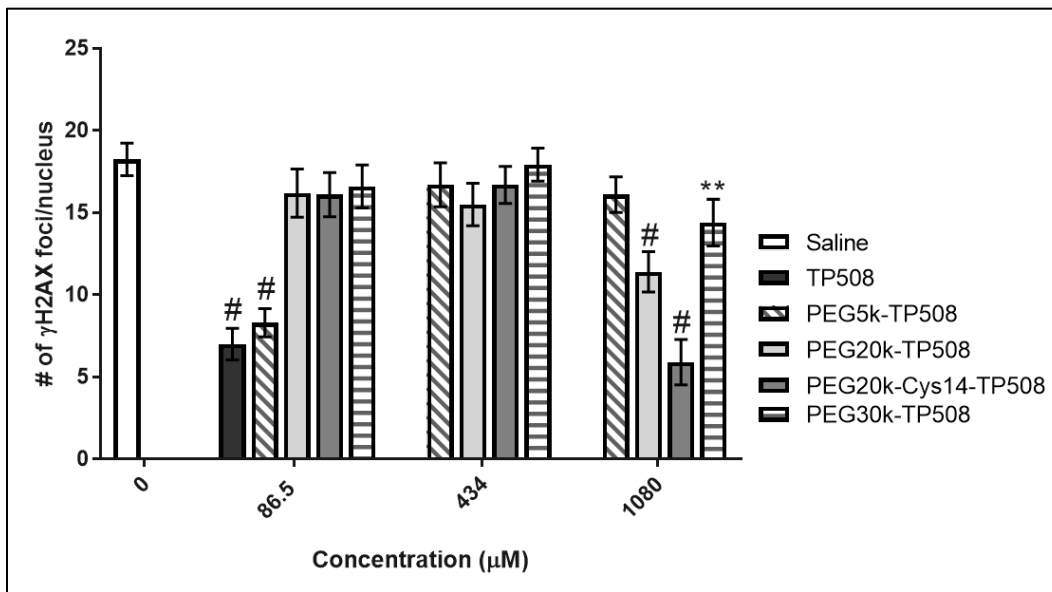


Figure 4.34 – Quantitation of the number of γ H2AX foci per nucleus in HDMEC pretreated with TP508 derivatives, at 5h post-6 Gy ionizing radiation. HDMEC cultured on glass coverslips in EGM2 media were pre-treated with 0.9% saline, 86.5 μ M TP508, or 86.5, 434, or 1080 μ M of each of the TP508 derivatives 1h prior to receiving 6 Gy ionizing radiation. Immunofluorescent imaging of samples fixed at 5h post-irradiation performed using anti- γ H2AX antibody to identify foci and DAPI to identify nuclei. Data presented as mean \pm 95% confidence interval, ** $p < 0.01$, # $p < 0.0001$.

PEG20k-TP508 and PEG30k-TP508 only showed activity in this assay at the 1080 μ M concentration. The PEG20k-TP508 pretreatment of HDMEC resulted in a mean of 11.4 foci/nucleus (adjusted p-value < 0.0001). Since this value is higher than that of the TP508 control, it is likely that while PEG20k-TP508 is biologically active at this concentration, it may be further away from its optimal concentration than the PEG20k-

Cys14-TP508 derivative at 1080 μM . Whether it is above or below the optimal concentration cannot be determined from the available data. The PEG30k-TP508 pretreatment of HDMEC resulted in a mean of 14.4 foci/nucleus (adjusted p-value of 0.009, designated as ** in Fig. 4.32). This is the lowest level of biological activity of any of the derivatives in this assay, and may suggest that 1080 μM is even further away from its optimal concentration than it was for PEG20k-TP508. However, since the 10x stock used to dose the cells was in excess of 350 mg/mL PEG30k-TP508, assaying this derivative at higher concentrations is impractical and may be of limited biological relevance.

SECTION 3: DISCUSSION

Chapter 5: Discussion and conclusions

A. GOAL OF PROJECT

The goal of this project was to evaluate the development of a TP508 derivative as a second-generation TP508 molecule that would have increased bioactivity following systemic injection. The hypothesis was that PEGylation of TP508 could increase both the half-life of TP508 in plasma and also increase the biological activity. A series of PEGylated TP508 molecules were designed and then synthesized and purified by American Peptide Company. In our laboratory the molecules were further characterized and their persistence in plasma was determined following injection into mice. The biological activity of these derivatives was then evaluated using a combination of *in vivo* and *in vitro* assays. A major hurdle in this project was establishing assays that could be used reproducibly and quantitatively for to test the hypothesis and validate activity of the derivatives. Using a combination of *in vivo* and *in vitro* assays, these studies identify two PEGylated TP508 derivatives with potential for future commercial development.

B. CHARACTERIZATION OF TP508 DERIVATIVES

Each of the PEGylated TP508 derivatives synthesized by American Peptide Company (Sunnyvale, CA) was delivered with a certificate analysis stating peptide purities of at least 95% by reversed phase HPLC. These results were confirmed by SDS-PAGE for each of the monovalent PEGylated TP508 derivatives (PEG5k-TP508, PEG20k-TP508,

PEG20k-Cys14-TP508 and PEG30k-TP508), where a single major band was observed for each of the derivatives. However, the tetravalent TP508 derivative produced 4 different bands of similar intensity. Since PEG does not migrate at the same rate per unit length as SDS-treated protein, the identity of each band could not be determined by size, but likely corresponded to incompletely reacted 4-arm PEG containing either 1, 2, 3 or 4 TP508 moieties. These bands all bound the Rb411 TP508B antibody in Western Blotting, confirming that they all contained TP508. Due to the mixture of species, the tetravalent TP508 derivative was deemed too impure for analysis of its biological activity *in vivo*, and was returned to the American Peptide Company.

The fluorescently-labeled variants of each derivative, created by adding TAMRA on a Lysine-Lysine-Lysine spacer to the N-terminal alanine of TP508, were injected i.v. into male CD-1 mice, who then had their blood collected at each timepoint for analysis of residual plasma fluorescence. The plasma half-life of the TP508 derivatives increased in a size-dependent manner, consistent with the hypothesis that the short plasma half-life is due to rapid renal clearance. TP508 had a plasma half-life of 13.7 minutes in this analysis, agreeing with literature values of 10-14 minutes (47). PEG5k-TP508 had the same plasma half-life as TP508. PEG20k-TP508 increased the plasma half-life of TP508 approximately 6-fold, while the PEG20k-Cys14-TP508 increased the plasma half-life of TP508 5-fold. These results are within error of each other at the level of sampling ($n = 3$ per timepoint) in the data set, but may also indicate slight differences in hydrodynamic volume of the molecule caused by attachment of the PEG20k to the center of the TP508 molecule versus attachment to its N-terminus. The PEG30k-TP508 resulted in a large increase in plasma half-life, approximately 19-fold. These results complete Aim 1 of this dissertation by confirming that PEGylation extended the plasma half-life of TP508.

C. BIOLOGICAL ACTIVITY OF THE TP508 DERIVATIVES *IN VIVO*

TP508 is currently being developed for use as a nuclear countermeasure to enhance survival and delay mortality in the event of a nuclear incident. To be an effective countermeasure, it must be able to protect subjects against the harmful effects of acute radiation syndromes when given as an injection up to 24h after exposure to ionizing radiation. Results of multiple studies have shown that a single injection of TP508 24h post exposure significantly increases animal survival [ref, ref]. The short peptide half-life in plasma suggests that by increasing plasma half-life a peptide derivative could be made that has greater activity or that can produce the same degree of radiomitigation with injection of much lower amounts of peptide. The PEGylated TP508 derivatives were assessed using three different *in vivo* biological assays that are relevant to development as a nuclear countermeasure. These assays included TP508 and TP508 derivative effects on: proliferation and mobilization of bone marrow stem/progenitor cells; aortic endothelial cell survival and sprouting *ex vivo*; and their ability to restore healing of wounds in mice that were exposed to radiation.

Results from all three *in vivo* assays for the biological activity of TP508 were in agreement with regard to the activity of the TP508 derivatives administered at equimolar doses. 100 μ g PEG30k-TP508 and PEG5k-TP508 treatment of naïve male CD-1 mice 24h prior to isolating femurs for IHC of the red marrow demonstrated that this region had enhanced proliferation compared to saline controls, at levels similar to that of the TP508 monomer. These derivatives also enhanced endothelial sprouting in aortic rings taken from the same mice, resulting in a 209% increase in sprouting at Day 6 over the saline control

for PEG5k-TP508 and a 168% for PEG30k-TP508. These sprouting levels were even greater than those of TP508, which displayed a 93% increase in sprouting over the saline control at this concentration. In addition, these derivatives also accelerated wound healing in male CD-1 mice exposed to 8Gy ionizing radiation. Irradiation reduces closure of a full-thickness 1.44 cm² dorsal wound from 9.5 mm²/day in unirradiated mice to 6 mm²/day. A 100 µg i.p. injection of TP508 increased the wound closure to 7.4 mm²/day in the 8Gy irradiated mice. Equimolar doses of the TP508 derivatives further enhanced the wound closure to 9 mm²/day for PEG5k-TP508 and 10 mm²/day for PEG30k-TP508, similar to the unirradiated control. These results all suggest that PEG5k-TP508 and PEG30k-TP508 enhance the biological activity of TP508 administered by injection, consistent with the dissertation hypothesis.

Surprisingly, there was not a simple correlation between increased PEG size and enhanced biological activity of TP508. Neither PEG20k-TP508 nor PEG20k-Cys14-TP508 displayed any significant differences in biological activity as compared to saline control. For the PEG20k-Cys14-TP508, it is possible that attaching the PEG20k to the central Cys14 residue blocks access of TP508 to its receptor, negating its activity. This does not apply in the case of PEG20k-TP508, where the PEG20k is attached to the same site (the N-terminus) as in PEG5k-TP508 and PEG30k-TP508, which both showed biological activity.

PEGylation of small proteins at one or more sites increases their hydrodynamic volume, slowing their renal clearance and extending their exposure to tissues for

therapeutic effect. This, in turn, is anticipated to increase the therapeutic efficacy of the peptide or protein or reduce the dosage required for therapeutic effect. Tradeoffs for this extended systemic exposure are that, due to the increased size of the molecule, the PEGylated peptide it may have slower tissue diffusion and a reduced specific activity for its target receptor. This reduced specific activity comes from both steric hindrance of receptor access to the peptide binding site, and from the fact that the binding interactions now tether a larger molecule to the receptor without any binding contribution from the PEG moiety. In simple terms, then, PEGylation represents a balance between enhancing the pharmacokinetics of a polypeptide through increased systemic exposure, and reducing its pharmacodynamics by reduced binding affinity (99). Based on current understanding of PEGylated polypeptides, biological activity of a monovalent, single-site PEGylated polypeptide should increase as PEG size increases, up until the point where the hydrodynamic volume of the PEG sterically hinders target binding, at which point biological activity is lost. However, the results from this study show that, for TP508, the results of PEGylation are discontinuous. PEG5k-TP508, which had the same plasma half-life as TP508 administered i.v., displayed as good or better activity than TP508 at the same molar concentration. At the next size up, PEG20k-TP508 displayed no enhancement in biological activity. However, as size was increased again, to PEG30k-TP508, enhanced biological activity was once again observed.

The key to this discontinuity lies in the balance between pharmacodynamics and pharmacokinetics of PEGylated TP508. Unlike many of the PEGylated antibodies and proteins which have been FDA approved, TP508 has a therapeutic window above which

its efficacy is reduced (48, 66). This introduces an additional factor affecting biological activity that could cause the discontinuity under two different sets of conditions. In the first case, PEG20k-TP508 and PEG30k-TP508 have similar, low specific activities as compared to TP508 and PEG5k-TP508. In this case, the 6-fold extension in half-life of TP508 is too low to maintain therapeutic efficacy while the 19-fold extension in half-life of PEG30k is sufficient for activity. In the second case, there is a small difference in specific activity between PEG5k-TP508 and PEG20k-TP508, and a larger decrease in specific activity from PEG20k-TP508 to PEG30k-TP508. Under those conditions, PEG20k-TP508 could have been at too high a concentration for biological activity. It is also possible that this condition would apply to the PEG20k-Cys14-TP508 derivative, if instead of completely inactivating TP508 it has a specific activity similar to PEG20k-TP508.

To experimentally determine which of the two cases prevailed, it was necessary to assess the specific activities of TP508 and the TP508 derivatives *in vitro*, where the increased plasma half-life is removed as a factor. In the absence of an identified, purified receptor, the binding affinity of each receptor cannot be precisely determined. Instead, it must be determined indirectly using assays for biological activity that provide evidence for the relative specific activity between derivatives.

D. RELATIVE SPECIFIC ACTIVITY OF THE PEGYLATED TP508 DERIVATIVES *IN VITRO*

Development of an *in vitro* assay for the biological activity of TP508 which would also have sufficient dynamic range to identify dose response differences and differentiate

between the specific activities of the TP508 derivatives proved challenging. Initial development of an RT-PCR assay for transcriptional response of key genes in WI-38 fibroblasts to TP508 was unsuccessful. These genes, originally identified in studies using the PhosphoImager platform as having up to 3.8-fold increases in transcription level, resulted in no more than a 1.4-fold increase by RT-PCR in response to TP508. This result may have indicated false positives in the PhosphoImager studies, or a reduced response to TP508 as cell passage number increased. These cells also failed to show a proliferative response with the MTT assay, further suggesting that they may have lost their responsiveness. To resolve the question of cell responsiveness, we attempted to develop a receptor-binding assay using TAMRA-labeled TP508. There was no measurable specific or non-specific binding of TAMRA-TP508 to WI-38 cells under the conditions employed. Therefore, further assay development focused on other activities of TP508 reported in literature.

Based on the *in vivo* effects of TP508 on endothelial sprouting from aortic rings, our next attempt to establish a suitable *in vitro* assay was to use the mouse aortic ring assay with *in vitro* dosing. In this case aortas were isolated from untreated naïve mice and were then treated post-isolation with TP508 or TP508 derivatives. As described previously, incorporating the use of the iBidi μ Slide format allowed endothelial sprout counting from a single confocal image rather than manually counting endothelial sprouts while adjusting the microscope to observe their 3D network. This in turn allowed for semi-automatic counting of endothelial sprouts using an image analysis macro for ImagePro 7.0 (see

Section 2 Chapter 4E, Appendix A). These adaptations reduced much of the variability seen in the standard aortic ring *in vitro* assay.

Screening various concentrations of TP508 demonstrated that, optimal enhancement of endothelial sprouting was seen at a TP508 concentration of 1 $\mu\text{g}/\text{mL}$ (434 nM). Interestingly, at concentrations above a critical concentration (in this case, 10 $\mu\text{g}/\text{mL}$) TP508 no longer enhanced endothelial sprouting and showed sprouting levels similar to that seen in saline controls. This reinforces the possibility that the discontinuity between PEG length and biological activity *in vivo* and lack of effect of PEG20k-TP508 derivatives could have been because either the effective activity of the PEG20k-derivatives was too low to be effective or above that of the effective concentration.

Using this *in vitro* it was possible to show that each TP508 derivative had its own concentration range for activity. PEG5k-TP508 stimulated endothelial sprouting over a wide range of concentrations from 1 $\mu\text{g}/\text{mL}$ to 50 $\mu\text{g}/\text{mL}$. PEG20k-TP508 enhanced sprouting in the range equivalent to 5 – 100 $\mu\text{g}/\text{mL}$ TP508 with a maximum equivalent to 50 $\mu\text{g}/\text{mL}$ TP508, suggesting a lower relative specific activity than PEG5k-TP508. PEG20k-Cys14-TP508 did not enhance sprouting activity across the entire concentration range, consistent with the hypothesis that specific activity is significantly decreased when TP508 is PEGylated at the Cys14 residue instead of the N-terminus. The PEG30k-TP508 results were somewhat unexpected, however, with an activity range equivalent to 1 – 30 $\mu\text{g}/\text{mL}$ TP508 and an optimum equivalent to 1 $\mu\text{g}/\text{mL}$ TP508. Based on the results of the

other derivatives, the activity of PEG30k-TP508 would be expected to occur at a concentration roughly 10-fold higher than what was observed.

This assay does have several weaknesses for comparing the specific activities of the different derivatives. First, addition of the derivatives to the media used for the first two days of incubation allows for extended stimulation of the aortic tissue, especially if there are differences in the degradation rate between TP508 and the TP508 derivatives. During this period it is necessary not to disturb the rings so that they do not detach from the Matrigel prior to invasion of the endothelial sprouts into the matrix, which aids in tethering the rings. The extended period between treatment and sprouting is also not ideal, as it allows potential confounding factors such as differences in media evaporation, to confound results. Finally, this assay is highly variable, making clear determination of differences between treatment levels difficult to perform without using a prohibitive number of mice. Therefore, other assays were evaluated.

We next evaluated a modified version of the endothelial tube assay that was designed to quantify rapid changes in endothelial cells. The endothelial tube formation assay offered some valuable insight into the mechanism of action of TP508. While 1 – 30 $\mu\text{g}/\text{mL}$ TP508 did not alter the extent of tube formation in HDMEC alone, there was substantial enhancement of total tube length in the 1:100 pericyte:HDMEC co-culture by 1 and 10 $\mu\text{g}/\text{mL}$ TP508, with a 1.67-fold increase over saline control at 16h with 1 $\mu\text{g}/\text{mL}$ and a 2.0-fold increase with 10 $\mu\text{g}/\text{mL}$ TP508. This is in the same concentration range that increased endothelial sprout formation in the *in vitro* mouse aortic ring assay. The evidence

that TP508 did not stimulate enhanced tube formation in HDMEC alone, but did so in a 1:100 co-culture with pericytes, suggests a role for cellular cross-talk in the *in vivo* activity of TP508. The data may also suggest that pericytes which have progenitor cell properties may be the primary cell type that is activated in certain populations of endothelial cells or in the isolated aortic rings. Determining the nature of this cross-talk or involvement of pericytes in TP508 activation of endothelial cells is beyond the scope of this dissertation research.

The third type of *in vitro* assay used involved TP508 acceleration of radiation-induced DNA DSB detected by analysis of γ H2AX binding to DSB. Because data for the number of γ H2AX foci/nucleus is gathered from 5 – 10 visual fields per replicate, generating hundreds nuclei for analysis, this assay allowed us to quantify differences in the biological activity of TP508 derivatives with a high degree of certainty. These experiments demonstrate the radioprotective effects of TP508 administered 1h prior to IR exposure. A pretreatment of HDMEC with 0.2 mg/mL TP508 administered 1h prior to 3 Gy IR significantly reduced the number of foci/nucleus compared to saline control at 5h and 9h, while pretreatment prior to 6 Gy IR resulted in significant decreases in the number of foci/nucleus at 2.5, 5 and 9h. Because the number of foci/nucleus is the same at 1h for both TP508 pretreatment and saline control, these results suggest that TP508 accelerates the repair of DNA DSB. The mechanisms of this accelerated repair in HDMEC in response to TP508 have not yet been investigated. However, they likely share features in common with human mesenchymal stem cells, such as increased levels phosphorylated Ataxia telangiectasia mutated (p-ATM) in response to IR with TP508 pretreatment, which in turn increases levels of phosphorylated (p-RAD50) (Rayavara, McVicar and Carney,

manuscript in preparation). These early events in DNA DSB repair are anticipated to enhance formation of the MRN complex (MRE11-RAD50-NBS1) that performs DSB repair in the homologous recombination (HR) pathway (100).

PEGylated TP508 derivatives were tested at molar concentrations equivalent to 1x, 5x, and 12.5x the level where TP508 accelerated DSB repair in HDMEC exposed to 6 Gy irradiation. PEG5k-TP508 was the only derivative to cause a reduced number of γ H2AX foci/nucleus at the 1x concentration (86.5 μ M). This indicated that the PEG5k modification at the N-terminus of TP508 had little to no effect on its *in vitro* activity. None of the derivatives had any difference from the saline control at the 5x concentration, including PEG5k-TP508, indicating a reduction in activity for this derivative going from 86.5 to 434 μ M. PEG20k-TP508, PEG30k-TP508, and PEG20k-Cys14-TP508 all displayed *in vitro* activity at the 12.5x concentration (1080 μ M). PEG20k-Cys14-TP508 had a similar number of γ H2AX foci/nucleus at 1080 μ M as TP508 and PEG5k-TP508 did at 86.5 μ M. This indicates that its specific activity is approximately 12.5-fold lower than that of TP508. The 1080 μ M PEG20k-TP508 treatment resulted in 11.4 foci/nucleus, as compared to 7.0 foci/nucleus for 86.5 μ M TP508. This would suggest that 1080 μ M PEG20k-TP508 is either slightly below or slightly above its optimum concentration. This would also be the case for 1080 μ M PEG30k-TP508 pretreatment, which resulted in 14.4 foci/nucleus 5h after IR.

These results describe the second case (described in Section 3 Chapter 5B) of relative specific activities of the PEGylated TP508 derivatives that accounts for the discontinuity in *in vivo* activity. PEG5k-TP508 has a similar plasma half-life to TP508 and

similar specific activity, accounting for its activity *in vivo* at the same concentration as TP508. PEG20k-TP508 and PEG20k-Cys14-TP508 increased the plasma half-life of TP508 5-6 fold. However, this was insufficient to overcome the approximate 12.5 fold loss in specific activity seen *in vitro*. PEG30k-TP508 also had a loss in specific activity on the order of 12.5x, but maintains biological activity *in vivo* because of its 19-fold increase in plasma half-life. These *in vitro* results complete Aim 3 and explain the unexpected loss of PEG20k-TP508 activity at equimolar doses to TP508 *in vivo*.

E. FUTURE DIRECTIONS

E (1). IDENTIFICATION OF THE TP508 RECEPTOR

A key step in integrating the body of knowledge about the TP508 peptide into the greater field of tissue repair, as well as in translating TP508 into an FDA-approved therapeutic drug, is identification of the TP508 receptor. While this was beyond the scope of this dissertation, I have identified 3 alternative approaches during my research that could be explored to confirm the identity of TP508-binding proteins.

There are major technical challenges in raising an antibody to TP508 with sufficient specificity and binding affinity to use in Co-IP approaches. TP508's lack of secondary structure means there is limited constraint of a binding motif to be exploited by an antibody. In addition, the TP508 amino acid sequence is highly conserved in mammalian prothrombin and thrombin, making it weakly immunogenic. There is also the issue of generating an antibody that does not obstruct the receptor binding domain of TP508. Also, as with antibodies raised to any short polypeptide sequence, new antibodies raised to

TP508 may have insufficient specificity due to binding to other proteins containing a homologous primary polypeptide sequence.

The first approach, therefore, uses an anti-PEG antibody in conjunction with one of the PEGylated TP508 derivatives that were shown to have biological activity in these studies. These are already commercially available (e.g. THE™ PEG Antibody, mAb, Mouse, Genscript cat# A01795), possess the requisite specificity and binding affinity to the PEG moiety. These PEG antibodies have been successfully used to bind PEGylated TP508 derivatives in Western blots during the course of this dissertation research. As a result, a PEG antibody-TP508 derivative pair could be directly substituted for the anti-TP508B antibody-TP508 binding pair in a traditional Co-IP approach. Prior affinity purification attempts suggest, however, that the receptor or binding protein may have altered conformation when solubilized from cell surface membranes. Therefore, additional studies will need to be conducted using a variety of non-denaturing detergents.

A second approach would be to use an aptamer raised to TP508 in place of an antibody in a pulldown approach. Aptamers are analogous to antibodies, but use a single, folded chain of nucleic acids whose secondary structure creates hydrogen bonding interactions to bind with high affinity to a polypeptide of interest. The aptamer generation approach, known as SELEX (see Figure 5.1, derived from Sriramoju et al. 2015) does not require any immunogenic property of the polypeptide, but instead produces a library of short nucleic acid sequences with a computationally predicted series of charge interactions with the target polypeptide, then uses high throughput technology to isolate which aptamers actually bind the peptide. These aptamers then form the base for another aptamer library

in an iterative affinity maturation approach until the desired binding affinity is reached. The aptamer can then be attached to biotin for convenience of use in Co-IP, using the high affinity biotin-avidin binding reaction ($K_d \sim 10^{-15}$ M) for capture. Base Pair Biotechnologies (Pearland, TX) has been identified as a commercial partner which can raise TP508 specific aptamers using this approach in as little as 8 – 12 weeks.

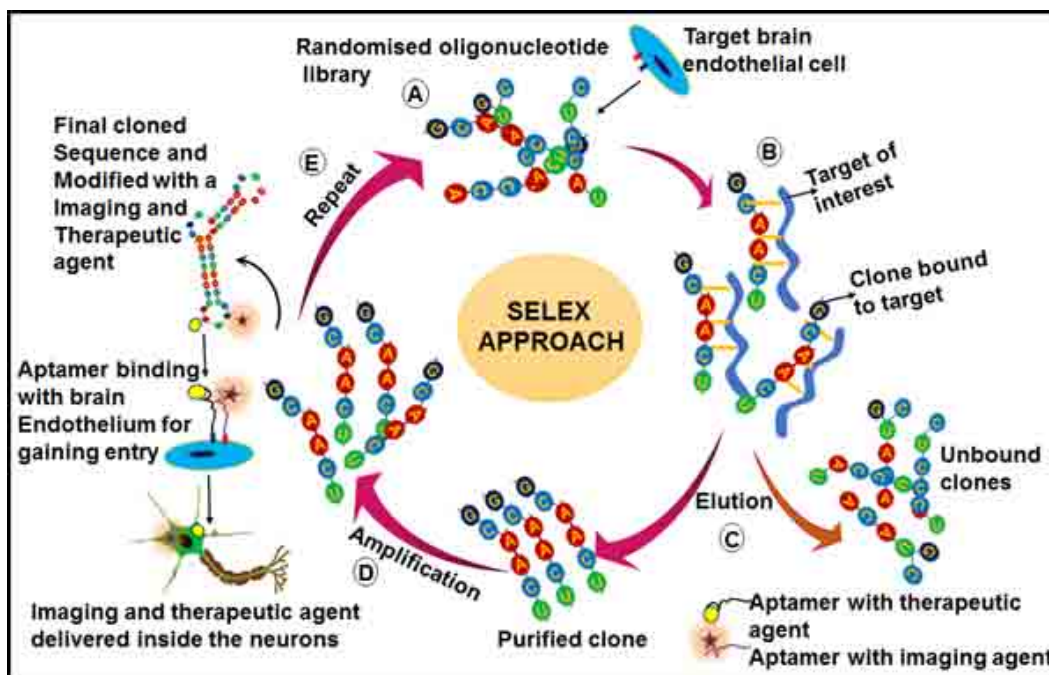


Figure 5.1 – The SELEX aptamer-generation approach.

A third approach uses a reagent specifically designed to overcome a number of weaknesses inherent in the Co-IP approach. It uses a TRICEPS™ reagent with 3 functional groups on a flexible backbone to enable (1) binding to a polypeptide ligand to a primary amine using an NHS ester; (2) crosslinking to a receptor or other protein binding partner

in cell cultures or tissue samples using a hydrazine group which is protected during binding of the ligand of interest, which then becomes deprotected under mild oxidizing conditions by addition of sodium periodate to the buffer containing tissue or cells; and (3) a biotin group for use in capturing the crosslinked ligand-receptor complex (Figure 5.2 adapted from Frei et al. This removes the need for an anti-TP508 antibody entirely for a Co-IP approach. The NHS ester chemistry which would be used for binding the TRICEPS™ reagent directly to TP508 has been shown not to prevent biological activity in the PEG5k-TP508 and PEG30k-TP508 derivatives. In addition, this chemistry makes it possible to attempt receptor purification from primary cell culture or tissue in the event that TP508 is interacting with a receptor more highly expressed in a stem or progenitor cell population rather than in terminally differentiated or immortalized cell cultures. This technology has been licensed by Dualsystems Biotech (Zurich, Switzerland) which offers this form of ligand-receptor capture as a service where the end-user supplies the ligand and frozen cell pellet for LC-MS analysis.

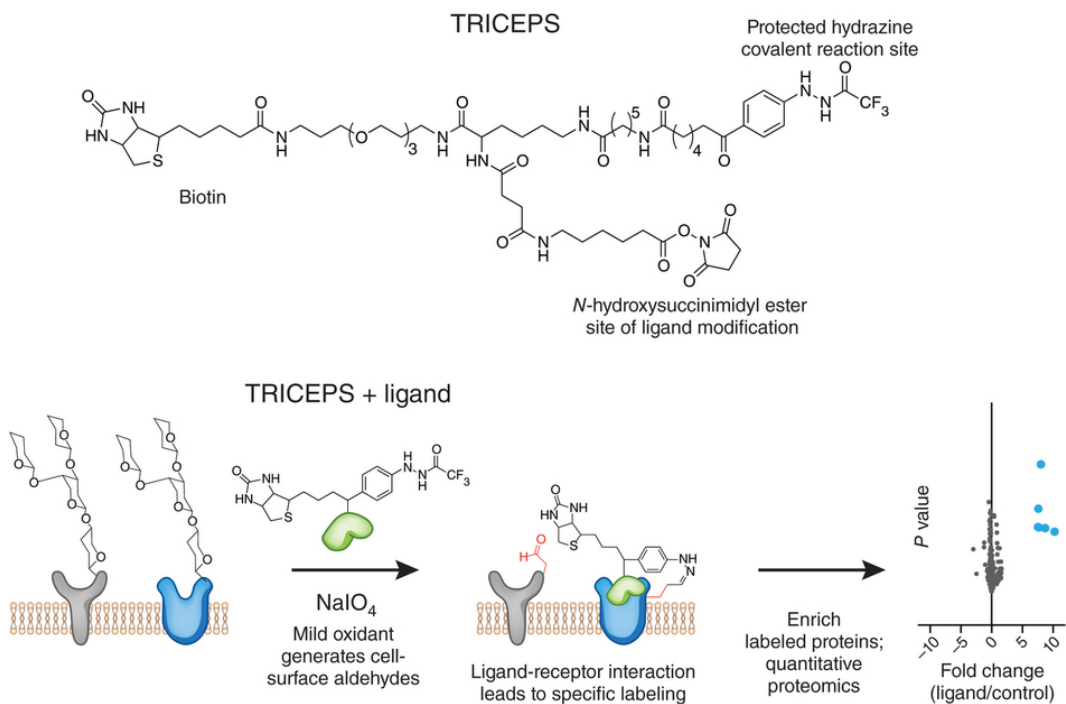


Figure 5.2 - TRICEPS™ reagent-based ligand-receptor capture.

E (2). NEXT STEPS WITH THE PEGYLATED TP508 DERIVATIVES

The results presented in this dissertation suggest the need for additional research into the tissue repair and radiomitigation effects of TP508 and its PEGylated derivatives. The observation that TP508 accelerates tube formation of HDMECs only in co-culture with pericytes (see Chapter 4 Section E2) suggests that cross-talk between these cell types may be necessary for the pro-angiogenic activity of TP508. Key elements of pericyte-endothelial cell interactions for endothelial tube formation and stabilization include: a) secretion of platelet-derived growth factor beta (PDGF- β) by endothelial cells for pericyte recruitment (92); b) increased expression of TGF- β and VEGF by pericytes (92); c) expression of matrix metalloproteinases (MMPs) TIMP-2 by endothelial cells and TIMP-

3 by pericytes for vascular remodeling (86); and d) enhanced generation of basement membrane components such as fibronectin (87, 88). Quantitation of growth factors and matrix metalloproteinases in media from pericyte:endothelial cell co-cultures after 18h incubation with and without TP508 using ELISA or multiplex ELISA may reveal differences at the protein level. RT-qPCR could be used to examine upregulation of mRNAs for basement membrane proteins in addition to those for the growth factors and MMPs previously mentioned. However, preparing 1:100 pericyte:HDMEC co-cultures that produce a consistent, reproducible response may prove challenging. For the purposes of creating a reproducible *in vitro* assay for the biological activity of TP508 which can be validated, it may be preferable to quantify changes to expression level of these proteins in response to TP508 in pericytes or HDMEC alone.

While it is of interest that the bone marrow in the red marrow region of healthy mice displayed enhanced PCNA expression in response to TP508, it is also important to determine if this also occurs in irradiated animals as part of the radiomitigation response to TP508 and/or TP508 derivatives. A number of femurs from mice exposed to 9 Gy ionizing radiation and injected with TP508 24h later were harvested and preserved during the studies presented in this dissertation as well as other aortic ring assay experiments performed by the Carney laboratory have been preserved for further study. Additional data could be mined from these samples to better understand the effects of TP508 and the TP508 derivatives in irradiated and non-irradiated bone marrow. It is possible, for example, that some effects of TP508 are greatly enhanced by prolonging bioavailability while others are less so. This bone marrow data would then help establish whether one of the PEGylated

derivatives identified in the current studies might be a better nuclear countermeasure for hematopoietic-acute radiation syndrome (H-ARS) than the TP508 monomer.

Finally, if PEG30k-TP508 and PEG5k-TP508 are to be evaluated as true second-generation drug candidates for radiomitigation, CD-1 mouse survival after LD_{70/30} doses of ionizing radiation with i.p. injection of the derivatives 24h after radiation exposure must be evaluated. However, since a 30% increase in survival requires approximately 26 mice per group to have sufficient statistical power to verify enhanced survival, an even larger population would be necessary to verify an incremental increase in survival between TP508 and a TP508 derivative. In addition, a marginal improvement in survival alone might not be sufficient to warrant further development of the PEGylated TP508 derivatives in comparison to the bulk of data regarding the safety, efficacy, manufacturing and formulation development already generated for TP508 monomer.

If I were to continue these studies, I would propose the evaluation of 26 mice per treatment at two doses: one that is the equimolar equivalent to the 10 mg/kg TP508 that previously demonstrated efficacy (66), and a second dose at the equimolar equivalent of 2.5 – 5 mg/kg TP508, below the threshold of efficacy for TP508. With an experiment performed in this manner, if the potency of the derivatives is such that they are above the therapeutic window at the equivalent of 10 mg/kg TP508, the lower dosage should show activity. Alternatively, if the PEGylated TP508 derivatives show a similar level of activity or slight improvement over TP508 at the equivalent of a 10 mg/kg dose, and also enhance survival at the lower dose, there is additional reason for further development of the derivatives. Not only would there be an argument for additional optimization of dose to

increase survival over TP508 monomer, a reduced dose for efficacy would also allow for stockpiling a greater number of doses against a nuclear incident using the same amount of synthesized TP508 by adding PEGylation step to the synthesis.

Due to the number of mice needed, and the large number of factors which can affect response to radiation, including timing of radiation exposure and dosing, stress level of the mice, gender differences, etc., these experiments may best be carried out by collaborator institutions which specialize in these types of studies. For instance, these studies might be carried out by the Armed Forces Radiobiology Research Institute (AFFRI, Bethesda, MD), which has already independently confirmed the efficacy of TP508 in enhancing survival in mice exposed to LD_{70/30} doses of ionizing radiation. Moreover, greater quantities of the PEGylated derivatives than were synthesized for this project would be required for these studies. Therefore, these studies are beyond the scope of this project at this time, unless further evidence is obtained to warrant the expense of manufacture and purification of large batches of these peptides.

F. CONCLUSIONS

PEGylation of TP508 increased the plasma half-life of the TP508 derivatives in a size-dependent manner, as anticipated. However, the *in vivo* biological activity of the PEGylated TP508 derivatives did not correlate directly with increased half-life. The PEG20k-TP508 and PEG20k-Cys14-TP508 derivatives showed a 5-7 fold enhancement in plasma half-life, but did not display biological activity *in vivo*. PEG5k-TP508 displayed enhanced *in vivo* activity over TP508 despite having the same biological half-life. PEG30k-TP508 increased plasma half-life on the order of 19-fold and also enhanced *in vivo*

biological activity. *In vitro* studies demonstrated that PEG5k-TP508 was active in accelerating the repair of DNA double stranded breaks at the same molar concentration as TP508, while the other derivatives were not active at 1x or 5x the molar concentration of TP508 displaying activity, but were active only at the 12.5x concentration. As a result, the extended biological half-lives of PEG20k-TP508 and PEG20k-Cys14-TP508 were insufficient to overcome their loss of specific activity when administered *in vivo*, while the extended biological half-life of TP508 outweighed its loss of specific activity. This work identifies PEG5k-TP508 and PEG30k-TP508 as potential second generation TP508 molecules for drug development.

SECTION 4: MATERIALS AND METHODS

A. TP508 DERIVATIVE PEPTIDE SYNTHESIS

All TP508, PEGylated TP508 derivatives, the truncated 14-mer variant of TP508 (RGDACEGDSGGPFV-NH₂), and tetramethylrhodamine (5-TAMRA) fluorescently-labeled TP508 and derivatives were synthesized by American Peptide Company (Sunnyvale, CA). PEG5k-, PEG20k-, and PEG30k-TP508 derivatives were synthesized using n-hydroxysuccinimidyl ester (NHS) functionalized PEGs to bind to the N-terminal amine using existing stocks of TP508. PEG20k-Cys14-TP508 was synthesized using a maleimide-functionalized PEG20k to covalently bind to TP508 at the internal cysteine residue at position 14 (Cys14) of TP508. Fluorescently labeled variants of the PEGylated TP508 derivatives were prepared by fresh synthesis with the inclusion of 5-tetramethylrhodamine (5-TAMRA) on a 3x Lysine residue spacer (Lys-Lys(5-TAMRA)-Lys) between the N-terminus of TP508 and the PEG moiety.

A TAMRA-TP508 dimer was synthesized from TAMRA-TP508 monomer using a dimerization and purification protocol based on Peptide Analysis Protocols Chapter 5 Section 3.1 (101). Briefly, 10 mL of 1 mM TAMRA-TP508 prepared in 18.2 mΩ deionized water was reacted with 80 μL 100 mM sodium phosphate, 5 mM EDTA pH 7.4 + 10 μL of freshly prepared 0.25 mM DTNB in 50 mM sodium phosphate, 2.5 mM EDTA pH 7.4 for 2h at 25°C. Sample was stored at -20°C and then dimer isolated by the Biomolecular Resource Facility using a preparative scale purification by reversed phase HPLC on a C18 column, with TAMRA-TP508 monomer and a TAMRA-TP508-TNB adduct reference standards for identification of the dimer fractions by retention time. Pooled dimer fractions

were frozen and dried using a SpeedVac and stored at -80°C until reconstitution. Dimer identity confirmed by dynamic light scattering on a Malvern ZetaSizer.

B. PLASMA HALF-LIFE

Male CD-1 mice aged 11-20 weeks were injected IV by tail vein injection with 100 μ L of 5 mg/mL TAMRA-TP508 in 0.9% saline for injection (Hospira) or the molar equivalent of TAMRA-labeled PEGk-TP508, PEG20k-TP508, PEG20k-Cys14-TP508, or TP508 dimer. Due to limitations in the amount of TAMRA-labeled PEG30k-TP508, as well as potential solubility issues, 100 μ L of the molar equivalent of 1 mg/mL TAMRA-TP508 (1/5th of the dosage for the other treatment groups) was used for determining plasma half-life for the PEG30k-TP508 derivative. At each timepoint, mice were euthanized by CO₂ asphyxiation followed by surgically opening the chest for blood collection. Whole blood was collected using 1 cc insulin syringes (Becton Dickinson cat. # 329412) and transferred into heparinized microfuge tubes. Assay development demonstrated that the most sensitive signal occurs in platelet-depleted plasma. Samples were first centrifuged at 1000 x g to pellet blood cells. Plasma fraction was then transferred to a clean microfuge tube and centrifuged at 15,000 x g for 10 min to pellet platelets. Platelet-depleted plasma was transferred to a clean microfuge tube. Samples were diluted 2x with 0.9% sterile saline (Hospira) in 96-well plates and measured for fluorescence on a microplate reader (ex: 530 nm, em: 590 nm). TP508 and TP508 derivative concentrations were determined from calibration curves with concentration standards prepared in the same matrix. Residual platelet-depleted plasma samples were retained for future testing stored at -20°C.

C. IN-GEL FLUORESCENCE ASSAY

Platelet-depleted plasma samples archived from biological half-life studies were thawed to 4°C. Samples were diluted to ~ 2 µg/mL TAMRA-TP508, then combined 1:1 with Laemmli sample buffer containing 5% β-mercaptoethanol. Samples were then heated to 95°C for 5 min, cooled to room temperature, and pulse centrifuged to collect sample at bottom of microfuge tubes. Samples were loaded to 18% acrylamide gels and run for 85 min at 120V, 50 mA/gel in 1x TGS buffer. After electrophoresis, gels were removed from cassettes, rinsed with distilled water, and assayed for fluorescence on a Fujifilm FLA-5100 instrument set at 100 micron resolution, 532 nm excitation, long pass red emission filter, 400V photomultiplier. Fluorescent intensities were converted to TAMRA-T508 concentration using a 3-point concentration curve of 5, 2, and 0.5 µg/mL TAMRA-TP508 spiked into mouse platelet-depleted plasma.

D. WI-38 CELL CULTURE

WI-38 cell cultures were initiated from frozen stocks archived in liquid nitrogen in 2006 at passage 3 after demonstration of specific binding to TP508. A 1 mL vial of cells were revived by thawing in a 37°C water bath for 1 minute and then adding the entire contents to a T-25 flask containing 5 mL DMEM/F12 growth media (DMEM/F-12 basal media (Gibco) supplemented with 10% FBS (Sigma-Aldrich), 1% 200 mM L-glutamine (Gibco) and 1% of 100x penicillin/streptomycin antibiotic (Gibco)). Cells were incubated at 37°C, 5% CO₂. Media was changed 2h into incubation after verifying cell attachment, then every 2-3 days thereafter. After reaching confluence 6-8 days after initial revival, cells were subcultured. To subculture, media was removed from T-25 flasks and cells were

washed with 5 mL DPBS. Cells were then detached using 1 mL 0.25% Trypsin-EDTA solution (Gibco) and incubating for 5 min at 37°C. Trypsinization was halted by the addition of 3 mL DMEM/F-12 growth media. Cells were collected in 15 mL Falcon tubes then centrifuged for 5 minutes at 1200 x g at room temperature. Supernatant was removed, cells were resuspended in fresh media, then split at a 1:6 ratio (~4,000 cells/cm²) to T-75 flasks containing 10 mL DMEM/F-12 growth media.

E. RNA ISOLATION FROM WI-38 CELLS

Cells were subcultured from T-75 flasks as above into 6- or 24-well plates as above, but at a concentration of 1×10^5 cells in 0.5 mL in DMEM/F-12 growth media, using 0.5 mL for 24-well plates or 2.0 mL for 6-well plates. Cells were then cultured for up to 48h in serum free media (DMEM/F-12 basal media supplemented with 1% 200 mM L-glutamine and 1% of 100x penicillin/streptomycin antibiotic) prior to stimulation with 0.1 – 10 μ M TP508 or saline as a control.

F. MTT ASSAY

WI-38 cells subcultured from passage 7 cells into 24-well plates at a concentration of 1×10^5 cells per in in 490 μ L DMEM/F-12 growth media. Added concentrated stocks of TP508 or thrombin in DPBS to bring final concentrations to 0, 0.1, 1 or 10 μ M TP508 and 0, 62.5 or 125 ng/mL thrombin. Cells were incubated for 24h at 37°C, 5% CO₂. Removed media and rinsed wells 1 x with 400 μ L DMEM media (+ Pen/Strep, + L-Glu, no FBS, no phenol red). Added 400 μ L DMEM media + 40 μ L 12 mM MTT in DPBS to wells and returned to incubator for 1.5h. Prepared a second plate with 400 μ L DMEM media + 40 μ L 12 mM MTT in DPBS as blank. Added 400 μ L 10% SDS in 0.01M HCl to

each well and returned plates to incubator for 2h. Plates read at 37°C using Synergy H1 plate spectrophotometer set to read absorbance at 570 nm after 15s, slow orbital shaking.

G. AORTIC RING ASSAY USING *IN VIVO* PRETREATMENT

Male CD-1 mice were injected intraperitoneally with 100 µg (2.5 mg/kg) TP508 or the molar equivalent of each of the TP508 derivatives in DPBS (Cellgro cat. # 21-030-CV). 24h post-injection, thoracic aortas were isolated, cleaned, and sectioned into rings ~ 0.5 mm in diameter. Rings were then embedded in 50 µL of Growth Factor Reduced Matrigel® (BD cat. # 356231) within 4-well chamber slides and overlaid with 250 µL EGM2-MV media (Lonza). Rings were incubated for 7 days at 37°C, 5% CO₂, with media changes every 2 – 3 days. On Days 4, 5 & 6, sprouts were manually counted *in situ* using phase contrast microscopy and imaged with a Spot RT camera at 40x magnification.

H. IMMUNOFLUORESCENT IMAGING OF AORTIC RINGS

On Day 7 post-embedding in Matrigel®, aortic rings cultured as per Section 4G were fixed using 200 µL per well 4% formalin for 30 minutes at room temperature. Wells were rinsed 2x with DPBS, then incubated with 1:200 dilution of mouse anti-CD31 (BD cat. # 553369) and 1:200 dilution of rabbit anti-α-NG2 (Millipore cat. # AB5320) in PBLEC (PBS + CaCl₂ + MgCl₂, 1 mM MnCl₂, 1% v/v Tween 20) overnight at 4°C. Washed wells 3x for 15 min each with 0.1% Triton X-100 DPBS at room temperature, added secondary antibody solution of 1:1000 of each of Alexa 594 anti-rabbit and Alexa 488 anti-mouse in PBLEC and incubated overnight at 4°C. Counterstained with 300 nM DAPI for 5 min at room temperature, then washed 3x for 15 min each with 0.1% Triton X-

100 DPBS at room temperature. Fluorescent images were taken using a Zeiss Axiovert II inverted fluorescent microscope with 2.5x and 10x objectives.

I. FEMUR SECTION IMMUNOHISTOCHEMISTRY

Femurs were isolated from the same mice used for the aortic ring assay. Femurs were surgically removed from euthanized mice after the thoracic aorta (described in section 4G), trimmed of excess tissue and rinsed with cold PBS. Femurs were then fixed in 10% buffered formalin overnight at 4°C. Bone decalcification was performed by storing femurs in formic acid (Sigma-Aldrich cat # 399388) for 72h at 4°C, followed by neutralization in DPBS for 2h at 4°C. Decalcified bones then stored in 70% ethanol at 4°C prior to paraffin embedding and sectioning. Longitudinal femur sections were labeled with proliferating cell nuclear antigen (PCNA) antibody conjugated to Alexa-594 antibody to identify proliferating cells, with DAPI counterstain to identify cell nuclei. H&E staining was performed on adjacent sections for contrast. Brightfield images of H&E stained sections taken using a Nikon TMS inverted microscope at 20x objective magnification. Fluorescent images were taken using a Zeiss Axiovert II inverted fluorescent microscope with 20x objective.

J. WOUND CLOSURE RATE IN A MURINE RADIATION COMBINED WITH INJURY (RCI) MODEL

Male CD-1 mice (n = 10 per treatment) received 8 Gy of ionizing radiation from a ¹³⁷Cs source, or sham treatment. At 24h post-irradiation, mice were injected intraperitoneally with 100 µL of either saline; or 43.4 nmol of TP508, PEG5k-TP508, PEG20k-TP508, PEG20k-Cys14-TP508, or PEG30k-TP508. At 48h post-irradiation,

anesthetized mice received a full-thickness 1.44 cm² dorsal excision wound. Wound areas were generated from images taken at Day 3, 5, 7, 10, 13 & 15 using a WoundZoom camera, which uses 4 positioning lasers to determine distance from wound and automatically calculate size of wound after user definition of the wound perimeter in the WoundZoom software. Rate of wound closure and standard error of rate was calculated from all data points per treatment from Day 3 – Day 15 using non-linear regression in SigmaPlot 12.

K. AORTIC EXPLANTS WITH *IN VITRO* TP508 TREATMENT

Aortas from male CD-1 mice were isolated, cleaned & sectioned prior to overnight incubation in serum-free media. On the following day, aortic rings were transferred to iBidi Angiogenesis μ Slides (iBidi cat. # 81506) or μ Plates (iBidi cat. # 89646) containing Growth Factor Reduced Matrigel®. Explants were incubated in EGM2-MV media containing TP508 or TP508 derivatives for two days, followed by media alone at 37°C, 5% CO₂. Media evaporation was minimized by adding media to the edges of the μ Plates, or incubating in sterile petri dishes containing Kimwipes soaked in DPBS. On Days 6, 7 & 8, sprouts were counted *in situ* using phase contrast microscopy on a Leica DMLB microscope.

L. ENDOTHELIAL TUBE FORMATION

HDMECs (Promocell # C-12215) pre-screened for VEGF responsiveness and primary human pericytes isolated from placenta (hPC-PL, Promocell cat # C-12980) were cultured separately prior to experiment. HDMEC were cultured in EGM2-MV media, while hPC-PL were cultured in Pericyte Growth Medium (Promocell # C-28040). Cells were grown to ~90% confluence prior to subculture or co-culture. On the day of

experiment, if irradiation was performed, cells were irradiated as separate cultures 1h prior to harvesting. Cells were harvested by trypsinization for 5 minutes at 37°C, then quenched with EGM2-MV media and transferred to 15 mL microfuge tubes. Cells were then pelleted by centrifuging at 300 x g for 3 minutes. Media was removed and cells were resuspended in Endothelial Basal Media, then counted using a Cellometer Mini cell counter (Nexcelom Bioscience). Cells were then transferred in the appropriate pericyte:HDMEC cell ratios (HDMEC alone, 1:1, 1:10 or 1:100) to microcentrifuge tubes. Cells were pelleted a second time at 300 x g for 3 minutes. Media was then replaced with fresh EBM containing various concentrations of TP508 or VEGF. Cells were seeded at concentration of 1×10^5 cells in 50 μ L volume into iBidi μ Slides containing 10 μ L growth factor reduced Matrigel® in the lower well. μ Slides were incubated at 37°C, 5% CO₂ within petri dishes containing Kimwipes soaked in sterile DPBS to minimize media evaporation. At timepoints between 2 and 44h after seeding, wells were imaged by phase contrast microscopy on a Leica DMLB microscope. All experiments were performed between cell passages 3 and 8 for both cell types. Quantitation of total tube length was performed using the Angiogenesis Analyzer plugin for ImageJ (<http://image.bio.methods.free.fr/ImageJ/?Angiogenesis-Analyzer-for-ImageJ>, last accessed Nov. 4, 2016)

M. γ H2AX ASSAY

HDMEC were subcultured at 10,000 – 25,000 cells per well into 24-well plates containing glass cover slips. Cells were incubated in 500 μ L EGM2-MV media overnight at 37°C at 5% CO₂. On the following day, media was changed, replacing it with 450 μ L EGM2-MV media plus either 50 μ L 0.9% saline, or 50 μ L of TP508 or TP508 derivative

at various concentrations in 0.9% saline 1h prior to irradiation. Cells were then exposed to either 3, 6, or 9 Gy ionizing radiation from a ionizing radiation using a ^{137}Cs Gamma Irradiator (Mark 30, Shephard and Associates, San Fernando, CA), then returned to incubator. At each timepoint, wells were rinsed with DPBS and then fixed with 4% formalin for 30 minutes at room temperature. HDMEC were permeabilized for 1h with 0.2% Triton X-100, then blocked overnight with 10% normal goat serum. Labeled cells with 1:1000 mouse anti γH2AX (Ser136) antibody (Millipore cat #05-636) primary antibody, then 1:500 Goat anti-mouse Alexa Fluor 488 conjugated secondary antibody (Life Tech cat# A-11001). Counterstaining of nuclei was performed by adding 300 nM DAPI in deionized water to samples for 5 minutes, then rinsing 3x with DPBS. Coverslips were then inverted and mounted onto glass slides using ProLong Gold mounting medium.

Fluorescent microscopy was performed at 4x objective on a Leica DMLB microscope using filter cubes for DAPI and Alexa 488 secondary antibody. At least 8 random fields per coverslip were imaged to ensure counting of speckles within at least 100 distinct nuclei. Images were automatically analyzed in CellProfiler to determine the number of cells for each nucleus, and exported to GraphPad Prism for statistical analysis. Mean and 95% confidence intervals were generated using descriptive statistics analysis of the histograms of γH2AX foci per nucleus for each treatment and timepoint. P-values adjusted for the multiple comparisons between groups were generated using the Kruskal-Wallis non-parametric test (also known as one-way ANOVA of ranks) to account for differences in number of nuclei analyzed per group and non-normal distribution of γH2AX foci per nucleus observed in histograms.

**Appendix A – Original macro by RJ Blatt for automated analysis of
endothelial sprouting in the *in vitro* mouse aortic ring assay using
ImagePro 7.0**

```
Sub Vessels()
Dim Y As Integer
Dim X As Integer
Dim IName As String * 255
Dim Subtract(1 To 2) As Integer
Dim Threshold1 As Integer
Dim RingRemoval(1 To 2) As Integer
Dim Distance As Integer
Dim Folder As Integer

Folder = IpStGetName("Select File", "M:\data\achs\Blatt", "*.TIF", IName)

Do While Folder <> 0
    ret = IpWsLoad(IName, "TIF")
    ret = IpDocGet(GETACTDOC, 0, IName)
    For X = 1 To 2
        Subtract(X) = IpWsConvertImage(IMC_GRAY, CONV_SCALE, 0, 0, 0,
0)
    Next X
    ret = IpAppSelectDoc(Subtract(2))
    ret = IpFltConvolveKernel("HIGAUSS.7x7", 7, 2)
    ret = IpAppSelectDoc(Subtract(1))
    Threshold1 = IpOpImageArithmetics(Subtract(2), 0.0, OPA_SUB, 1)
    ret = IpDocCloseEx(Subtract(1))
    ret = IpDocCloseEx(Subtract(2))
    For Y = 1 To 2
        ret = IpAppSelectDoc(Threshold1)
        ret = IpSegShow(0)
        ret = IpSegPreview(ALL_W_B)
        ret = IpSegSetRange( 0, 0, 8)
        RingRemoval(Y) = IpSegCreateMask(MASK_BILEVELNEW, 0, 0)
        ret = IpSegReset()
        ret = IpLutSetAttr(LUT_CONTRAST, -2)
        ret = IpFltClose(MORPHO_3x3CROSS, 1)
    Next Y
    ret = IpAppSelectDoc(RingRemoval(1))
```

```
ret = IpFltClose(MORPHO_11x11OCTAGON, 3)
ret = IpFltDistance(50, 2)
```

```
'Private Sub SetupCount_Size1()
ret = IpBlbSetAttr(BLOB_AUTORANGE,0)
ret = IpBlbSetAttr(BLOB_BRIGHTOBJ,1)
ret = IpBlbSetAttr(BLOB_MEASUREOBJECTS,1)
ret = IpBlbSetAttr(BLOB_ADDCOUNT,1)
ret = IpBlbSetAttr(BLOB_FILTEROBJECTS,1)
ret = IpBlbSetAttr(BLOB_LABELCOLOR,1)
ret = IpBlbSetAttr(BLOB_LABELMODE,0)
ret = IpBlbSetAttr(BLOB_OUTLINEMODE,2)
ret = IpBlbSetAttr(BLOB_SMOOTHING,0)
ret = IpBlbSetAttr(BLOB_CLEANBORDER,0)
ret = IpBlbSetAttr(BLOB_FILLHOLES,0)
ret = IpBlbSetAttr(BLOB_CONVEX,0)
ret = IpBlbSetAttr(BLOB_MINAREA,1)
ret = IpBlbSetAttr(BLOB_8CONNECT,0)
ret = IpBlbEnableMeas(BLBM_ALL, 0)
ret = IpBlbEnableMeas(BLBM_AREA, 1)
ret = IpBlbSetFilterRange(BLBM_AREA, 35000, 10000000)
ret = IpSegSetRange(0, 1, 30)
```

```
Distance = IpSegCreateMask(MASK_BILEVELINPLACE, 0,0)
ret = IpDocCloseEx(RingRemoval(1))
ret = IpMacroStop("Here is where you pick your object outline", 0)
ret = IpAoiManager(AOISHOWDLG, "ring1")
ret = IpAoiManager(AOIADD, "ring1")
ret = IpDocCloseEx(Threshold1)
ret = IpDocCloseEx(Distance)
ret = IpAppSelectDoc(RingRemoval(2))
ret = IpAoiShow(FRAME_NONE)
ret = IpAoiManager(AOISSET, "ring1")
ret = IpWsFill(0, 3, 0)
ret = IpAoiShow(FRAME_RESET)
ret = IpMacroStop("Here is where you pick your counting outline",0)
ret = IpAoiManager(AOISHOWDLG, "count")
ret = IpAoiManager(AOIADD, "count")
ret = IpAoiManager(AOISSET, "count")
ret = IpOpShow(0)
```

```
ret = IpBlbShow(1)
```

```
'Private Sub SetupCount_Size2()
ret = IpBlbSetAttr(BLOB_LABELMODE, 0)
```

```

ret = IpBlbSetAttr(BLOB_OUTLINEMODE, 5)
ret = IpBlbSetAttr(BLOB_AUTORANGE, 1)
ret = IpBlbSetAttr(BLOB_BRIGHTOBJ, 1)
ret = IpBlbSetAttr(BLOB_FILLHOLES,0)
ret = IpBlbSetAttr(BLOB_MEASUREOBJECTS,1)
ret = IpBlbSetAttr(BLOB_ADDCOUNT,1)
ret = IpBlbSetAttr(BLOB_FILTEROBJECTS,1)
ret = IpBlbSetAttr(BLOB_LABELCOLOR,1)
ret = IpBlbSetAttr(BLOB_SMOOTHING,0)
ret = IpBlbSetAttr(BLOB_CLEANBORDER,0)
ret = IpBlbSetAttr(BLOB_CONVEX,0)
ret = IpBlbSetAttr(BLOB_MINAREA,1)
ret = IpBlbSetAttr(BLOB_8CONNECT,0)
ret = IpBlbEnableMeas(BLBM_ALL, 0)
ret = IpBlbEnableMeas(BLBM_DENDRITES, 1)
ret = IpBlbEnableMeas(BLBM_AREA, 1)
ret = IpBlbSetFilterRange(BLBM_AREA, 75.0, 1000000.0)
ret = IpBlbEnableMeas(BLBM_MINORAX, 1)
ret = IpBlbSetFilterRange(BLBM_MINORAX, 10.0, 1000000.0)
ret = IpBlbEnableMeas(BLBM_BRANCHLEN, 1)

ret = IpSCalSelect("(none)")
ret = IpBlbCount()
ret = IpBlbUpdate(0)
ipClassifiers(0) = BLBM_AREA
ret = IpBlbShowAutoClass(ipClassifiers(0), 1, 4, 1, 1)
ret = IpBlbSaveClasses("", S_LEGEND+S_DDE)
ret = IpMacroStop("Fix DDE options and Check Count; Then Click Continue", 0)
ret = IpDocCloseEx(RingRemoval(2))
ret = IpBlbShow(0)
Folder = IpStGetName("Select File, if Finished Select Cancel",
"M:\data\achs\Blatt", "*.TIF", IName)
Loop
End Sub

```

Appendix B – Optimized macro used for analysis of TP508 and TP508

derivative biological activity in ImagePro Plus 7.0

```
Sub Vessels()
Dim Y As Integer
Dim X As Integer
Dim IName As String * 255
Dim Subtract(1 To 2) As Integer
Dim Threshold1 As Integer
Dim RingRemoval(1 To 2) As Integer
Dim Distance As Integer
Dim Folder As Integer

Folder = IpStGetName("Select File", "C:\Users\Scott McVicar\Documents\Carney Lab",
"*.TIF", IName)

Do While Folder <> 0
    ret = IpWsLoad(IName, "TIF")
    ret = IpDocGet(GETACTDOC, 0, IName)
    For X = 1 To 2
        Subtract(X) = IpWsConvertImage(IMC_GRAY, CONV_SCALE, 0, 0, 0,
0)
    Next X
    ret = IpAppSelectDoc(Subtract(2))
    ret = IpFltConvolveKernel("HIGAUSS.7x7", 7, 2)
    ret = IpAppSelectDoc(Subtract(1))
    Threshold1 = IpOpImageArithmetics(Subtract(2), 0.0, OPA_SUB, 1)
    ret = IpDocCloseEx(Subtract(1))
    ret = IpDocCloseEx(Subtract(2))
    For Y = 1 To 2
        ret = IpAppSelectDoc(Threshold1)
        ret = IpSegShow(0)
        ret = IpSegPreview(ALL_W_B)
        ret = IpSegSetRange( 0, 0, 8)
        RingRemoval(Y) = IpSegCreateMask(MASK_BILEVELNEW, 0, 0)
        ret = IpSegReset()
        ret = IpLutSetAttr(LUT_CONTRAST, -2)
        ret = IpFltClose(MORPHO_3x3CROSS, 1)
    Next Y
    ret = IpAppSelectDoc(RingRemoval(1))
    ret = IpFltClose(MORPHO_11x11OCTAGON, 3)
    ret = IpFltDistance(50, 2)
```

```

Private Sub SetupCount_Size1()
ret = IpBlbSetAttr(BLOB_AUTORANGE,0)
ret = IpBlbSetAttr(BLOB_BRIGHTOBJ,1)
ret = IpBlbSetAttr(BLOB_MEASUREOBJECTS,1)
ret = IpBlbSetAttr(BLOB_ADDCOUNT,1)
ret = IpBlbSetAttr(BLOB_FILTEROBJECTS,1)
ret = IpBlbSetAttr(BLOB_LABELCOLOR,1)
ret = IpBlbSetAttr(BLOB_LABELMODE,0)
ret = IpBlbSetAttr(BLOB_OUTLINEMODE,2)
ret = IpBlbSetAttr(BLOB_SMOOTHING,1)
ret = IpBlbSetAttr(BLOB_CLEANBORDER,0)
ret = IpBlbSetAttr(BLOB_FILLHOLES,0)
ret = IpBlbSetAttr(BLOB_CONVEX,0)
ret = IpBlbSetAttr(BLOB_MINAREA,1)
ret = IpBlbSetAttr(BLOB_8CONNECT,0)
ret = IpBlbEnableMeas(BLBM_ALL, 0)
ret = IpBlbEnableMeas(BLBM_AREA, 1)
ret = IpBlbSetFilterRange(BLBM_AREA, 25000, 10000000)
ret = IpSegSetRange(0, 1, 30)

```

```

Distance = IpSegCreateMask(MASK_BILEVELINPLACE, 0,0)

```

```

ret = IpDocCloseEx(RingRemoval(1))
ret = IpAppSelectDoc(DOCSEL_PREVID)
ret = IpDocMove(716, 0)
ret = IpAppSelectDoc(DOCSEL_PREVID)
ret = IpAppSelectDoc(DOCSEL_PREVID)
ret = IpMacroStop("Here is where you pick your object outline", 0)
ret = IpAoiManager(AOISHOWDLG, "ring1")
ret = IpAoiManager(AOIADD, "ring1")
ret = IpDocCloseEx(Threshold1)
ret = IpDocCloseEx(Distance)
ret = IpAppSelectDoc(RingRemoval(2))
ret = IpAoiShow(FRAME_NONE)
ret = IpAoiManager(AOISSET, "ring1")
ret = IpWsFill(0, 3, 0)
ret = IpAoiShow(FRAME_RESET)
ret = IpMacroStop("Here is where you pick your counting outline",0)
ret = IpAoiManager(AOISHOWDLG, "count")
ret = IpAoiManager(AOIADD, "count")
ret = IpAoiManager(AOISSET, "count")
ret = IpOpShow(0)

ret = IpBlbShow(1)

```

```

Private Sub SetupCount_Size2()
ret = IpBlbSetAttr(BLOB_LABELMODE,0)
ret = IpBlbSetAttr(BLOB_OUTLINEMODE,3)
ret = IpBlbSetAttr(BLOB_AUTORANGE,1)
ret = IpBlbSetAttr(BLOB_BRIGHTOBJ,1)
ret = IpBlbSetAttr(BLOB_FILLHOLES,0)
ret = IpBlbSetAttr(BLOB_MEASUREOBJECTS,1)
ret = IpBlbSetAttr(BLOB_ADDCOUNT,1)
ret = IpBlbSetAttr(BLOB_FILTEROBJECTS,1)
ret = IpBlbSetAttr(BLOB_LABELCOLOR,1)
ret = IpBlbSetAttr(BLOB_SMOOTHING,5)
ret = IpBlbSetAttr(BLOB_CLEANBORDER,0)
ret = IpBlbSetAttr(BLOB_CONVEX,0)
ret = IpBlbSetAttr(BLOB_MINAREA,1)
ret = IpBlbSetAttr(BLOB_8CONNECT,0)
ret = IpBlbEnableMeas(BLBM_ALL, 0)
ret = IpBlbEnableMeas(BLBM_DENDRITES, 1)
ret = IpBlbEnableMeas(BLBM_AREA, 1)
ret = IpBlbSetFilterRange(BLBM_AREA, 100, 10000000.0)
ret = IpBlbEnableMeas(BLBM_MAJORAX, 1)
ret = IpBlbSetFilterRange(BLBM_MAJORAX, 15, 1000000.0)
ret = IpBlbEnableMeas(BLBM_MINORAX, 1)
ret = IpBlbSetFilterRange(BLBM_MINORAX, 3, 1000000.0)
ret = IpBlbEnableMeas(BLBM_BRANCHLEN, 1)

ret = IpSCalSelect("(none)")
ret = IpBlbCount()
ret = IpBlbUpdate(0)
ipClassifiers(0) = BLBM_AREA
ret = IpBlbShowAutoClass(ipClassifiers(0), 1, 2, 1, 1)
ret = IpBlbSaveClasses("", S_LEGEND+S_DDE)
ret = IpMacroStop("Fix DDE options and Check Count; Then Click Continue", 0)
ret = IpDocCloseEx(RingRemoval(2))
ret = IpBlbShow(0)
Folder = IpStGetName("Select File, if Finished Select Cancel",
"M:\data\achs\Blatt", "*.TIF", IName)
Loop
End Sub

```

Bibliography

1. Glenn KC, Frost GH, Bergmann JS, Carney DH. Synthetic peptides bind to high-affinity thrombin receptors and modulate thrombin mitogenesis. *Pept Res.* 1988;1(2):65-73.
2. Pineda AO, Carrell CJ, Bush LA, Prasad S, Caccia S, Chen ZW, Mathews FS, Di Cera E. Molecular dissection of Na⁺ binding to thrombin. *J Biol Chem.* 2004;279(30):31842-53. doi: 10.1074/jbc.M401756200.
3. Carney DH, Stiernberg J, Fenton JW. Initiation of proliferative events by human alpha-thrombin requires both receptor binding and enzymic activity. *J Cell Biochem.* 1984;26(3):181-95. doi: 10.1002/jcb.240260306.
4. Carney DH, Redin W, McCroskey L. Role of high-affinity thrombin receptors in postclotting cellular effects of thrombin. *Semin Thromb Hemost.* 1992;18(1):91-103. doi: 10.1055/s-2007-1002414.
5. Tsopanoglou NE, Pipili-Synetos E, Maragoudakis ME. Thrombin promotes angiogenesis by a mechanism independent of fibrin formation. *Am J Physiol.* 1993;264(5 Pt 1):C1302-7.
6. Cirino G, Cicala C, Bucci MR, Sorrentino L, Maraganore JM, Stone SR. Thrombin functions as an inflammatory mediator through activation of its receptor. *J Exp Med.* 1996;183(3):821-7.
7. Strukova SM. Thrombin as a regulator of inflammation and reparative processes in tissues. *Biochemistry (Mosc).* 2001;66(1):8-18.
8. Trejo J. Protease-activated receptors: new concepts in regulation of G protein-coupled receptor signaling and trafficking. *J Pharmacol Exp Ther.* 2003;307(2):437-42. doi: 10.1124/jpet.103.052100.
9. Carney DH, Redin W, McCroskey L. Role of high-affinity thrombin receptors in postclotting cellular effects of thrombin. *Semin Thromb Hemost.* 1992;18(1):91-103. doi: 10.1055/s-2007-1002414.
10. Carney DH, Stiernberg J, Fenton JW. Initiation of proliferative events by human alpha-thrombin requires both receptor binding and enzymic activity. *J Cell Biochem.* 1984;26(3):181-95. doi: 10.1002/jcb.240260306.
11. Sower LE, Payne DA, Meyers R, Carney DH. Thrombin peptide, TP508, induces differential gene expression in fibroblasts through a nonproteolytic activation pathway. *Exp Cell Res.* 1999;247(2):422-31. doi: 10.1006/excr.1998.4372.
12. Naldini A, Carraro F, Baldari CT, Paccani SR, Bernini C, Keherly MJ, Carney DH. The thrombin peptide, TP508, enhances cytokine release and activates signaling events. *Peptides.* 2004;25(11):1917-26. doi: 10.1016/j.peptides.2004.05.017.

13. Bizios R, Lai L, Fenton JW, Malik AB. Thrombin-induced chemotaxis and aggregation of neutrophils. *J Cell Physiol.* 1986;128(3):485-90. doi: 10.1002/jcp.1041280318.
14. Olszewska-Pazdrak B, Bergmann J, Fuller G, Carney D. Thrombin and Thrombin Peptides in Wound Healing and Tissue Repair. In: Maragoudakis M, Tsopanoglou N, editors. *Thrombin: Physiology and Disease*: Springer; 2009. p. 115-32.
15. Carney DH, Herbosa GJ, Stiernberg J, Bergmann JS, Gordon EA, Scott D, Fenton JW. Double-signal hypothesis for thrombin initiation of cell proliferation. *Semin Thromb Hemost.* 1986;12(3):231-40. doi: 10.1055/s-2007-1003559.
16. Tsopanoglou NE, Papaconstantinou ME, Flordellis CS, Maragoudakis ME. On the mode of action of thrombin-induced angiogenesis: thrombin peptide, TP508, mediates effects in endothelial cells via alphavbeta3 integrin. *Thromb Haemost.* 2004;92(4):846-57. doi: 10.1160/TH04-04-0208.
17. Derkach DN, Wadekar SA, Perkins KB, Rousseau E, Dreiza CM, Cheung-Flynn J, Ramos HC, Ugarova TP, Sheller MR. RGD-dependent binding of TP508 to integrin alphavbeta3 mediates cell adhesion and induction of nitric oxide. *Thromb Haemost.* 2010;104(1):172-82. doi: 10.1160/TH09-07-0447.
18. Norfleet AM, Bergmann JS, Carney DH. Thrombin peptide, TP508, stimulates angiogenic responses in animal models of dermal wound healing, in chick chorioallantoic membranes, and in cultured human aortic and microvascular endothelial cells. *Gen Pharmacol.* 2000;35(5):249-54.
19. Vartanian KB, Chen HY, Kennedy J, Beck SK, Ryaby JT, Wang H, Hoying JB. The non-proteolytically active thrombin peptide TP508 stimulates angiogenic sprouting. *J Cell Physiol.* 2006;206(1):175-80. doi: 10.1002/jcp.20442.
20. Wang Y, Wan C, Szöke G, Ryaby JT, Li G. Local injection of thrombin-related peptide (TP508) in PPF/PLGA microparticles-enhanced bone formation during distraction osteogenesis. *J Orthop Res.* 2008;26(4):539-46. doi: 10.1002/jor.20495.
21. Olszewska-Pazdrak B, Hart-Vantassell A, Carney DH. Thrombin peptide TP508 stimulates rapid nitric oxide production in human endothelial cells. *J Vasc Res.* 2010;47(3):203-13. doi: 10.1159/000255963.
22. Fossum TW, Olszewska-Pazdrak B, Mertens MM, Makarski LA, Miller MW, Hein TW, Kuo L, Clubb F, Fuller GM, Carney DH. TP508 (Chrysalin) reverses endothelial dysfunction and increases perfusion and myocardial function in hearts with chronic ischemia. *J Cardiovasc Pharmacol Ther.* 2008;13(3):214-25. doi: 10.1177/1074248408321468.
23. Freyberg S, Song YH, Muehlberg F, Alt E. Thrombin peptide (TP508) promotes adipose tissue-derived stem cell proliferation via PI3 kinase/Akt pathway. *J Vasc Res.* 2009;46(2):98-102. doi: 10.1159/000142727.
24. Pernia SD, Berry DL, Redin WR, Carney DH. A synthetic peptide representing the thrombin receptor-binding domain enhances wound closure in vivo. *SAAS Bull Biochem Biotechnol.* 1990;3:8-12.

25. Norfleet AM, Huang Y, Sower LE, Redin WR, Fritz RR, Carney DH. Thrombin peptide TP508 accelerates closure of dermal excisions in animal tissue with surgically induced ischemia. *Wound Repair Regen.* 2000;8(6):517-29.
26. Ryaby JT, Sheller MR, Levine BP, Bramlet DG, Ladd AL, Carney DH. Thrombin peptide TP508 stimulates cellular events leading to angiogenesis, revascularization, and repair of dermal and musculoskeletal tissues. *J Bone Joint Surg Am.* 2006;88 Suppl 3:132-9. doi: 10.2106/JBJS.F.00892.
27. Carney DH, Olszewska-Pazdrak B. Could rusalptide acetate be the future drug of choice for diabetic foot ulcers and fracture repair? *Expert Opin Pharmacother.* 2008;9(15):2717-26. doi: 10.1517/14656566.9.15.2717.
28. Wang H, Li X, Tomin E, Doty SB, Lane JM, Carney DH, Ryaby JT. Thrombin peptide (TP508) promotes fracture repair by up-regulating inflammatory mediators, early growth factors, and increasing angiogenesis. *J Orthop Res.* 2005;23(3):671-9. doi: 10.1016/j.orthres.2004.10.002.
29. Hanratty BM, Ryaby JT, Pan XH, Li G. Thrombin related peptide TP508 promoted fracture repair in a mouse high energy fracture model. *J Orthop Surg Res.* 2009;4:1. doi: 10.1186/1749-799X-4-1.
30. Li X, Wang H, Touma E, Qi Y, Rousseau E, Quigg RJ, Ryaby JT. TP508 accelerates fracture repair by promoting cell growth over cell death. *Biochem Biophys Res Commun.* 2007;364(1):187-93. doi: 10.1016/j.bbrc.2007.07.202.
31. Oyamada S, Osipov R, Bianchi C, Robich MP, Feng J, Liu Y, Burgess TA, Bell TM, Sheller MR, Sellke FW. Effect of dimerized thrombin fragment TP508 on acute myocardial ischemia reperfusion injury in hypercholesterolemic swine. *J Pharmacol Exp Ther.* 2010;334(2):449-59. doi: 10.1124/jpet.110.166348.
32. Chu LM, Osipov RM, Robich MP, Feng J, Sheller MR, Sellke FW. Effect of thrombin fragment (TP508) on myocardial ischemia reperfusion injury in a model of type 1 diabetes mellitus. *Circulation.* 2010;122(11 Suppl):S162-9. doi: 10.1161/CIRCULATIONAHA.109.928374.
33. Osipov RM, Bianchi C, Clements RT, Feng J, Liu Y, Xu SH, Robich MP, Wagstaff J, Sellke FW. Thrombin fragment (TP508) decreases myocardial infarction and apoptosis after ischemia reperfusion injury. *Ann Thorac Surg.* 2009;87(3):786-93. doi: 10.1016/j.athoracsur.2008.12.021.
34. Fossum TW, Olszewska-Pazdrak B, Mertens MM, Makarski LA, Miller MW, Hein TW, Kuo L, Clubb F, Fuller GM, Carney DH. TP508 (Chrysalin) reverses endothelial dysfunction and increases perfusion and myocardial function in hearts with chronic ischemia. *J Cardiovasc Pharmacol Ther.* 2008;13(3):214-25. doi: 10.1177/1074248408321468.
35. Papareddy P, Rydengård V, Pasupuleti M, Walse B, Mörgelin M, Chalupka A, Malmsten M, Schmidtchen A. Proteolysis of human thrombin generates novel host defense peptides. *PLoS Pathog.* 2010;6(4):e1000857. doi: 10.1371/journal.ppat.1000857.

36. Prasanna PG, Narayanan D, Hallett K, Bernhard EJ, Ahmed MM, Evans G, Vikram B, Weingarten M, Coleman CN. Radioprotectors and Radiomitigators for Improving Radiation Therapy: The Small Business Innovation Research (SBIR) Gateway for Accelerating Clinical Translation. *Radiat Res.* 2015;184(3):235-48. doi: 10.1667/RR14186.1.
37. Ryaby JT, Sheller MR, Levine BP, Bramlet DG, Ladd AL, Carney DH. Thrombin peptide TP508 stimulates cellular events leading to angiogenesis, revascularization, and repair of dermal and musculoskeletal tissues. *J Bone Joint Surg Am.* 2006;88 Suppl 3:132-9. doi: 10.2106/JBJS.F.00892.
38. Rodgers KE. Technology evaluation: Chrysalin (Orthologic). *Curr Opin Mol Ther.* 2005;7(3):264-72.
39. Stiernberg J, Norfleet AM, Redin WR, Warner WS, Fritz RR, Carney DH. Acceleration of full-thickness wound healing in normal rats by the synthetic thrombin peptide, TP508. *Wound Repair Regen.* 2000;8(3):204-15.
40. Norfleet AM, Huang Y, Sower LE, Redin WR, Fritz RR, Carney DH. Thrombin peptide TP508 accelerates closure of dermal excisions in animal tissue with surgically induced ischemia. *Wound Repair Regen.* 2000;8(6):517-29.
41. Li G, Ryaby JT, Carney DH, Wang H. Bone formation is enhanced by thrombin-related peptide TP508 during distraction osteogenesis. *J Orthop Res.* 2005;23(1):196-202. doi: 10.1016/j.orthres.2004.05.006.
42. Sheller MR, Crowther RS, Kinney JH, Yang J, Di Jorio S, Breunig T, Carney DH, Ryaby JT. Repair of rabbit segmental defects with the thrombin peptide, TP508. *J Orthop Res.* 2004;22(5):1094-9. doi: 10.1016/j.orthres.2004.03.009.
43. Hedberg EL, Kroese-Deutman HC, Shih CK, Crowther RS, Carney DH, Mikos AG, Jansen JA. Effect of varied release kinetics of the osteogenic thrombin peptide TP508 from biodegradable, polymeric scaffolds on bone formation in vivo. *J Biomed Mater Res A.* 2005;72(4):343-53. doi: 10.1002/jbm.a.30265.
44. Wang Y, Wan C, Szöke G, Ryaby JT, Li G. Local injection of thrombin-related peptide (TP508) in PPF/PLGA microparticles-enhanced bone formation during distraction osteogenesis. *J Orthop Res.* 2008;26(4):539-46. doi: 10.1002/jor.20495.
45. Osipov RM, Robich MP, Feng J, Clements RT, Liu Y, Glazer HP, Wagstaff J, Bianchi C, Sellke FW. Effect of thrombin fragment (TP508) on myocardial ischemia-reperfusion injury in hypercholesterolemic pigs. *J Appl Physiol* (1985). 2009;106(6):1993-2001. doi: 10.1152/japplphysiol.00071.2009.
46. Osipov RM, Bianchi C, Clements RT, Feng J, Liu Y, Xu SH, Robich MP, Wagstaff J, Sellke FW. Thrombin fragment (TP508) decreases myocardial infarction and apoptosis after ischemia reperfusion injury. *Ann Thorac Surg.* 2009;87(3):786-93. doi: 10.1016/j.athoracsur.2008.12.021.
47. Chu LM, Osipov RM, Robich MP, Feng J, Sheller MR, Sellke FW. Effect of thrombin fragment (TP508) on myocardial ischemia reperfusion injury in a model of type

- 1 diabetes mellitus. *Circulation*. 2010;122(11 Suppl):S162-9. doi: 10.1161/CIRCULATIONAHA.109.928374.
48. Oyamada S, Osipov R, Bianchi C, Robich MP, Feng J, Liu Y, Burgess TA, Bell TM, Sheller MR, Sellke FW. Effect of dimerized thrombin fragment TP508 on acute myocardial ischemia reperfusion injury in hypercholesterolemic swine. *J Pharmacol Exp Ther*. 2010;334(2):449-59. doi: 10.1124/jpet.110.166348.
49. Pozzi N, Chen Z, Di Cera E. How the Linker Connecting the Two Kringles Influences Activation and Conformational Plasticity of Prothrombin. *J Biol Chem*. 2016;291(12):6071-82. doi: 10.1074/jbc.M115.700401.
50. Shen Y, Maupetit J, Derreumaux P, Tufféry P. Improved PEP-FOLD Approach for Peptide and Miniprotein Structure Prediction. *J Chem Theory Comput*. 2014;10(10):4745-58. doi: 10.1021/ct500592m.
51. Derkach DN, Wadekar SA, Perkins KB, Rousseau E, Dreiza CM, Cheung-Flynn J, Ramos HC, Ugarova TP, Sheller MR. RGD-dependent binding of TP508 to integrin α v β 3 mediates cell adhesion and induction of nitric oxide. *Thromb Haemost*. 2010;104(1):172-82. doi: 10.1160/TH09-07-0447.
52. Zheng JC, Lei N, He QC, Hu W, Jin JG, Meng Y, Deng NH, Meng YF, Zhang CJ, Shen FB. PEGylation is effective in reducing immunogenicity, immunotoxicity, and hepatotoxicity of α -momorcharin in vivo. *Immunopharmacol Immunotoxicol*. 2012;34(5):866-73. doi: 10.3109/08923973.2012.666979.
53. Kochendoerfer G. Chemical and biological properties of polymer-modified proteins. *Expert Opin Biol Ther*. 2003;3(8):1253-61. doi: 10.1517/14712598.3.8.1253.
54. Chilukuri N, Sun W, Naik RS, Parikh K, Tang L, Doctor BP, Saxena A. Effect of polyethylene glycol modification on the circulatory stability and immunogenicity of recombinant human butyrylcholinesterase. *Chem Biol Interact*. 2008;175(1-3):255-60. doi: 10.1016/j.cbi.2008.05.020.
55. Kinstler O, Molineux G, Treuheit M, Ladd D, Gegg C. Mono-N-terminal poly(ethylene glycol)-protein conjugates. *Adv Drug Deliv Rev*. 2002;54(4):477-85.
56. Zalipsky S. Functionalized poly(ethylene glycol) for preparation of biologically relevant conjugates. *Bioconjug Chem*. 1995;6(2):150-65. PubMed PMID: 7599259.
57. Veronese FM. Peptide and protein PEGylation: a review of problems and solutions. *Biomaterials*. 2001;22(5):405-17.
58. Busnelli M, Kleinau G, Muttenthaler M, Stoev S, Manning M, Bibic L, Howell LA, McCormick PJ, Di Lascio S, Braida D, Sala M, Rovati GE, Bellini T, Chini B. Design and Characterization of Superpotent Bivalent Ligands Targeting Oxytocin Receptor Dimers via a Channel-Like Structure. *J Med Chem*. 2016;59(15):7152-66. doi: 10.1021/acs.jmedchem.6b00564.
59. Berguig GY, Convertine AJ, Frayo S, Kern HB, Procko E, Roy D, Srinivasan S, Margineantu DH, Booth G, Palanca-Wessels MC, Baker D, Hockenbery D, Press OW, Stayton PS. Intracellular delivery system for antibody-Peptide drug conjugates. *Mol Ther*. 2015;23(5):907-17. doi: 10.1038/mt.2015.22.

60. Terskikh AV, Le Doussal JM, Cramer R, Fisch I, Mach JP, Kajava AV. "Peptabody": a new type of high avidity binding protein. *Proc Natl Acad Sci U S A*. 1997;94(5):1663-8.
61. Carney DH, Mann R, Redin WR, Pernia SD, Berry D, Heggors JP, Hayward PG, Robson MC, Christie J, Annable C. Enhancement of incisional wound healing and neovascularization in normal rats by thrombin and synthetic thrombin receptor-activating peptides. *J Clin Invest*. 1992;89(5):1469-77. doi: 10.1172/JCI115737.
62. Bergmann JS, Dowdy Z, Carney DH. Demonstration of Specific Binding of TP508 to Receptors on Fibroblasts and Coronary Artery Endothelial Cells by Photo-Affinity Cross-Linking. American Society of Cell Biology Annual Meeting; San Diego, California: Molecular Biology of the Cell; 2006. p. 3555.
63. Sower LE, Payne DA, Meyers R, Carney DH. Thrombin peptide, TP508, induces differential gene expression in fibroblasts through a nonproteolytic activation pathway. *Exp Cell Res*. 1999;247(2):422-31. doi: 10.1006/excr.1998.4372.
64. Mandal SK, Rao LV, Tran TT, Pendurthi UR. A novel mechanism of plasmin-induced mitogenesis in fibroblasts. *J Thromb Haemost*. 2005;3(1):163-9. doi: 10.1111/j.1538-7836.2004.01054.x.
65. Kantara C, Moya SM, Houchen CW, Umar S, Ullrich RL, Singh P, Carney DH. Novel regenerative peptide TP508 mitigates radiation-induced gastrointestinal damage by activating stem cells and preserving crypt integrity. *Lab Invest*. 2015. doi: 10.1038/labinvest.2015.103.
66. Olszewska-Pazdrak B, McVicar SD, Rayavara K, Moya SM, Kantara C, Gammarano C, Olszewska P, Fuller GM, Sower LE, Carney DH. Nuclear Countermeasure Activity of TP508 Linked to Restoration of Endothelial Function and Acceleration of DNA Repair. *Radiat Res*. 2016. doi: 10.1667/RR14409.1.
67. Baker M, Robinson SD, Lechertier T, Barber PR, Tavora B, D'Amico G, Jones DT, Vojnovic B, Hodivala-Dilke K. Use of the mouse aortic ring assay to study angiogenesis. *Nat Protoc*. 2012;7(1):89-104. doi: 10.1038/nprot.2011.435.
68. Kleinman HK, Martin GR. Matrigel: basement membrane matrix with biological activity. *Semin Cancer Biol*. 2005;15(5):378-86. doi: 10.1016/j.semcancer.2005.05.004.
69. Nicosia RF, Ottinetti A. Modulation of microvascular growth and morphogenesis by reconstituted basement membrane gel in three-dimensional cultures of rat aorta: a comparative study of angiogenesis in matrigel, collagen, fibrin, and plasma clot. *In Vitro Cell Dev Biol*. 1990;26(2):119-28.
70. Olszewska-Pazdrak B, Carney DH. Systemic administration of thrombin peptide TP508 enhances VEGF-stimulated angiogenesis and attenuates effects of chronic hypoxia. *J Vasc Res*. 2013;50(3):186-96. doi: 10.1159/000348250.
71. Huang Y, Yang Z, Li A. [An experimental study of the effects of thrombin receptor activating peptide (TP508) on healing of ischemic wound and flap survival in rats]. *Zhonghua Shao Shang Za Zhi*. 2001;17(6):339-41.

72. Pang Y, Tsigkou O, Spencer JA, Lin CP, Neville C, Grottkau B. Analyzing Structure and Function of Vascularization in Engineered Bone Tissue by Video-Rate Intravital Microscopy and 3D Image Processing. *Tissue Eng Part C Methods*. 2015;21(10):1025-31. doi: 10.1089/ten.TEC.2015.0091.
73. Rudolph R, Vande Berg J, Schneider JA, Fisher JC, Poolman WL. Slowed growth of cultured fibroblasts from human radiation wounds. *Plast Reconstr Surg*. 1988;82(4):669-77.
74. Qu JF, Cheng TM, Xu LS, Shi CM, Ran XZ. [Effects of total body irradiation injury on the participation of dermal fibroblasts in tissue repair]. *Sheng Li Xue Bao*. 2002;54(5):395-9.
75. Akita S. Treatment of Radiation Injury. *Adv Wound Care (New Rochelle)*. 2014;3(1):1-11. doi: 10.1089/wound.2012.0403.
76. Wang J, Boerma M, Fu Q, Hauer-Jensen M. Radiation responses in skin and connective tissues: effect on wound healing and surgical outcome. *Hernia*. 2006;10(6):502-6. doi: 10.1007/s10029-006-0150-y.
77. Tibbs MK. Wound healing following radiation therapy: a review. *Radiother Oncol*. 1997;42(2):99-106.
78. Gholobova D, Decroix L, Van Muylder V, Desender L, Gerard M, Carpentier G, Vandeburgh H, Thorrez L. Endothelial Network Formation Within Human Tissue-Engineered Skeletal Muscle. *Tissue Eng Part A*. 2015;21(19-20):2548-58. doi: 10.1089/ten.TEA.2015.0093.
79. DeCicco-Skinner KL, Henry GH, Cataisson C, Tabib T, Gwilliam JC, Watson NJ, Bullwinkle EM, Falkenburg L, O'Neill RC, Morin A, Wiest JS. Endothelial cell tube formation assay for the in vitro study of angiogenesis. *J Vis Exp*. 2014(91):e51312. doi: 10.3791/51312.
80. Zudaire E, Gambardella L, Kurcz C, Vermeren S. A computational tool for quantitative analysis of vascular networks. *PLoS One*. 2011;6(11):e27385. doi: 10.1371/journal.pone.0027385.
81. Chen YB, Lan YW, Chen LG, Huang TT, Choo KB, Cheng WT, Lee HS, Chong KY. Mesenchymal stem cell-based HSP70 promoter-driven VEGFA induction by resveratrol alleviates elastase-induced emphysema in a mouse model. *Cell Stress Chaperones*. 2015;20(6):979-89. doi: 10.1007/s12192-015-0627-7.
82. Chiang JH, Yang JS, Lu CC, Hour MJ, Chang SJ, Lee TH, Chung JG. Newly synthesized quinazolinone HMJ-38 suppresses angiogenic responses and triggers human umbilical vein endothelial cell apoptosis through p53-modulated Fas/death receptor signaling. *Toxicol Appl Pharmacol*. 2013;269(2):150-62. doi: 10.1016/j.taap.2013.03.007.
83. Blatt RJ, Clark AN, Courtney J, Tully C, Tucker AL. Automated quantitative analysis of angiogenesis in the rat aorta model using Image-Pro Plus 4.1. *Comput Methods Programs Biomed*. 2004;75(1):75-9. doi: 10.1016/j.cmpb.2003.11.001.

84. Lundholt BK, Scudder KM, Pagliaro L. A simple technique for reducing edge effect in cell-based assays. *J Biomol Screen*. 2003;8(5):566-70. doi: 10.1177/1087057103256465.
85. Guo S, Lok J, Liu Y, Hayakawa K, Leung W, Xing C, Ji X, Lo EH. Assays to examine endothelial cell migration, tube formation, and gene expression profiles. *Methods Mol Biol*. 2014;1135:393-402. doi: 10.1007/978-1-4939-0320-7_32.
86. Saunders WB, Bohnsack BL, Faske JB, Anthis NJ, Bayless KJ, Hirschi KK, Davis GE. Coregulation of vascular tube stabilization by endothelial cell TIMP-2 and pericyte TIMP-3. *J Cell Biol*. 2006;175(1):179-91. doi: 10.1083/jcb.200603176.
87. Stratman AN, Malotte KM, Mahan RD, Davis MJ, Davis GE. Pericyte recruitment during vasculogenic tube assembly stimulates endothelial basement membrane matrix formation. *Blood*. 2009;114(24):5091-101. doi: 10.1182/blood-2009-05-222364.
88. Stratman AN, Davis GE. Endothelial cell-pericyte interactions stimulate basement membrane matrix assembly: influence on vascular tube remodeling, maturation, and stabilization. *Microsc Microanal*. 2012;18(1):68-80. doi: 10.1017/S1431927611012402.
89. Traktuev DO, Merfeld-Clauss S, Li J, Kolonin M, Arap W, Pasqualini R, Johnstone BH, March KL. A population of multipotent CD34-positive adipose stromal cells share pericyte and mesenchymal surface markers, reside in a periendothelial location, and stabilize endothelial networks. *Circ Res*. 2008;102(1):77-85. doi: 10.1161/CIRCRESAHA.107.159475.
90. Cuthbertson RA, Mandel TE. Anatomy of the mouse retina. Endothelial cell-pericyte ratio and capillary distribution. *Invest Ophthalmol Vis Sci*. 1986;27(11):1659-64.
91. Frank RN, Turczyn TJ, Das A. Pericyte coverage of retinal and cerebral capillaries. *Invest Ophthalmol Vis Sci*. 1990;31(6):999-1007.
92. Geevarghese A, Herman IM. Pericyte-endothelial crosstalk: implications and opportunities for advanced cellular therapies. *Transl Res*. 2014;163(4):296-306. doi: 10.1016/j.trsl.2014.01.011.
93. Staton CA, Reed MW, Brown NJ. A critical analysis of current in vitro and in vivo angiogenesis assays. *Int J Exp Pathol*. 2009;90(3):195-221. doi: 10.1111/j.1365-2613.2008.00633.x.
94. Carpenter AE, Jones TR, Lamprecht MR, Clarke C, Kang IH, Friman O, Guertin DA, Chang JH, Lindquist RA, Moffat J, Golland P, Sabatini DM. CellProfiler: image analysis software for identifying and quantifying cell phenotypes. *Genome Biol*. 2006;7(10):R100. doi: 10.1186/gb-2006-7-10-r100.
95. González JE, Lee M, Barquinero JF, Valente M, Roch-Lefèvre S, García O. Quantitative image analysis of gamma-H2AX foci induced by ionizing radiation applying open source programs. *Anal Quant Cytol Histol*. 2012;34(2):66-71.

96. Suzuki M, Suzuki K, Kodama S, Watanabe M. Phosphorylated histone H2AX foci persist on rejoined mitotic chromosomes in normal human diploid cells exposed to ionizing radiation. *Radiat Res.* 2006;165(3):269-76.
97. Kataoka Y, Murley JS, Baker KL, Grdina DJ. Relationship between phosphorylated histone H2AX formation and cell survival in human microvascular endothelial cells (HMEC) as a function of ionizing radiation exposure in the presence or absence of thiol-containing drugs. *Radiat Res.* 2007;168(1):106-14. doi: 10.1667/RR0975.1.
98. Sokolov M, Neumann R. Lessons learned about human stem cell responses to ionizing radiation exposures: a long road still ahead of us. *Int J Mol Sci.* 2013;14(8):15695-723. doi: 10.3390/ijms140815695.
99. Fishburn CS. The pharmacology of PEGylation: balancing PD with PK to generate novel therapeutics. *J Pharm Sci.* 2008;97(10):4167-83. doi: 10.1002/jps.21278.
100. Chapman JR, Taylor MR, Boulton SJ. Playing the end game: DNA double-strand break repair pathway choice. *Mol Cell.* 2012;47(4):497-510. doi: 10.1016/j.molcel.2012.07.029.
101. Dunn BMP, Michael W. *Peptide Analysis Protocols*: Humana Press; 1994. 335 p.

Vita

Scott Davenport McVicar was born on December 8, 1978 in Steinbach, Manitoba, Canada to Grant Davenport McVicar and Sheila Jeannine McVicar (née Curtis). He obtained his Bachelor of Science at the University of Winnipeg with a double major in biochemistry and physics. During his time at the University of Winnipeg he earned seven awards and scholarships, including the Board of Regents Special Entrance Scholarship and the President's Award of Merit in Science. Upon graduation, he entered the biotechnology industry as a research analytical biochemist. At Cangene Corporation, a Canadian pharmaceutical company specializing in recombinant human protein therapeutics, his comparability studies on Cangene's liquid formulated recombinant human growth hormone (Accretropin™) formed part of a successful New Drug Application to the U.S. FDA. Dr. McVicar then moved to California to work at Codexis, a biotechnology company specializing in directed evolution of enzymes to replace costly steps of synthesis of active pharmaceutical intermediates and commodity chemicals with biocatalysis. His work at Codexis encompassed a broad array of projects from epoxide ring opening and closing reactions catalyzed by halohydrin dehalogenase to the breakdown of cellulosic biomass and production of cellulosic biofuels. During this time, he received 3 employee recognition awards for his scientific contributions and earned co-inventor credit on US Patent 8,187,856 for Recombinant Halohydrin Dehalogenase Polypeptides. Dr. McVicar joined the Graduate School of Biomedical Sciences at the University of Texas Medical Branch (UTMB) in 2010. His research in the laboratory of Dr. Darrell Carney focuses on the modification of tissue repair peptide TP508 for improved efficacy in mitigating the

damaging effects of ionizing radiation. This research is supported by grants from NIH/NIAID and has been published in Radiation Research, with an additional original research article currently in review by the American Association of Pharmaceutical Sciences Journal. He also acts as a consultant for Chrysalis BioTherapeutics, which is developing TP508 for radiomitigation and other therapeutic applications, on peptide formulation and assay development.

Permanent address: 3507 Borden Gully Drive, Dickinson, Texas 77539

This dissertation was typed by Scott McVicar.